Quantification of deformation processes in the Torlesse accretionary wedge, New Zealand

Dissertation zur Erlangung des Grades

„Doktor der Naturwissenschaften“

am Fachbereich Geowissenschaften
der Johannes Gutenberg – Universität Mainz

Hagen Karl Deckert

geboren in Erlenbach am Main

Mainz, August 2003

Erklärung

Ich versichere hiermit, die vorliegende Arbeit selbständig und nur unter Verwendung der angegebenen Quellen und Hilfsmittel verfasst zu haben.

Mainz, August 2003

Tag der mündlichen Prüfung: 14.11.2003

Summary

In this study structural data, strain determinations, and geochemical analyses are used to explore the tectonic evolution of the Torlesse accretionary wedge, New Zealand. The results provide information on the significance of deformation mechanisms and mass transfer, which additionally allow to comment on the flow paths and exhumation history of high-pressure rocks within this tectonic setting.

The Torlesse wedge in New Zealand's South Island represents a long-lived accretionary wedge that formed above a south-westward-dipping subduction zone during Permian to Late Cretaceous convergence between the Pacific oceanic plate and the east Gondwana margin. Investigations in this study were concentrated on the Otago Schist that is interpreted as the former fore-arc high of the Torlesse wedge. The Otago Schist forms a 150 km-wide, NW trending two-sided arch, that mainly consists of monotonous series of metamorphosed sandstones and mudstones. Metamorphic conditions range from prehnite-pumpellyite facies for the non-schistose rocks at the flanks to greenschist facies with peak metamorphic temperatures and pressures of 350-400°C and 8-10 kbar in the centre.

Absolute finite strain measurements in low-grade sandstones from the flanks of the wedge indicate an average volume loss of c. 20% (S_V = 0.78). Microstructural evidence prove a mainly coaxial deformation in the rocks. Strain in the low-grade sandstones and relative finite strain estimated in metapelites by X-ray texture goniometry, show both prolate and oblate strain symmetries with a significant maximum shortening. Because of strong variations in the orientation of principal stretching directions local stretches average out on the regional scale. Tensor average calculations of regional deformation denote uniaxial shortening along a subvertical maximum shortening axis (S_Z=0.87). Absolute strain data in upper wedge levels additionally reveal only minor shortening along the maximum and intermediate stretching axes (S_X=0.95, S_Y=0.94). The results indicate the complexity between local and regional deformation in three-dimensions.

Volume change is expressed in metasomatic mobilisation of silica due to pressure solution and results in a geochemical fractionation of the rocks. Systematic changes of residual element/SiO_2 ratios with volume strain are used to calculate volume strain in outcrops of deeper crustal levels, in which volume strain cannot be determined directly by absolute strain work. As a reference to which measured element ratios can be compared to, the protolith composition of the rocks was determined. Therefore samples that were already examined for volume strain were analysed for their chemical composition. Adding the amount of dissolved silica to the respective composition of the metamorphosed and deformed sandstone allowed to determine the protolith composition of the rocks. Chemical compositions of high-grade zones differ from the protolith composition denote a loss of 15 % silica despite a modal abundance of 15 to 33% of veins in the deeper levels of the wedge. Summarising, absolute strain data in higher and geochemical estimates in deeper levels of the wedge both indicate significant mass loss of up to 20% volume loss. This implies that uniaxial shortening is mainly compensated by significant mass-transfer volume strain instead of orogen-parallel extension. As sinks for

the dissolved material are unknown it must be assumed that the material was removed out of the wedge in an open-system mass transfer.

Strain results are also used to explore the degree of coupling between the accretionary wedge and the subducted plate. Maximum shear strains were determined from deviatoric finite strain data in the highest-grade pelitic rocks of the Torlesse wedge. After accretion at the base of the wedge the rocks accumulated strain as they were moved through the entire wedge to the surface. The rocks therefore provide a record of the deformation operating within the wedge. Calculated shear strains range between $\gamma = 1.06$ and 3.16. These results were compared to expected shear strains calculated by a simple geometric model that considers a variety of different convergence velocities and exhumation rates. Overall, the results indicate that the Torlesse wedge is strongly decoupled from the subducted Pacific plate. This is supported by the coaxial nature of deformation in the metamorphosed sandstones.

Results imply that deformation within the wedge is mainly driven by sedimentary fluxes in and out of the wedge and not by shear stresses transmitted from the down going plate. In this context the subvertical uniaxial shortening suggests that ductile thinning assisted the exhumation of the Otago Schist. Coevally, ductile thinning keeps the Torlesse wedge in a subcritical configuration and counteracts the underplating of rocks at its base. Normal faulting also aided the exhumation of the Otago Schist but not as a result of a supercritical wedge geometry. All known Mesozoic normal sense shear zones in the Otago Schist, like the Rise-Shine-, Cromwell-Gorge-, and Hyde-Macraes-Shear-Zones formed during a post-convergent New Zealand wide rifting after subduction processes ceased in the Late Cretaceous.

Zusammenfassung

In dieser Studie werden strukturgeologische Daten, Verformungsabschätzungen und geochemische Analysen benutzt, um die tektonische Entwicklung des Torlesse-Akkretionskeils in Neuseeland zu untersuchen. Die Ergebnisse enthalten Informationen über die Signifikanz von Deformationsmechanismen und Massenverschiebungen. Zusätzlich ergeben sich Einblicke über Fließpfade und Exhumierungsgeschichte hochdruckdeformierter Gesteine in diesem geotekonischen Szenario.

Der Torlesse-Keil in der Südinsel von Neuseeland stellt einen langlebigen Akkretionskeil dar. Er entwickelte sich während der südwest gerichteten Subduktion der ozeanischen Pazifischen Platte unter den Ostrand Gondwanas während des Perms bis in die späte Kreide. Die Untersuchungen in dieser Studie konzentrieren sich auf die Region des Otago Schist, der als ehemalige äußere Schwelle des Torlesse-Keils interpretiert wird. Der Otago Schist stellt einen 150 km breiten, Nordwest verlaufenden Bogen dar, der hauptsächlich aus monotonen Sand- und Tonsteinserien aufgebaut ist. Die metamorphen Bedingungen reichen von der Prehnit-Pumpellyit-Fazies in den ungeschieferten Flanken, bis zur Grünschiefer-Fazies mit maximalen P-T Bedingungen von 8-10 kbar und 350-400°C im Zentrum des Bogens.

Absolute, finite Verformungsmessungen, in niedriggradigen Sandsteinen von den Flanken des Keils, zeigen einen durchschnittlichen Volumenverlust von ca. 20% (S_V = 0.78) an. Mikrostrukturelle Erkenntnisse belegen eine koaxiale Deformation in den Gesteinen. Die Verformungen in den niedriggradigen Sandsteinen und relative finite Verformungsabschätzungen in Metapeliten, die durch Röntgentexturgoniometrie gewonnen wurden, zeigen sowohl prolate als auch oblate Symmetrien mit einer signifikanten maximalen Verkürzung. Durch die starke Variation in den Orientierungen der Hauptverformungsrichtungen werden lokale Streckungen im regionalen Maßstab allerdings gemittelt. Tensordurchschnittsberechnungen der regionalen Deformation zeigen eine uniaxiale Verkürzung entlang der subvertikalen maximalen Verkürzungsachse (S_Z = 0.87). Absolute Verformungsdaten in den oberen Stockwerken des Keils enthüllen zusätzlich, dass entlang der maximalen und intermediären Streckungsachsen nur sehr schwache Verkürzung stattfand (S_X = 0.95, S_Y = 0.94). Die Ergebnisse belegen die komplexen Unterschiede zwischen lokaler und regionaler Deformation im dreidimensionalen Raum.

Volumenveränderung drückt sich in der metasomatischen Mobilisierung von SiO_2 durch Drucklösung aus und schlägt sich in einer geochemischen Fraktionierung der Gesteine nieder. Die systematische Beziehung von Volumenverformung zu immobilen Element/SiO_2 Verhältnissen erlaubt auch die Volumenverformungsbestimmung in tiefer krustalen Aufschlüssen. In diesen ist es nicht möglich Volumenverformung direkt durch absolute Verformungsdaten zu ermitteln. Als Referenz, zu der die gemessenen Elementverhältnisse verglichen werden können, wurde die Protolitzusammensetzung der Gesteine bestimmt. Hierfür wurden die Gesteine, die bereits auf ihre Volumenveränderung erforscht wurden, auf ihre chemische Zusammensetzung untersucht. Das Hinzufügen des Betrags an gelöstem SiO_2 zu der jeweiligen Zusammensatzung der metamorphen und deformierten Sandsteine erlaubt es, auf den Protolit rückzuschließen. Die chemische Zusammensetzung höhergradiger Zonen weicht von der Protolitzusammensetzung ab und zeigt einen Verlust von 15% SiO_2 an,

obwohl in den tiefern Einheiten des Keils 15-33% Quarzadern vorzufinden sind. Zusammenfassend deuten die absoluten Verformungsdaten in den höheren und geochemische Abschätzungen in den tieferen Stockwerken des Keils einen signifikanten Volumenverlust von bis zu 20% an. Da Speicherorte für das gelöste Material nicht bekannt sind, muss angenommen werden, dass das Material in einem offenen System aus dem Keil abtransportiert wurde.

Die Verformungsergebnisse werden außerdem benutzt, um den Grad der Kopplung zwischen Akkretionskeil und subduzierter Platte zu untersuchen. In den höchstgradigen pelitischen Gesteinen des Torlesse-Keils wurden maximale Scherverformungswerte bestimmt. Nach der Akkretion an der Basis des Keils akkumulierten die Gesteine die Verformung auf ihrem Weg durch den Keil an die Erdoberfläche. Damit haben sie die Deformation im inneren des Keils aufgezeichnet. Die ermittelten Scherwerte variieren zwischen $\gamma = 1.06$ und 3.16. Diese Ergebnisse werden mit Scherwerten verglichen, die mittels eines einfachen Modells, das verschiedene Konvergenzgeschwindigkeiten und Exhumierungsraten berücksichtigt, berechnet wurden. Insgesamt zeigen die Resultate, dass der Torlesse-Keil stark von der subduzierten Pazifischen Platte entkoppelt ist. Dieses Ergebnis wird durch die, in den metamorphen Sandsteinen ermittelte, koaxiale Deformation unterstützt.

Die Resultate implizieren, dass die Deformation im Keil hauptsächlich durch den Fluß der Sedimente in und aus dem Keil bestimmt wird und nicht durch Scherstress, der von der subduzierten Platte auf den Keil übertragen wird. In diesem Zusammenhang legt die subvertikale Verkürzung nahe, dass duktile Plättung die Exhumierung des Otago Schist gefördert hat. Zeitgleich sorgt die duktile Plättung auch dafür, den Keil in einer subkritischen Konfiguration zu halten und wirkt damit der Unterplattung an der Basis des Keils entgegen. Abschiebungen trugen auch zur Exhumierung des Otago Schist bei, aber nicht als Folge einer superkritischen Keilsymmetrie. Vielmehr formten sich alle bekannten mesozoischen Abschiebungen, wie die Rise-and-Shine-, Cromwell-Gorge- und Hyde-Macraes-Scherzone, während eines post-konvergenten neuseelandweiten Riftprozess nach der Beendigung der Subduktion in der späten Kreide.

Zusammenfassung für Fachfremde

Die Südinsel Neuseelands stellte im Mesozoikum (Erdmittelalter, ca. 250-65 Mio. Jahre vor heute) einen Bereich zweier miteinander kollidierender Erdplatten dar. Die ozeanische Pazifische Platte wurde auf Grund ihrer höheren Gesteinsdichte unter den damalig existierenden Kontinent Gondwana geschoben (subduziert). Im Grenzbereich der beiden Platten, der Subduktionszone, bildete sich ein sogenannter Akkretionskeil aus. Dieser stellt eine Anhäufung von Sedimenten dar, die sowohl vom Kontinent als auch im geringeren Maße von der ozeanischen Platte stammen. Da die Sedimente im Gegensatz zu der ozeanischen Platte eine geringere Dichte aufweisen, werden sie nur in begrenztem Maße mit in die Tiefe gezogen. Der Großteil der Sedimente wird von der unterlagernden, ozeanischen Platte abgeschabt und zu einem Akkretionskeil direkt vor dem Kontinent zusammengeschoben (Abb. 1). Dieser Prozess gleicht einem Bulldozer der Sand vor sich herschiebt (Abb. 2).
In dieser Studie wird untersucht welche Mechanismen in welchem Maße die Gesteine während des Zusammenschiebens im Torlesse Akkretionskeil in Neuseeland, deformieren. Die Ergebnisse geben zusätzlich Aufschluß, wie es dazu kommen kann, dass Gesteine, die einst bis zu 30 km tief subduziert wurden, nun wieder an der Erdoberfläche anzutreffen sind (Exhumierung). Dies ist möglich, da die Gesteine die Deformationen die sie auf ihrem Weg durch den Akkretionskeil erleiden, gleich einem Flugschreiber aufzeichnen.
Verformungsmessungen an Sand- und Tonsteinen zeigen, dass die Gesteine innerhalb des Akkretionskeils, in der zur Erdoberfläche vertikalen Richtung, bis zu 20% verkürzt wurden. Diese Verkürzung entstand durch den Deformationsprozess der Drucklösung (d.h. Material wurde gelöst und vom Gestein wegtransportiert). In den andern Richtungen ergibt sich fast keine Längenänderung im Vergleich zum undeformierten Zustand. Dies bedeutet, dass die Gesteine bis zu 20% ihres ursprünglichen Volumens, das sie besessen haben bevor sie in den Akkretionskeil geschoben wurden, verloren haben.

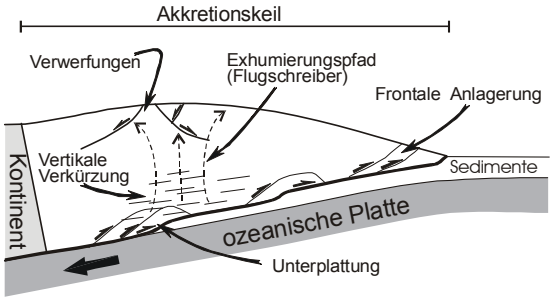

Abb.1 Akkretionskeil. Sedimente werden durch frontale Anlagerung oder Unterplattung von der subduzierten Platte abgeschabt und dem Keil zugeführt.

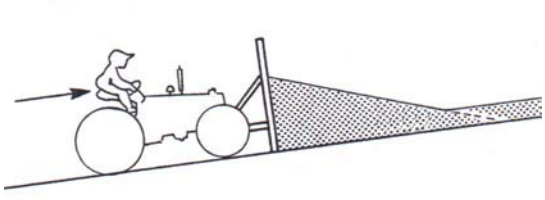

Abb.2 Bulldozer-Keil (aus Dahlen 1990). Sand wird durch den Bulldozer zu einer Keilform zusammengeschoben. Dies gleicht der Entwicklung eines Akkretionskeils im Bereich zweier kollidierender Platten.

In den tieferen Bereichen des Akkretionskeilen, bei höheren Temperaturen um 300°C, werden Verformungsmechanismen wie z.B. plastisches Fließen aktiv. Die angewandten Verfahren zur Verformungsabschätzung eigenen sich aber nur in Gesteinen, die ausschließlich durch Drucklösung deformiert wurden. Daher wird versucht eine mögliche Volumenveränderung in den tieferen Gesteinen mittels chemischer Gesteinsanalysen zu bestimmen. Das Element Zirkonium ist im Gegensatz zu SiO_2 (Quarz) wesentlich schwerer in Fluiden zu lösen. Da nahezu ausschließlich Quarz in den Gesteinen gelöst wird, bedeutet dies, dass höhere Zr/Quarz Verhältnisse gleichbedeutend mit einem höheren Volumenverlust sind. Die Ergebnisse der chemischen Untersuchung belegen auch in den tieferen Teilen des Akkretionskeils einen Volumenverlust von ca. 20%.
Hat sich ein Akkretionskeil erst einmal entwickelt, so wächst er in einer sich selbstähnlichen Art und Weise durch die ständige Anlieferung neuer Sedimentmassen und versucht eine stabile Konfiguration aufrecht zu erhalten. Sedimente werden nicht nur frontal angelagert, sondern z.T. erst in der Tiefe an den Keil angeschweißt (Unterplattung). Dadurch würde der Keil aus seiner stabilen Geometrie gerissen. Die in dieser Studie ermittelte starke vertikale Verkürzung mit den verbundenen Volumenverlusten wirkt dem entgegen und hält so die stabile Konfiguration aufrecht.
Die Exhumierung der einst tief versenkten Gesteine erfolgt teilweise durch die angesprochene vertikale Verkürzung und zum Teil auf Grund von Verwerfungen die, ähnlich Hangrutschungen, Material von den auflagernden Schichten abtransportieren und so darunterliegende Gesteinseinheiten freilegen.
Zuletzt erlauben die Verformungsergebnisse dieser Studie die Kopplung des Akkretionskeils und der ozeanischen Platte abzuschätzen. Eine starke Kopplung würde eine starke Zerscherung der Gesteine im Akkretionskeil mit sich führen. Mit Hilfe eines einfachen Modells werden verschiedene Szenarien starker oder wenig starker Kopplung berechnet. Im Vergleich mit den tatsächlich ermittelten Scherwerten in den Gesteinen des Torlesse Keils wird deutlich, dass die Kopplung nur sehr gering war. Somit wird die Verformung der Gesteine weniger durch das Aneinandervorbeigleiten der Pazifischen Platte am Akkretionskeil, als durch Deformation im inneren des Keils beeinflusst.

Literatur:

Dahlen, F.A. 1990. Critical taper model of fold-and-thrust belts and accretionary wedges. *Annual reviews of Earth and Planetary Sciences*, **18**, 55-99.

An dieser Stelle möchte ich mich bei meinem Betreuer in Mainz bedanken, der mich durch diese Arbeit führte und mir immer mit Rat und Tat bei Seite stand. Diese Arbeite profitierte außerdem von der Hilfe meiner Kollegen an der Yale University, USA und am GNS in Dunedin, Neuseeland.
Nicht zuletzt gilt mein Dank auch meinen Freunden und Kollegen in Mainz, die mir mit ihrer Unterstützung in vielerlei Hinsicht geholfen haben.

Table of content

Chapter 3
Shear coupling at subduction zones – Implications from X-ray texture goniometry on phyllosilicate-rich rocks from the Torlesse accretionary wedge, New Zealand

Chapter 4
Tectonic significance of Cretaceous bivergent extensional shear zones in the Torlesse accretionary wedge, Central Otago Schist, New Zealand

Preface

All chapters, including multiple author chapters, are solely written by Hagen Deckert unless stated otherwise. Research and results presented in all chapters, including multiple author chapters, are the sole work of Hagen Deckert unless stated otherwise. Uwe Ring and Mark Brandon have supervised the work. Nick Mortimer helped during field work and Jeffrey Rahl offered some absolute strain data.

The work presented in this thesis aims to quantify deformation processes in the Torlesse accretionary wedge, New Zealand. Investigation are based on geochemical analyses, absolute and relative finite strain determinations, and deformation structures obtained from fieldwork.

Chapter 1 addresses differences between local and regional scale deformation, and volume strain in low-grade rocks of the Torlesse wedge. Chapter 1 was written by Hagen Deckert and Jeffrey Rahl, supervised by Mark Brandon and Uwe Ring. Part of this research was presented at the *GSA Penrose Conference: Three-Dimensional Flow, Fabric Development, and Strain in Deformed Rocks and the Significance for Mountain Building Processes: New Approaches. Monte Verita, Switzerland*. Title: *Deckert, H., Brandon, M.T., Ring, U., Mortimer, N. & Maxelon, M. 2002. Absolute strain and volume loss in the Otago Schist, New Zealand.* EBSD measurements and tensor average calculations were performed by H. Deckert. 30% of the absolute strain measurements have been produced by Jeffrey Rahl (Yale University).

In Chapter 2 the geochemical fractionation in metamorphosed sandstones is investigated. New chemical rock composition data are used to estimate volume strain in deeper levels of the Torlesse wedge. Co-authors for this study are Uwe Ring, Mark Brandon, and Jeffrey Rahl. XRF-measurements used in Chapter 2 were performed by XRAL laboratories, Don Mills, Ontario.

Chapter 3 investigates the coupling between subducted plate and the Torlesse wedge. Additionally it comprises new relative strain data that are used to discuss regional deformation in the Otago Schist. The Chapter is identical to a manuscript submitted to "*Journal of Structural Geology*" in April 2003 entitled "*Deckert, H. & Brandon M.T. Shear coupling at subduction zones – Implications from X-ray texture goniometry on phyllosilicate-rich rocks from the Torlesse subduction wedge, New Zealand*." X-ray texture goniometry was performed by Hagen Deckert.

Chapter 4 discusses the significance of Mesozoic shear zones in the Otago Schist and tries to explain why the shear zones are not related to syn-convergent normal faulting but instead have to be seen in a post-subduction context. The chapter is identical with the manuscript *"Deckert, H., Ring, U. & Mortimer, N. 2002. Tectonic significance of Cretaceous bivergent extensional shear zones in the Torlesse accretionary wedge, Central Otago Schist, New Zealand"*, which was published in December 2002.

Local and regional mass-transfer deformation in the Torlesse accretionary wedge, New Zealand

Hagen Deckert[a], Jeffrey Rahl[b], Mark Brandon[b], and Uwe Ring[a]

[a] Institut für Geowissenschaften, Johannes Gutenberg-Universität, Becherweg 21, 55099 Mainz, Germany
[b] Kline Geology Laboratory, Yale University, P.O. Box 208109, 210 Whitney Avenue, New Haven,CT 06520-8109, U.S.A

To be submitted to the *Journal of Structural Geology*.

Abstract

Absolute deformation measurements are presented for a suite of samples from the Torlesse accretionary wedge exposed in the Otago region of the South Island, New Zealand. These data constrain the three-dimensional pattern of within-wedge ductile flow on both local and regional scales. Microstructural evidence indicates that deformation in the flanks of the Otago uplift was coaxial and dominated by solution mass-transfer processes. We find that local strains are both prolate and oblate with a mass-transfer volume loss typically about 20%. Individual samples typically show significant maximum shortening stretches (S_z). However, variation in the orientation of the principal strain axes leads to an averaging out of local features of the deformation field at a larger scale. Regional deformation is characterized by a uniaxial shortening (S_z = 0.87) with minor shortening in the regional foliation plane (the maximum (S_x) and intermediate (S_y) stretches are 0.95 and 0.94 respectively). Regional ductile flow involved shortening in all directions, compensated by a mass-transfer volume stretch (S_v) of about 0.78. These results highlight the complex relationship between local and regional deformation in three-dimensions.

Introduction

Deformation measurements contain direct information about the kinematics of ancient orogenic belts. Such data provide an opportunity to explore many important tectonic processes in subduction wedges, including the nature of margin-perpendicular deformation (whether shortening or extension), the significance of margin-parallel shearing, and the pattern of flow within the wedge. A rock accumulates strain as it is subducted and exhumed, thus providing a record of the deformation processes operating within the wedge. Regional deformation may be heterogeneous caused by significant local variations in the orientation of the principal strain directions. An important problem in structural geology is the interaction of local deformations to accommodate deformation on a regional scale.

This study focuses on deformation analysis on samples from the Otago Schist exposed in the South Island, New Zealand. Traditionally, there have been several tectonic models proposed to explain the fabrics exposed in the Otago Schist. Early work (e.g., Coombs et al., 1976; Wood, 1978; Mortimer, 1993) envisioned deformation as developing during discrete orogenic episodes that corresponded to the accretion of allochtonous terranes. Another idea is that the fabrics in the Otago Schist are related to syn-contractional extension, as has been increasingly recognized in many convergent settings (e.g., the Appennines) (Forster & Lister, 2003). However, the only extensional faults that have been identified in Otago appear to be related to post-convergence rifting (Deckert et al., 2002).

As an alternative to these models, we consider the Otago Schist as the remnants of an accretionary wedge that formed along the Mesozoic margin of Gondwana (Korsch & Wellman, 1988). In this scenario, the fabrics record progressive deformation of sediments advecting through the the wedge system. The Otago wedge is well-suited for this study for several reasons: 1) Despite its ancient age, the Otago Schist is well-preserved and has not been greatly deformed since the Mesozoic. This is indicated by the presence of a Cretaceous-Miocene peneplain surface that is present throughout the Otago region that itself is deformed only by broad, late-Cenozoic folds; 2) Previous work has placed constraints on the P-T-t history of the wedge (e.g., Mortimer, 2000) that provide a geologic framework for interpreting strain measurements; 3) Deformation throughout much of the currently exposed parts of the wedge was accommodated predominantly by pressure solution (Norris & Bishop, 1990), allowing the application of several methods that have been recently developed to measure absolute strains in these types of rocks (Feehan and Brandon, 1999; Ring & Brandon, 1999).

Previously published regional strain work in the Otago region is limited to a study of deformed conglomerates (Norris & Bishop, 1990). The present study is one of two papers focusing on regional deformation in the Otago Schist (see Deckert & Brandon, this volume). We present 54 new absolute strain determinations from the flanks of the Otago Schist, which we interpret to represent the former forearc high of the Torlesse wedge. We show that deformation within the schist was predominantly coaxial, and illustrate how local variations in the deformation field are balanced out over larger scales. This effect leads to a regional deformation of a smaller magnitude than that recorded in individual samples. Finally, we propose that the observed shortening within the wedge was accommodated not by extension but rather by open-system mass-transfer of material out of the subduction wedge.

Geologic setting

New Zealand represents the long-lived growth of Gondwana in response to the subduction-driven processes of terrane accretion and magmatic addition. In this paper we focus on the geology of the Permian-Cretaceous Torlesse accretionary wedge, that was built during the subduction of the oceanic Pacific plate under the East Gondwana margin. In present coordinates, the ancient subduction system faces to the northeast, with the magmatic arc (Median Batholith) located in southern part of the South Island. The fossil trench located offshore to the north of the South Island. Between the Torlesse wedge and the arc lie the sediments of the fore-arc basin, represented by the Brook Street, Murihiku, and Maitai units (Fig. 1).. The composition of these sediments requires that the arc was built on oceanic (rather than continental) crust (MacKinnon, 1983). The fore-arc sediments are floored by the remnant oceanic crust preserved in the Dun Mountain Ophiolite Belt (part of the Maitai). Together, these units act as a structural lid, or backstop, to the Torlesse wedge, which is composed of the mainly greywacke sandstone-dominated Caples and Torlesse Terranes (Fig. 1). The Torlesse wedge grew by accretion of Permian and Triassic sandstones of the Caples Terrane and Permian and Triassic sandstones of the older part of the Torlesse Terrane. Torlesse and Caples rocks are distinguished by sedimentary provenance, with the Caples derived from an immature island arc source and the Torlesse, from a more evolved continental source (Mortimer & Roser 1992).

The Otago Schist represents the metamorphosed and penetratively deformed parts of the Caples and older Torlesse terranes that were exhumed in the forearc high of the subduction wedge. The broad structure of the forearc high is preserved as a large, roughly 150-km wide antiform. Penetrative foliation is subhorizontal in the core of the structure and dips moderately away in the flanks (Fig. 1). Mesoscopic lineations may be consistently

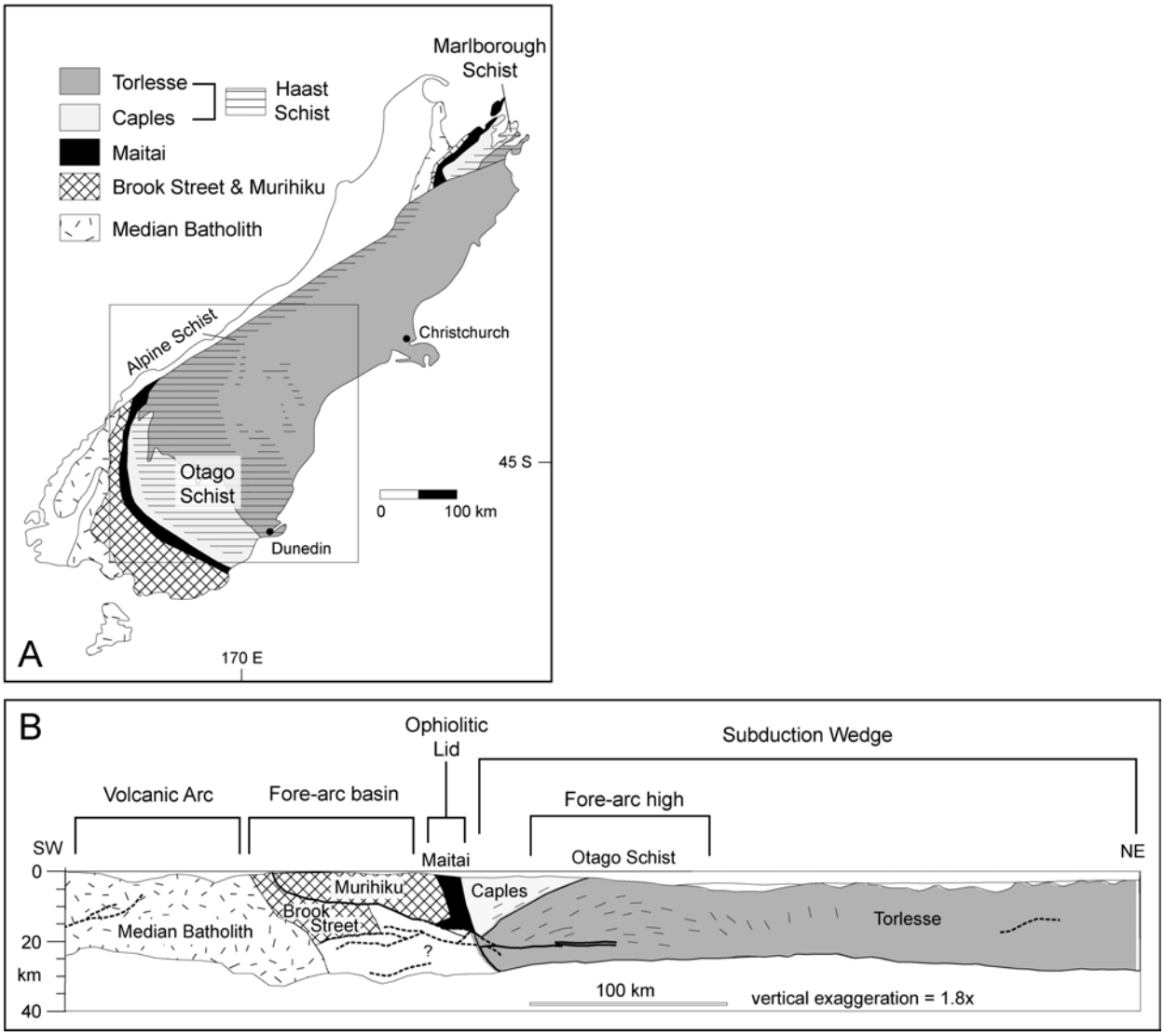

Fig. 1. A) Simplified geologic map of the pre-Cretaceous basement of the South Island, New Zealand (after Mortimer et al., 1999). B) Interpretative cross-section of the South Island, based on an interpretation by Mortimer et al. (2002) of a crustal seismic reflection profile.

oriented on a local scale, though their directions vary strongly across the region (Mortimer, 1993).Metamorphic grade ranges from prehnite-pumpellyite facies along the flanks of the Otago Schist antiform to greenschist facies along its axis. Maximum P-T conditions are estimated to be 0.8-1.0 MPa and 350-400°C within the core of the Otago culmination (Mortimer, 2000).

The main rock type within the Otago Schist is a lithologically monotonous metagreywacke. The lack of distinctive marker horizons impedes the identification of the regional structure. To overcome these difficulties, previous workers have subdivided the Otago Schist into “textural zones” (TZs) (e.g., Bishop, 1972). A recent study has defined these zones on the basis of white mica grain size and the degree of foliation development in the schist (Turnbull et al., 2001) (Fig. 2).The textural zones roughly correlate with stuctural

depth (Mortimer, 2003), deformation (Norris and Bishop, 1990), and metamorphic grade. It has been suggested (Norris and Bishop, 1990) that an important transition in the mode of deformation occurs as textural zone increases, from pressure-solution deformation at low TZ to dislocation creep at higher TZ. We confirm below that crystal plasticity becomes an additional deformation mechanism between textural zones 2A and 2B.

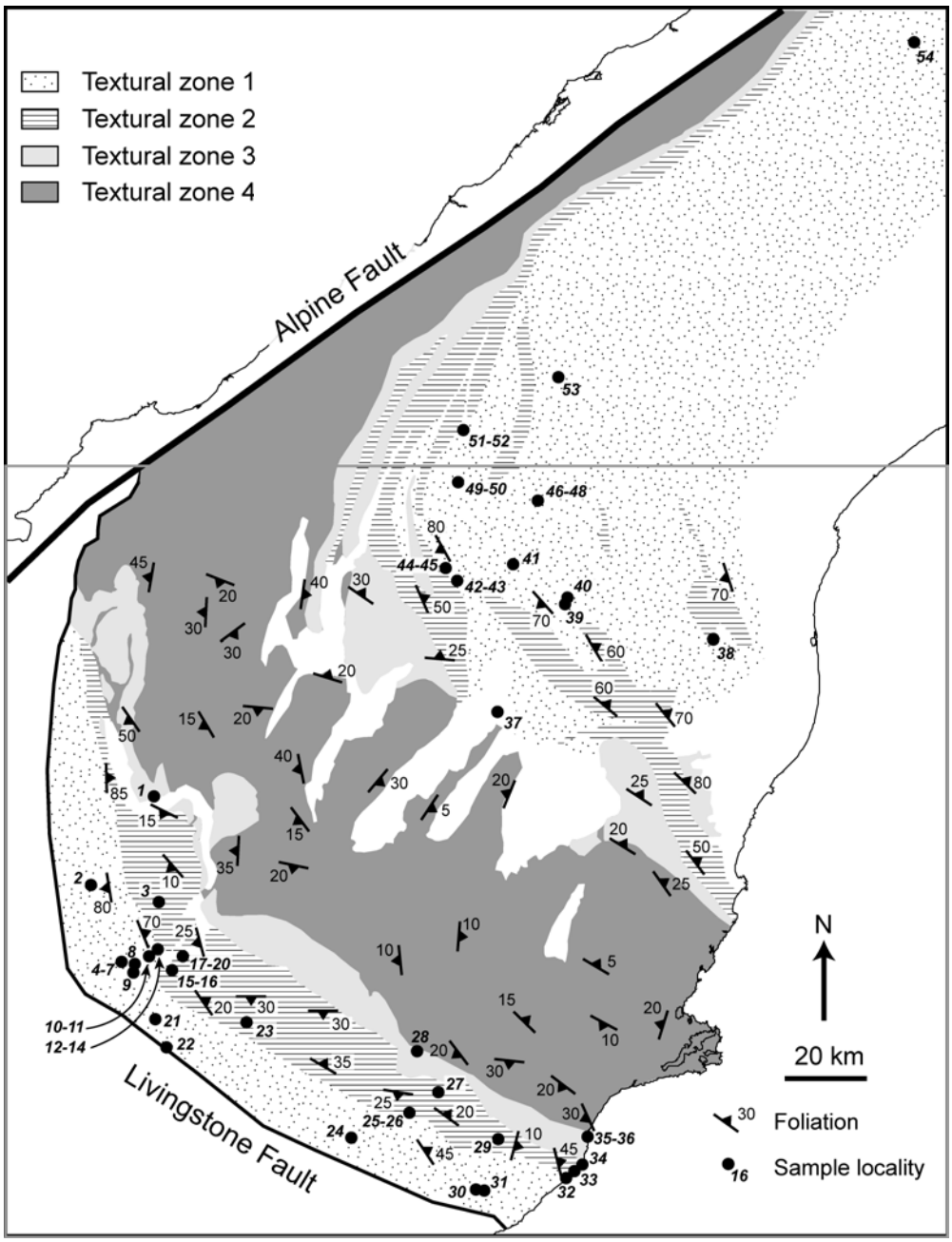

Fig. 2. Map of the study area. Sample localities are indicated by the black circles with bold italic numbers. The orientation of dominant foliation is shown after Mortimer (1993).

Deformation in the Torlesse wedge proceeded until the mid-Cretaceous. At about 105 Ma, Otago Schist clasts can be found in mid-Cretaceous graben sediments, demonstrating the exposure of the rocks of the Torlesse wedge by that time (Korsch & Wellman 1988, Adams & Raine 1988). This corresponds to a widely developed initial phase of rifting that ultimately resulted in the opening of the Tasman Sea by 85 Ma (Kamp, 1986). Between 105-85 Ma widespread erosion resulted in peneplanation of much of the southern South Island, creating the Waipounamu Erosion Surface (WES) (Bishop, 1994; LeMasurier & Landis, 1996). Miocene - Recent deformation related to formation of the Alpine Fault folded the surface that is exposed over large areas of eastern Otago region. However, deformation was only mild, so that the penetrative deformation recorded in the Otago Schist can be attributed to the Mesozoic.

Microstructural observations and deformation mechanisms

The metasediments of the Otago region are largely composed of sand-sized grains of quartz, feldspar and volcanic-lithic grains. Quartz, albite, pumpellyite, titanite, phengite and chlorite are also present in the groundmass. Microstructural observations indicate that the deformed sandstones of the Otago region can be classified into two types: one in which pressure solution operates as the dominant deformation mechanism, and another in which dislocation creep plays a significant role (Norris and Bishop, 1990).

54 samples of TZ1 (unfoliated) and TZ2A (weakly foliated) sandstones were sampled from both the Caples and Torlesse Terranes on either side of the Otago Schist antiformal culmination (Fig. 2). In low TZ rocks (typically < TZ 2B), deformation appears to have been dominated by solution mass-transfer processes. Evidence for pressure solution includes truncated mineral grains, the development of mica-rich dissolution seams. Generally, detrital quartz grains are devoid of undulose extinction, subgrain boundaries, deformed rutile inclusions, and other microstructures indicative of intragranular dislocation creep processes. Furthermore, fibrous overgrowths are commonly visible along the edges of large quartz and feldspar grains (Fig. 3). These fibers are generally straight and parallel to the macroscopic extension direction, indicating that any vorticity related to the deformation was negligible (Ring and Brandon, 1999; Ring et al., 2001). Some grain boundary sliding must accompany this deformation, in order to accommodate the divergence of two grains due to the precipitation of fibrous material between them. However, we interpret this as a secondary process, active only to prevent accommodation problems from developing within the rock.

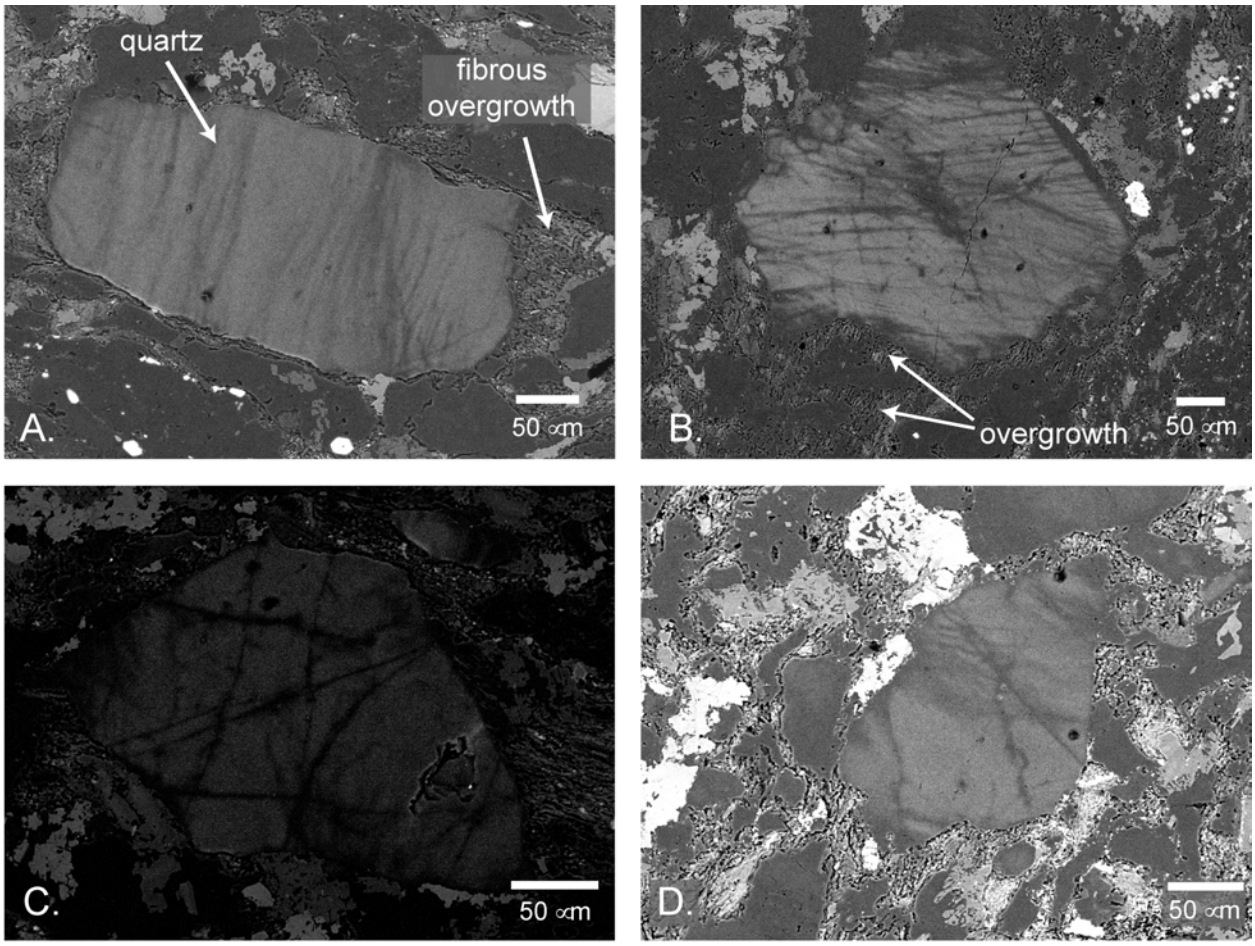

Fig. 3**.** Combined cathodoluminescence (CL) and electron back-scatter images (BSE) of samples from the Otago Schist. The large grains in the center of each image are quartz. The CL reveals internal fractures and deformation lamellae. However, these features do not have a systematic relationship to deformation features in the rock, such as the orientation of fibrous overgrowth. Thus, we interpret these features as inherited from the original source rock rather than as forming in situ due to deformation. The BSE portion of the image clearly shows the fibrous nature of the quartz overgrowth along the margins of many of the grains. There is no evidence of any non-fibrous overgrowths within the quartz grains.

One important issue for our study focuses on the nature of the reprecipitated material. Our strain measurement technique requires that the original detrital grain dimensions can be identified optically (see below). If reprecipitated material grows in crystallographic continuity with the deforming grain, our methods can significantly overestimate the actual strain. In a variety of studies of quartz veins, both observational and experimental, it has been demonstrated that the crystallographic nature of the vein material is controlled by the amount of surrounding pore space (Hilgers et al, 2000; Urai et al, 1991; Fischer & Brantley, 1992). If a growth surface is free and surrounded by fluid, the vein material tends to grow in crystallographic continuity with the wall rock. However, both theory and experiments have shown that fibrous vein material will precipitate when the available pore space is negligible.

Thus, fibre overgrowths observed in the Otago rocks suggests that deformation proceeded in the absence of significant porosity.

To ensure that there are no additional overgrowths in crystallographic continuity with the parent grains, we conducted reconnaissance cathodoluminescene (CL) work (Fig. 3). The quartz grains display cracks and deformation lamellae. However, our observations indicate that these features do not display any systematic relationship within each sample. Thus, we regard these features as inherited from the sedimentary source, rather than as forming in situ. We did not observe crystallographically continuous overgrowths, confirming our ability to identify the reprecipitated material solely through optical means.

In higher TZ rocks (generally > TZ 2A) larger clasts show evidence of internal deformation, including recrystallization and subgrain development. These microstructures indicate that dislocation creep was active in these rocks. However, we note that diffusion creep continues to play a significant role in accommodating the deformation in these rocks. Both the fibrous overgrowth and micaceous solution seams are more abundant in the higher TZ rocks, suggesting that reprecipitation remained important even while dislocation creep deformation took place. It is difficult to assess the relative importance of the competing deformation mechanisms, but it is clear that one mechanism did not dominate bulk deformation.

These microstructural interpretations are supported by an investigation of five samples using electron backscatter diffraction (EBSD) on quartz (Fig. 4). In samples collected from low textural zones (< TZ 2A), quartz fails to show any preferred orientation. This confirms that dislocation creep was not active at lower textural zone conditions. In contrast, the higher textural zone samples (beginning at TZ 2B) display a well developed orientation (Fig. 4), suggesting that the initiation of intracrystalline deformation occurs between textural zones 2A and 2B**.**

Methods for strain analysis

Feehan & Brandon (1999) and Ring& Brandon (1999) presented techniques specifically designed to measure absolute strain in pressure-solved sandstones. These are the Projected Dimension Strain (PDS) method, for quantifying shortening strains, and the Mode method, for measuring extensional strains. However, as described below, the PDS method in particular requires that the marker grains have experience no internal deformation. Thus, these methods can not be applied to the higher TZ rocks that contain abundant evidence for dislocation creep deformation. For this reason, the deformation measurements reported here are restricted to samples from the flanks of the Otago antiform, where the lower TZ (TZ 1 and 2a) rocks outcrop (Fig. 2).

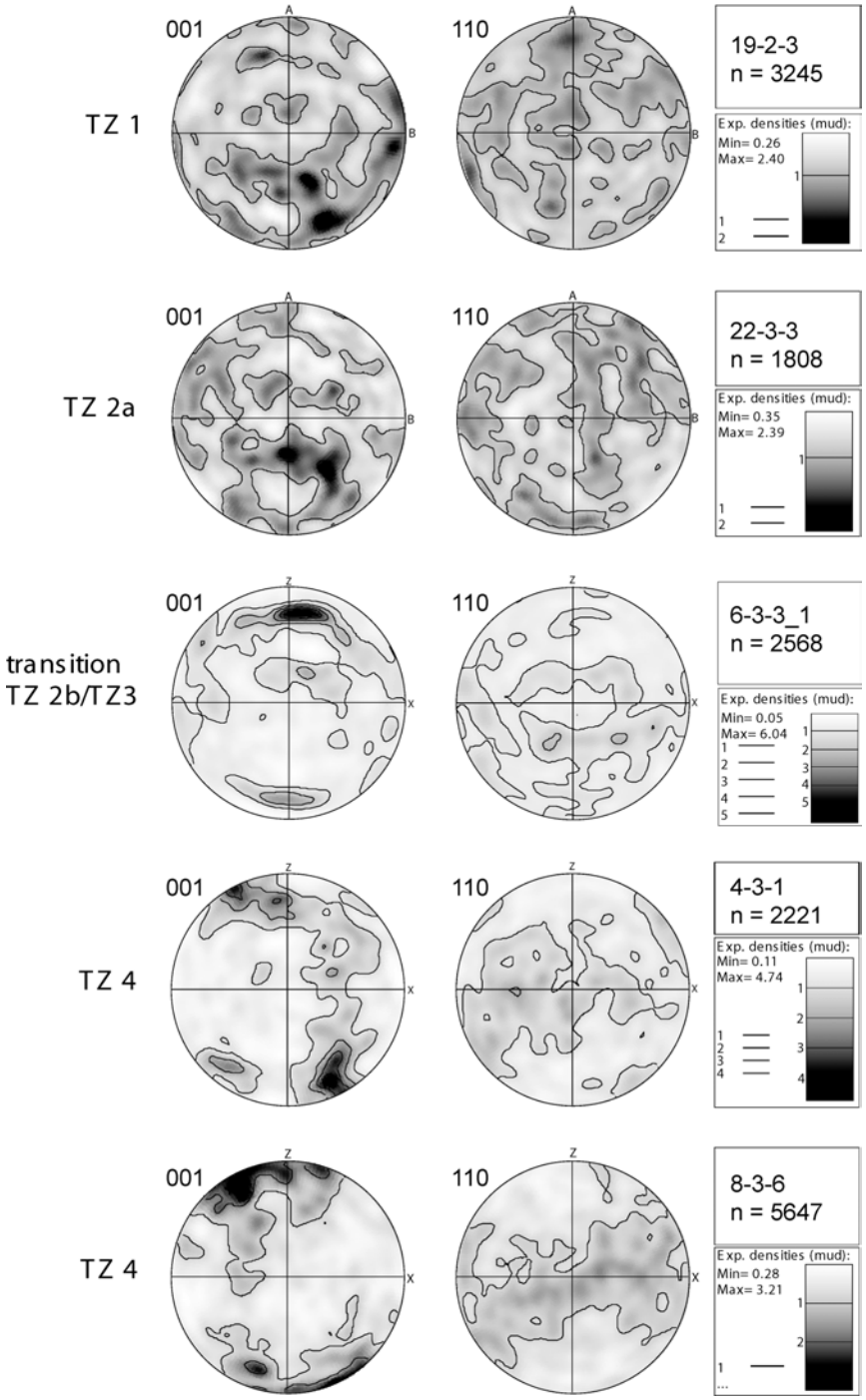

Fig. 4. Lower hemisphere, equal area stereonets showing electron back-scatter diffraction orientation data for 001 and 110 lattice directions in quartz from five samples of the Otago Schist. Lower textural zone samples (TZ 1 and TZ 2a) show no lattice preferred orientation (LPO), indicating that dislocation glide was not active, which is consistent with other evidence indicating that grain-boundary pressure solution was the dominant deformation mechanism for these textural zones. In contrast, rocks from TZ 2b and higher do show quartz LPO, indicating that intracrystalline deformation has occurred.

A companion study, based on X-ray texture goniometry, focuses on deformation in the higher TZ rocks from the deepest parts of exhumed fore-arc high (Deckert & Brandon this issue).

Projected dimension strain (for shortening strains)

Feehan & Brandon (1999) note that in rocks deformed only through diffusion creep processes, extension is accommodated through the precipitation of material along the edges of grains. If the newly precipitated material can be distinguished from the original grain material, the original grain dimension in the extension direction can be identified. Thus, the lengths of the original quartz grains in the extension direction can be used as a reference against which absolute strains can be estimated. Dissolution reduces the observed grain dimension in the shortening direction by removing original grain material. The measured average lengths in the shortening direction can be compared to the average original grain length in the extension direction to yield the stretch (S), where S = (final length)/(initial length).

Two orthogonal thin sections were prepared for each of the samples, one section parallel the foliation plane (the XY plane), and another parallel to the maximum and minimum stretch directions (the XZ plane). X, Y, and Z to denote the maximum, intermediate, and minimum extension directions respectively. For samples with no obvious lineation direction in hand sample, the extension direction was taken to be parallel to fibrous overgrowths observed in the foliation plane (XY section). The Otago samples generally show extension in one principal direction and shortening in the other two principal directions. Thus, PDS shortening stretches were measured in both the XZ and XY sections.

In general, a two-dimensional thin section will not intersect individual grains through the plane that would lead to the largest cross section. Thus, measurements made in 2D thin sections will underestimate of the amount of shortening experienced by individual grains (Fig. 5). Feehan & Brandon (1999) present a relationship between the observed, biased stretch and the actual stretch experienced by a rock by the integration of the observed stretches in all possible sections passing through a truncated sphere parallel to the shortening direction. However, their analysis assumes no shortening in the Y direction. In cases in which $S_y < 1$, the correction factor in the XZ section is obtained by integrating stretches observed in each XZ section between $-S_y$ and $+S_y$. The corrected stretches in both the X and Y directions are thus dependent on each other, and must be determined numerically using the observed stretches in the X and Y directions.

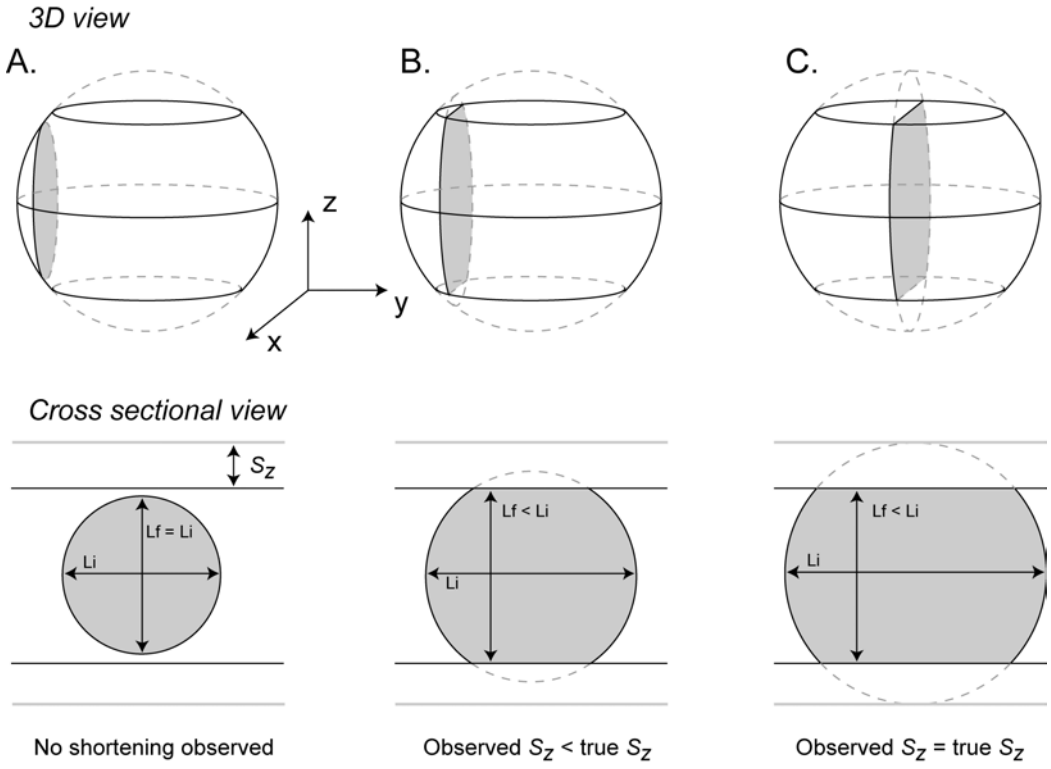

Fig. 5. Schematic illustration of the bias in estimating the magnitude of shortening in a truncated sphere due to using two-dimensional sections. For cross-sections far from the the center of the grain (A), no shortening may be observed (the initial length, Li, is equal to the final length, Lf). Generally, the stretch observed in most sections will be less than the actual stretch (B). It is only in cases where the thin section passes through the center of the grain (C) that the true stretch will be observed.

Mode method (for extensional strains)

The growth of veins is one means of accommodating extension in the bulk rock. However, in the lower textural zone rocks of the Otago region, vein material typically comprises a small proportion of the observed outcrops, typically less than 3% (Cox, 1991; Breeding and Ague, 2002). Another means of accommodating extension in pressure-solved rocks is through the precipitation of fibre overgrowth. In rocks with unidirectional fibers, the relationship between the modal abundance of overgrowth, m, and the extensional stretch, S_x, is described by: $S_x = 1/(1-m)$ (Ring & Brandon, 1999). A prerequisite for this to work is that the microscopist can clearly distinguish whether a given point in a thin section is an overgrowth or not. To minimize operator biases, we used several criteria to guide us in our recognition of fibrous overgrowth:

1) Overgrowths are recognized on the basis of their fibrous habit and their proximity to detrital grains of quartz or feldspar. They typically have a mineralogy consisting of quartz, albite, chlorite.
2) An individual thin section typically has minor three-dimensionality to it, and there are many cases where a given (x,y) coordinate would correspond to fibrous overgrowth at

one level and the edge of a grain at a different depth. Thus, we were careful to make all measurements at a single depth within the thin section, to avoid over- or under-estimating the abundance of overgrowth.

In order to quantify the abundance of fibrous overgrowth, we performed either point counting or line integration in the XZ thin sections using a computer-driven optical microscope. Multiple analyses by different operators varied by no more than 5% modal abundance.

Results

Local deformation

Using the PDS and Mode methods described above, the three principal stretches Sx, Sy, and Sz were determined for each sample (Fig. 6; Table 1). Individual hand samples generally show non-plane deformation, including both prolate and oblate strain symmetry (Fig. 6a). The conventional octahedral shear strain γoct can be used as a measure of the average distortion a sample suffered. It can be calculated by the amount of shear strain that is recorded by a material line and plane during deformation and is independent from strain geometry (Brandon 1995). In general, the distortional strains exhibited by individual samples are small, with octahedral shear strains typically about 0.6 or less (Fig. 6b). Because volume strain has to be considered for strain type even samples with an oblate symmetry tend to be constrictional (Fig. 6d). The fibrous overgrowths that accommodate extension are uncurved, indicating that the deformation was coaxial (Fig. 3).

Individual samples show only minor extension (< 5%) along Sx. This indicates that shortening was balanced not by corresponding extension but rather by mass-transfer volume loss. For the Otago samples, the volume stretch (Sv = Sx * Sy * Sz) is typically around Sv = 0.78. The volume strain shows a good correlation with the maximum shortening strain, indicating that the shortening was accomplished largely by mass-transfer volume loss (Fig. 6c). The correlation between the octahedral shear strain and the volume strain suggests that distortion is accomplished primarily by the mass-transfer deformation (Fig. 6b). There do not appear to be any differences in the magnitude or geometry of deformation in samples from the northern or southern flank of the forearc high.

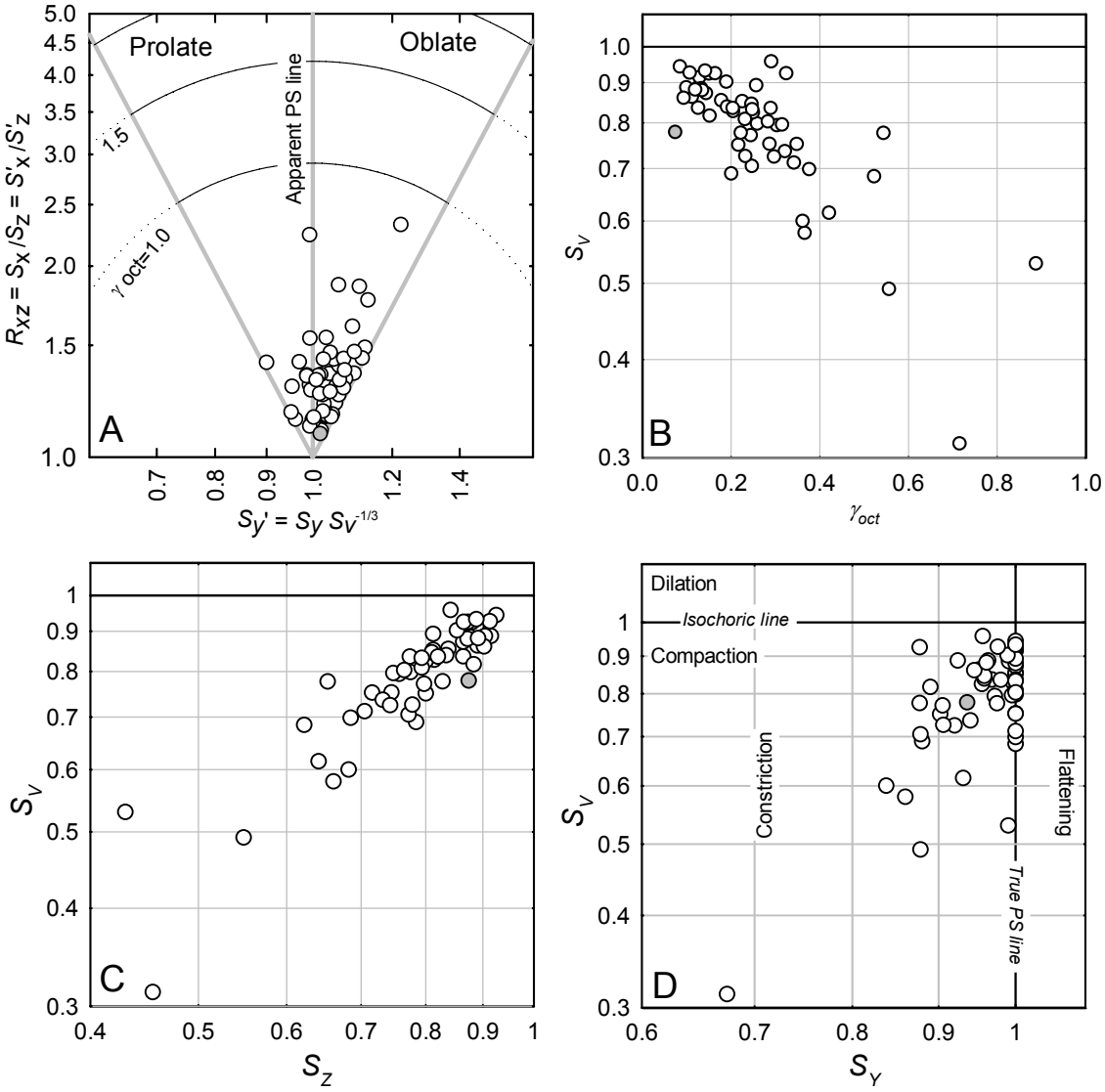

Fig. 6. Strain plots using the methods of Brandon (1995). The grey circle represent the strain values for the tensor average of all samples. See text for further information.

Regional deformation

Strain recorded at the local scale must reflect the nature of the deformation on the scale of the entire convergent wedge. In order to integrate the local measurements into a coherent estimate of the strain at the regional scale, we have applied the Hencky-tensor averaging method of Brandon (1995). The local deformation measurements are transformed into a natural-strain tensor form. The Hencky-tensor average is a straightforward component-by-component average of the data from the individual natural tensors. A requirement for this method is that the vorticity of the deformation is negligible. The straight fibrous overgrowths indicate that this requirement is met in the Otago rocks (Fig. 3).

When the data from both the northern and southern flanks of the forearc high are combined to form a single regional tensor average, the principal stretches S_x, S_y, and S_z, are 0.95, 0.94, and 0.87. The flattening plane for this regional tensor average dips moderately to the ENE.

Discussion

Local versus regional deformation

Local strain measurements record the deformation that has accrued at a specific spatial point in a deformational field. These data are sensitive to minor variations in the larger strain field. However, when the bulk deformation in a volume larger than that of an individual sample is considered, local deviations from the bulk strain field will tend to be averaged out. In other words, an extension observed at one sample locality may be balanced by a similarly oriented shortening in another location. Thus, the deformation at a regional scale may be of a smaller magnitude than what would be indicated by considering individual samples. This is similar to the findings of Feehan & Brandon (1999), Ring & Brandon (1999) and Ring et al. (2001) who also investigated local and regional deformation in accretionary wedges and fold-and-thrust belts. However, in some collisional orogens, e.g. the Alps, deformation is much more organized and characterized by flat-lying foliations and stretching lineations whose trend does not scatter much (and if so this scatter is commonly caused by later folding) (e.g., Ratschbacher et al. 1991). In this case "scaling-up" of local observations is less problematic.

In the case of the Otago samples, our results indicate that there are significant differences in the pattern of deformation at the regional and local scales. The distortional strains exhibited in local samples are in general much greater than the bulk deformation at the regional scale. For example, the octahedral shear strain for every individual sample is greater than that for the regional tensor average (Fig. 6b). On most of the strain plots, the regional

tensor average falls off of the trend defined by the local strain measurements. Note that the volume strain is similar for both the local and regional measurements. This is because volume stretch is a scalar quantity that is insensitive to orientation direction. Thus, tensor averaging will reduce the magnitude of distortional strain without affecting the volume stretch.

This finding highlights the important role that the scale of observation plays in the assessment of geologic deformation. Because deformation at one locality may be balanced by deformation at another locality, local samples will always show deformation of a greater magnitude than what has occurred at the regional scale. If the goal of structural analysis is gain insight into the regional tectonics, our results demonstrate that it is may be misleading to simply "scale up" local observations to a larger scale. When spatial variations in the geometry of deformation exist, it is necessary to integrate observations from a scale large enough to capture the bulk regional deformation. In general, the larger the volume of rock studied, the smaller the magnitude of the distortional component deformation.

Volume strain

The mass-transfer deformation in the Otago wedge displays both open-system and closed-system behavior on the scale of a hand sample. Some of the dissolved material is locally redeposited as fibrous overgrowth, but the bulk of the material (~20%) appears to have been transported out of the sample volume. All samples exhibit mass-loss deformation, and there is no obvious sink for this missing material (see Chapter 2).

We acknowledge this is an as-yet unresolved problem, but it is one common to subduction wedges, as large mass-loss strains have now been reported in many convergent wedge settings, including the Franciscan complex (Ring and Brandon, 1999), the San Juan-Cascade nappes (Feehan & Brandon, 1999), and the Helvetic wedge of Switzerland (Ring et al., 2001). The main paradox is that the solubility of quartz is relatively low (Manning 1994), and a tremendous amount of fluid is required to remove one-third of the original rock mass. One possible solution, suggested by Ring et al. (2001), invokes within-wedge fluid circulation. Fluids may repeatedly pass through the wedge, thus generating large net fluid fluxes with a limited amount of fluid. This type of fluid circulation is how other insoluable elements, such as gold, are consolidated.

The mass-transfer strains would be easier to understand if the solubility of quartz was higher. One possibility is that the organic acids bound up in sediments may significantly increase the solubility of silica (Hajash et al. 1998), thereby reducing the net fluid flux required to allow the observed mass-transfer strains.

Coaxial deformation and shear-coupling at the base of the wedge

Our strain results also have important implications regarding the strength of the boundary between the downgoing plate and the Torlesse wedge. The coaxial nature of the deformation, denoted from straight fibre overgrowth and the relatively small strain values both indicate that the shear coupling between the downgoing plate and the wedge was minimal. The coaxial deformation is also indicated by the fact that the orientation of the foliation does not change in different lithologies. If the coupling would be strong, shearing should be expected to accumulated in softer phyllosilicate-rich rocks. Thus, the schistosity should be rotated towards the shear plane, but this cannot be found in the Otago Schist. These observations are consistent with the findings of Deckert & Brandon (this volume), who use X-ray texture measurements of phyllosilicates to demonstrate that shear strain in the Otago wedge are small to account for a strong coupling between the subducted plate and the wedge. Thus, the observed deformation appears to be related to processes internal to the wedge rather than being imposed from below.

Conclusions

Our structural investigation of the exhumed Mesozoic Torlesse accretionary wedge reveals that significantly different views of deformation may be obtained by focusing on local versus regional deformation. Along the flanks of the Otago Schist, individual samples generally exhibit non-plane, mass-transfer volume loss strains, with minor extension in one principal direction and shortening in the other two principal directions. In contrast, the regional deformation is characterized by shortening in all directions, with the maximum shortening stretch generally much less than for individual samples. These results demonstrate that care must be taken when extrapolating local observations to understand deformation at a regional scale,

Deformation along the flanks of the Otago antiform was dominated by open-system pressure solution processes that led to a significant mass-loss volume stretch (S_v = 0.78). The coaxial nature of the deformation suggests that the coupling between the downgoing plate and the overlying convergent wedge too weak to drive simple-shear deformation in the wedge. Thus, deformation in the Otago wedge appears to result purely from within-wedge processes.

References

Bishop, D.G., 1972. Progressive metamorphism from prehnite-pumpellyite to greenschist facies in the Danseys Pass area, Otago, New Zealand. *Geological Society of America Bulletin* 83, 3177-3198.

Bishop, D. G. 1994. Extent and regional deformation of the Otago peneplain. *Institute of Geological & Nuclear Sciences Science Report* 94/1, 10 pp.

Bradshaw, J.D., Weaver, S.D., and Muir, R.J., 1996. Mid-Cretaceous oroclinal bending of New Zealand terranes. *New Zealand Journal of Geology and Geophysics* 39, 461-468.

Brandon, M.T., 1995. Analysis of geologic strain data in strain-magnitude space. *Journal of Structural Geology* 17, 1375-1385.

Breeding, C.M., and Ague, J.J., 2002. Slab-derived fluids and quartz-vein formation in an accretionary prism, Otago Schist, New Zealand. *Geology* 30, 499-502.

Coombs, D.S., Landis, C.A., Norris, R.J., Sinton, J.M., Bons, D.J., and Craw, D., 1976. The Dun Mountain Ophiolite Belt, New Zealand, its tectonic setting, constitution and origin, with special reference to the southern portion. *American Journal of Science* 276, 561-603.

Cox, S., 1991. Veins, Fluid, Fractals, Scale & Schist. Ph.D. thesis. University of Otago

Deckert, H., Ring, U., and Mortimer, N., 2002. Tectonic significance of Cretaceous bivergent extensional shear zones in the Torlesse accretionary wedge, central Otago Schist, New Zealand. *New Zealand Journal of Geology & Geophysics* 45, 537-547.

Deckert and Brandon (this volume)

Feehan, J.G., and Brandon, M.T., 1999. Contribution of ductile flow to exhumation of low-temperature, high-pressure metamorphic rocks: San Juan-Cascade nappes, NW Washington State. *Journal of Geophysical Research* 104, 10883-10902.

Forster, M.A., and Lister, G.S. 2003. Cretaceous metamorphic core complexes in the Otago Schist, New Zealand. *Australian Journal of Earth Sciences* 50, 181-198.

Hajash, A., Carpenter, T. D. & Dewers, T. A. 1998. Dissolution and time-dependent compaction of albite sand: experiments at 100ºC and 160ºC in pH-buffered organic acids and distilled water. *Tectonophysics* 295, 93-115.

Kamp, P. J. J. 1986. Late Cretaceous-Cenozoic tectonic development of the southwest Pacific region. *Tectonophysics* 121, 225-251.

Korsch, R. J. and Wellman, H. W. 1988. The geological evolution of New Zealand and the New Zealand region. In: *The Ocean Basins and Margins* (edited by Nairn, A. E. M., Stehli, F. G. & Uyeda, S.) 7B. Plenum Publishing Corporation, 411-482.

LeMasurier, W.E., and Landis, C.A., 1996. Mantle-plume activity recorded by low-relief erosion surfaces in West Antarctica and New Zealand. *Geological Society of America Bulletin* 108, 1450-1466.

Little, T.A., Mortimer, N., and McWilliams, M., 1999. An episodic Cretaceous cooling model for the Otago-Marlborough Schist, New Zealand, based on 40Ar/39Ar white mica ages. *New Zealand Journal of Geology & Geophysics* 42, 305-325.

MacKinnon, T. C., 1983. Origin of the Torlesse terrane and coeval rocks, South Island, New Zealand. *Geological Society of America Bulletin* 94, 967-985.

Manning, C. E. 1994. The solubility of quartz in H_2O in the lower crust and upper mantle. *Geochimica et Cosmochemica Acta* 58, 4831-4839.

Mortimer, N, 1993. Jurassic tectonic history of the Otago Schist, New Zealand. *Tectonics* 12, 237-244.

Mortimer, N. & Roser, B. P. 1992. Geochemical evidence for the position of the Caples-Torlese boundary in the Otago Schist, New Zealand. *J.Geol.Soc.London* 149, 967-977.

Mortimer, N., Tulloch, A.J., Spark, R.N., Walker, N.W., Ladley, E., Allibone, A., and Kimbrough, D.L., 1999. Overview of the Median Batholith, New Zealand: a new interpretation of the geology of the Median Tectonic Zone and adjacent rocks. *Journal of African Earth Sciences* 29, 257-268.

Mortimer, N., 2000. Metamorphic discontinuities in orogenic belts: example of the garnet-biottie-albite zone in the Otago Schist, New Zealand. *International Journal of Earth Science* 89, 295-306.

Mortimer, N., Davey, F.J., Melhuish, A., Yu, J., and Godfrey, N.J., 2002. Geological interpretation of a deep seismic reflection profile across the Eastern Province and Median Batholith, New Zealand: crustal architecture of an extended Phanerozoic convergent orogen. *New Zealand Journal of Geology and Geophysics* 45, 349-363.

Mortimer, N., 2003. Regional structure of the Otago Schist, New Zealand, from an isopach map of foliation. *American Journal of Science*, in press.

Norris, R.J., and Bishop, D.G., 1990. Deformed conglomerates and textural zones in the Otago Schists, South Island, New Zealand. *Tectonophysics* 174, 331-349.

Platt, J.P., 1986. Dynamics of orogenic wedges and the uplift of high-pressure metamorphic rocks. *Geological Society of America Bulletin* 97, 1037-1053.

Ramsay, J.G., and Wood, D.S., 1973. The geometric effects of volume change during deformation prcoesses. *Tectonophysics* 16, 263-277.

Ratschbacher, L., Frisch, W., Linzer, H.-G. & Merle, O. 1991. Lateral extrusion in the Eastern Alps, Part II: structural analysis. *Tectonics* 10(2), 257-271.

Ring, U., and Brandon, M.T., 1999. Ductile deformation and mass loss in the Franciscan Subduction Complex: implications for exhumation processes in accretionary wedges. In: Ring, U., Brandon, M.T., Lister, G.S., and Willett, S.D. (eds), Exhumation Processes: Normal Faulting, Ductile Flow and Erosion. Geological Society, London, Special Publications, 154, 55-86.

Ring, U., Brandon, M.T., and Ramthun, A., 2001. Solution-mass-transfer deformation adjacent to the Glarus thrust, with implications for the tectonic evolution of the Alphine wedge in eastern Switzerland. *Journal of Structural Geology* 23, 1491-1505.

Turnbull, I.M., Mortimer, N., and Craw, D., 2001. Textural zones in the Haast Schist – a reappraisal. *New Zealand Journal of Geology and Geophysics* 44, 171-183.

Wood, B.L., 1978. The Otago Schist megaculmination: Its possible origin and tectonic significance in the Rangitata Orogen of New Zealand. *Tectonophysics* 47, 339-368.

Table 1: Absolute strain and volume strain

	Max..Extension			Intermed. Extension			Max. Shortening					
Sample	tr.	pl.	Sx	tr.	pl.	Sy	tr.	pl.	Sz	Sv	NZ North	NZ East
0T19-2-1	121	58	1	298	32	0.99	29	1	0.53	0.52	5632800	2249100
0T19-2-3	134	71	1.02	330	19	0.878	238	5	0.55	0.49	5632800	2250100
0C8-3-2b	234	60	1.1	331	5	1	62	30	0.62	0.68	5562100	2158300
0C19-3-1	20	33	1.03	112	4	0.931	209	57	0.64	0.61	5491400	2186900
0C21-3-1	52	69	1.04	216	20	0.902	308	5	0.80	0.75	5534100	2138700
0C22-3-1a	2	16	1.05	92	2	0.924	188	74	0.92	0.89	5509400	2152100
0C22-3-2a	23	58	1.01	194	31	1	286	4	0.75	0.75	5506800	2151700
Ca98-91	182	12	1.02	86	26	0.674	294	61	0.46	0.31	5455700	2293300
Ca98-92	186	25	1.02	69	45	1	295	35	0.69	0.7	5455700	2293300
BB99-51	348	22	1.01	250	19	1	123	60	0.71	0.71	5442500	2286800
BB99-52	131	1	1.02	41	40	0.86	223	50	0.66	0.58	5444900	2289300
2C-1	65	36	1.02	164	12	1	270	51	0.84	0.85	5483600	2162000
2C-6	25	7	1.05	122	43	1	288	46	0.81	0.85	5492600	2158500
P61686	103	29	1	197	7	0.968	300	60	0.86	0.84	5455200	2219900
BB99-53	262	4	1.03	171	19	1	6	70	0.78	0.8	5447200	2291400
AW-1-1	162	21	1.02	261	22	0.951	34	59	0.89	0.86	5510320	2147924
AW1-2	159	8	1.01	271	69	1	66	19	0.86	0.87	5510320	2147924
AW2-1	318	25	1.03	192	52	1	61	27	0.89	0.91	5510146	2148129
AW2-3	104	8	1.02	11	22	0.991	213	62	0.88	0.89	5510146	2148129
AW3-1	355	76	1.02	112	6	0.963	203	12	0.90	0.89	5528789	2159828
AW4-1	17	27	1.05	123	29	1	252	48	0.88	0.92	5507393	2163705
AW4-2	15	27	1.06	149	54	1	273	22	0.87	0.93	5507393	2163705
AW5-1	30	27	1.02	285	27	1	157	50	0.93	0.94	5512170	2156842
AW5-2	12	27	1.01	135	46	1	264	31	0.87	0.88	5512170	2156842
AW6-1	105	29	1.1	357	30	1	230	46	0.81	0.89	5513966	2159357
AW6-2	351	38	1.07	151	50	0.989	253	10	0.85	0.9	5513966	2159357
AW7-1	167	20	1.08	73	12	1	314	67	0.77	0.84	5511909	2167045
AW7-3	158	9	1.08	62	31	0.972	262	57	0.76	0.79	5511909	2167045
AW7-4	156	16	1.07	61	17	0.995	285	66	0.75	0.8	5511909	2167045
AW7-5	158	25	1.05	253	10	1	2	63	0.72	0.75	5511909	2167045
LP99/20	305	76	1	103	13	0.88	194	5	0.78	0.69	5629300	2252200
NZ97-1	66	49	1.02	208	34	0.997	312	20	0.81	0.83	5796766	2394824
NZ97-3	324	53	1.19	147	37	0.956	56	2	0.84	0.96	5514175	2159445
NZ97-5	254	42	1.22	3	20	0.877	111	41	0.87	0.93	5692400	2284100
NZ97-15	169	23	1.08	263	9	0.955	12	65	0.80	0.83	5469550	2246763
NZ97-16	51	46	1.22	305	15	0.975	202	40	0.65	0.78	5439000	2258500
NZ97-17	20	15	1.05	190	75	0.838	109	2	0.68	0.6	5438600	2261200
000301-1A	17	17	1.04	122	41	0.976	268	44	0.91	0.93	5463053	2237720
000301-1B	7	34	1.05	130	39	0.958	251	33	0.83	0.84	5463053	2237720
000303-1	345	70	1.04	204	16	0.878	111	12	0.77	0.7	5659502	2252845
000303-4	296	86	1.09	206	0	0.958	116	4	0.81	0.85	5659502	2252845
000304-2	158	30	1.05	338	60	1	248	0	0.89	0.93	5675419	2254999
000304-4	340	58	1.02	185	30	1	88	11	0.79	0.81	5675663	2254685
000304-5	347	35	1.07	155	54	0.905	253	6	0.80	0.77	5610642	2332314
000305-4	52	62	1.07	185	20	0.94	282	19	0.73	0.74	5654009	2277780
000305-5	52	72	1.06	176	10	0.92	269	14	0.74	0.72	5654009	2277780
000305-7	28	55	1.07	168	28	0.877	268	19	0.83	0.78	5654009	2277780
000307-4	108	44	1.01	15	3	0.945	282	46	0.90	0.86	5623708	2287006
010309-4	91	67	1.05	320	16	1	225	17	0.79	0.83	5588233	2265302
99311-1	159	28	1.03	68	1	0.906	336	62	0.78	0.73	5621894	2286297

Table 1 continued

	Max..Extension			Intermed. Extension			Max. Shortening					
Sample	tr.	pl.	Sx	tr.	pl.	Sy	tr.	pl.	Sz	Sv	NZ North	NZ East
99311-6	104	76	1.05	284	14	1	194	0	0.77	0.8	5634082	2269935
99312-1	283	61	1.03	21	4	0.961	113	29	0.89	0.88	5628955	2254526
99319-6	333	50	1.04	203	28	0.98	98	26	0.82	0.84	5482217	2240011
99320-5	185	1	1.04	93	61	0.89	275	29	0.88	0.82	5454820	2265341
Tensor avger.	**349**	**4**	**0.95**	**87**	**65**	**0.94**	**258**	**25**	**0.87**	**0.78**		

Geochemical fractionation and volume strain in pressure solved sandstones

Hagen Deckert[a], Mark T. Brandon[b], Uwe Ring[a], Jeffrey Rahl[b]

[a] Institut für Geowissenschaften, Johannes Gutenberg-Universität, Becherweg 21, 55099 Mainz, Germany
[b] Kline Geology Laboratory, Yale University, P.O. Box 208109, 210 Whitney Avenue, New Haven, CT 06520-8109, U.S.A

To be submitted to *Geology*.

Abstract

Geochemical fractionation and regional mass transfer of silica are explored by comparing volume strain and geochemical compositions of 47 metamorphosed sandstones from the Mesozoic Torlesse accretionary wedge, New Zealand. Published absolute strain measurements show that pressure solution processes in the low-grade samples caused 4 to 69% loss of silica. Adding those volume losses to the respective geochemical composition of deformed and metamorphosed sandstones, it is possible to determine the protolith composition for the rocks. The correlation of Al_2O_3, MgO, and TiO_2 with SiO_2 in the backcalculated protolith compositions shows that the rocks were already chemically fractionated by sedimentary sorting. Zr is used to evaluate regional mass transfer of silica on the base of geochemical fractionation. Chemical inhomogeneities between hand scale samples are suppressed by using average outcrop values. Zr/SiO_2 ratios in outcrops of lowest-grade rocks show a well-defined regression line defined by c. 20% silica loss. Chemical compositions of high-grade zones differ from this reference line relative to the amount of volume change in the outcrops. High-grade zones are characterised by a loss of 15% silica. A removal of the dissolved material out of the wedge seems likely because of missing sinks for the dissolved silica.

Introduction

Many geochemical and strain studies found evidence for large amounts of deformation-related volume change in accretionary wedges, fold-and-thrust belts, and shear zones (Breeding & Ague 2002, Newman & Mitra 1993, Ring 1996, Ring et al. 2001, Steyrer & Sturm 2002). Volume strain, S_V, can have three different sources (Fig. 1). (1) Loss of porosity, e.g. during compaction (Bray & Karig 1985, Paterson et al. 1995) and (2) change in grain density during mineral phase transitions (Austrheim et al. 1997). Here we focus on a third possibility for volume strain, the change of mass due to dissolution processes (Ramsay & Wood 1973, Ring & Brandon 1999, Ring et al. 2001, Wright & Henderson 1992). This implies open-system mass transfer causing fractionation of the residual rock during dissolution. Different components will have different solubilities and thus the rock becomes depleted in the more soluble components such as silica and enriched in the more insoluble components such as Mg, Ti, Al, and Zr. The chemical composition of the altered rock can be used to estimate volume strain. However, it has to be shown that the geochemical fractionation was caused by mass change and not by sedimentary sorting processes or different source areas, i.e. the protolith reference frame needs to be rigorously established.

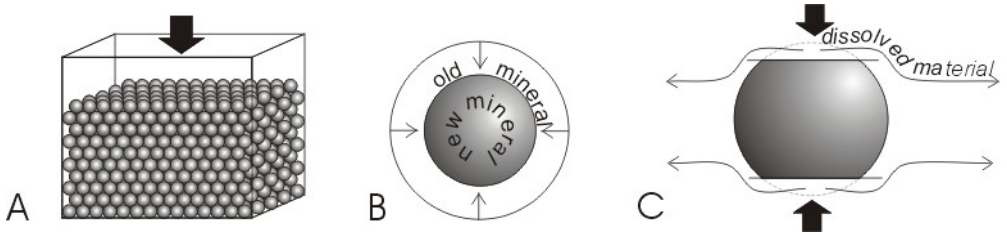

Fig. 1. Three different sources of volume strain. A) Compaction. B) Density change. C) Volume loss due to dissolution processes. In contrast to compaction and density change, dissolution causes also a mass change in the analysed rocks.

In a study of metamorphosed sandstones in the Torlesse accretionary wedge, New Zealand, Breeding & Ague (2002) tried to reconcile observed geochemical fractionation processes with volume change. Their results indicate systematic regional scale variations in average outcrop compositions, that they attributed to addition or removal of silica from a protolith with a specific geochemical composition. The hitch in this approach is the definition of the protolith to which measured compositions can be compared to. The protolith issue is the general problem of geochemical methods for quantifying volume strain and also constraining the provenance of deformed and metamorphosed rocks.

In this paper we present a conceptional overview on how to analyse geochemical fractionation processes using new geochemical data from rocks with known volume strain. We examine the fractionation problem by looking at the residual enrichment of trace elements

and by studying systematic changes of major and trace elements as a function of mass transfer strain. Rahl et al. (2003) report absolute strain data and thus volume strains from those samples. With this independent information we attempt to find the protolith composition and dissolution component (Fig. 2). The determination of the protolith enables to recognise possible variations in the original composition of the rocks that may conceal any systematic chemical fractionation. Moreover, with known protolith compositions measured chemical element ratios can be used to evaluate regional mass transfer in the Torlesse accretionary wedge.

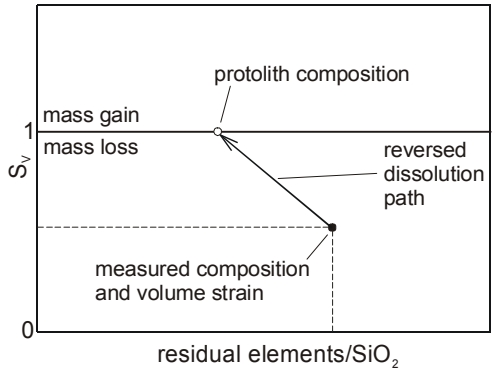

Fig. 2. Determination of protolith composition. The amount of silica that was lost during pressure solution processes, known from the study of Rahl et al. (2003), is added to the current geochemical composition along the dissolution path. Protolith compositions are characterised by lower residual elements versus SiO2 ratios.

Tectonic setting and previous work

To tackle the problem of geochemical fractionation we focus on the Torlesse accretionary wedge, New Zealand, that was already the target of volume strain studies by Rahl et al. (2003) and Breeding & Ague (2002). The Torlesse accretionary wedge formed during subduction of the Pacific plate underneath the eastern Gondwana margin between the Permian and the Late Cretaceous (Korsch & Wellman 1988, MacKinnon 1983, Mortimer & Tulloch 1996). It consists of the Caples and Torlesse metasedimentary units that comprise monotonous series of sandstones and mudstones. Geochemical differences between both terranes suggest spatially separated source areas (Mortimer & Roser 1992, Roser et al. 1993). Based on meso- and microstructural changes in the metasedimentary rocks the monotonous rocks are subdivided into four different textural zones (TZ) (Bishop 1972a, Hutton & Turner 1936, Turnbull et al. 2001). In this study we only distinguish between low-grade textural zones, comprising TZ 1 and 2, and high-grade textural zones consisting of TZ 3 and 4. Low-grade rocks are weakly foliated and contain hardly any veins. High-grade rocks are well foliated and characterised by 15-33% veins (Breeding & Ague 2002). Metamorphic conditions range from prehnite-pumpellyite facies to greenschist facies with peak

metamorphic temperatures and pressures of 350-400°C and 8-10 kbar in high-grade rocks (Mortimer 2000, Turnbull 2000).

Two approaches were used to analyse volume change in the Torlesse wedge. Rahl et al. (2003) measured absolute finite strain in pressure solved low-grade metasandstones from the Torlesse and Caples terranes. This work shows that only a minor part of the dissolved material is precipitated in-situ as fibre overgrowth, while most of the silica left the rock. Volume loss in the samples ranges between 4 to 69% with an average of c. 20% (Table 1). The geochemical study of Breeding & Ague (2002) used systematic regional differences in outcrop Zr/SiO_2 ratios to estimate volume change and mass transfer in the Torlesse wedge. In their study, ~25 samples per outcrop were analysed, whereas high-grade rocks also include vein material. Most of the individual specimens have different Zr/SiO_2 compositions (Breeding & Ague (2002) data rep.). Those local variations were suppressed by calculating an average outcrop composition. Averages of Zr and SiO_2 values of TZ1 outcrops show a positive correlation along a well-defined trend line (Fig. 3). This compositional trend is

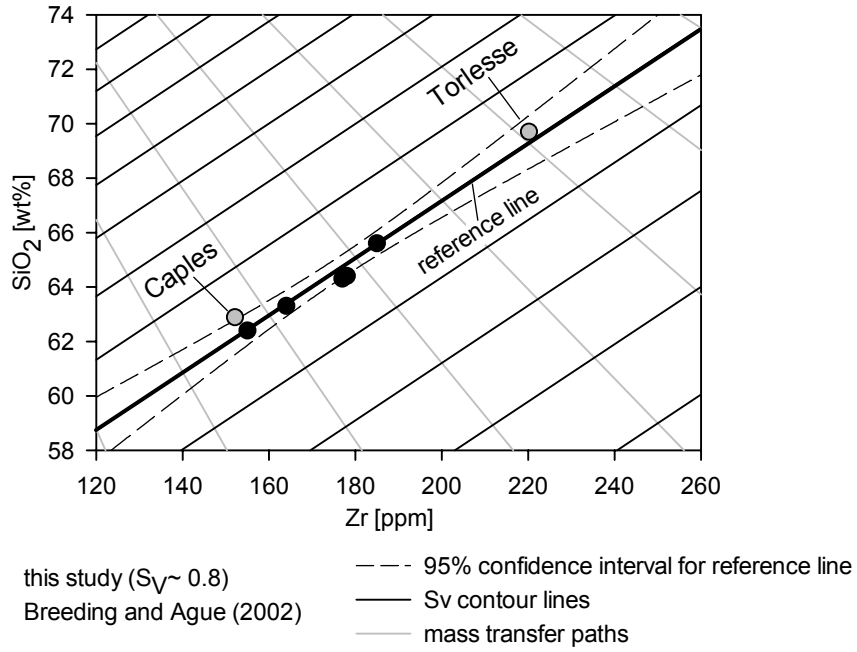

Fig. 3. Zr/SiO_2 averages of TZ 1 outcrops plot on a well-defined trend line, to which Breeding & Ague (2002) attributed a protolith composition with no volume change (i.e. S_V = 1); note that Caples and Torlesse TZ 1 averages analysed in this study plot along this reference line. Rahl et al (2003) determined a volume strain of S_V = 0.8 for those rocks. Contour lines mark compositions with equal amounts of volume strain. Negatively sloped mass transfer paths indicate how given compositions vary with changing amount of silica.

thought to be the result of sedimentary sorting processes that led to different proportions of psammite and pelite in a single outcrop. Breeding & Ague (2002) argued that this trend line represents the protolith composition where samples experienced no volume change (i.e. S_V=1). Addition or loss of silica results in negatively sloped compositional trajectories at high

angles to the protolith array (Fig. 3) (Ague 1994, Breeding & Ague 2002). Mass changes in higher-grade zones were calculated by the deviation of the outcrop Zr/SiO2 ratios from the protolith line. This made Breeding & Ague (2002) come to the conclusion that externally derived silica in quartz veins is responsible for a mass addition of c. 11% in high-grade textural zones.

Geochemistry and volume strain

To examine chemical fractionation entailed by volume strain, we use 47 samples of the Rahl et al.(2003) study with known volume strain and analysed them for their geochemical composition. Major and trace elements were quantitatively determined by XRF measurements (Table 1). TiO_2, MgO, and Al_2O_3 are considered immobile elements (Ague 1994) and show negative correlation with SiO_2 (Fig. 4) (see also Breeding & Ague (2002)). The negative correlation may be attributed to two different processes: (1) Certain elements may be separated into different grain size fractions as a result of sedimentary sorting mechanisms. This process is commonly used to explain the accumulation of Al, Mg, and Fe in pelitic rocks (Ague 1997, Moss et al. 1995). (2) Metasomatic SiO_2 mobilisation by dissolution processes results in a loss of initial rock mass, leading to a residual enrichment of immobile elements depending on relative mineral solubilities (Ague 1994, Ague 1997, Roser & Korsch 1999).

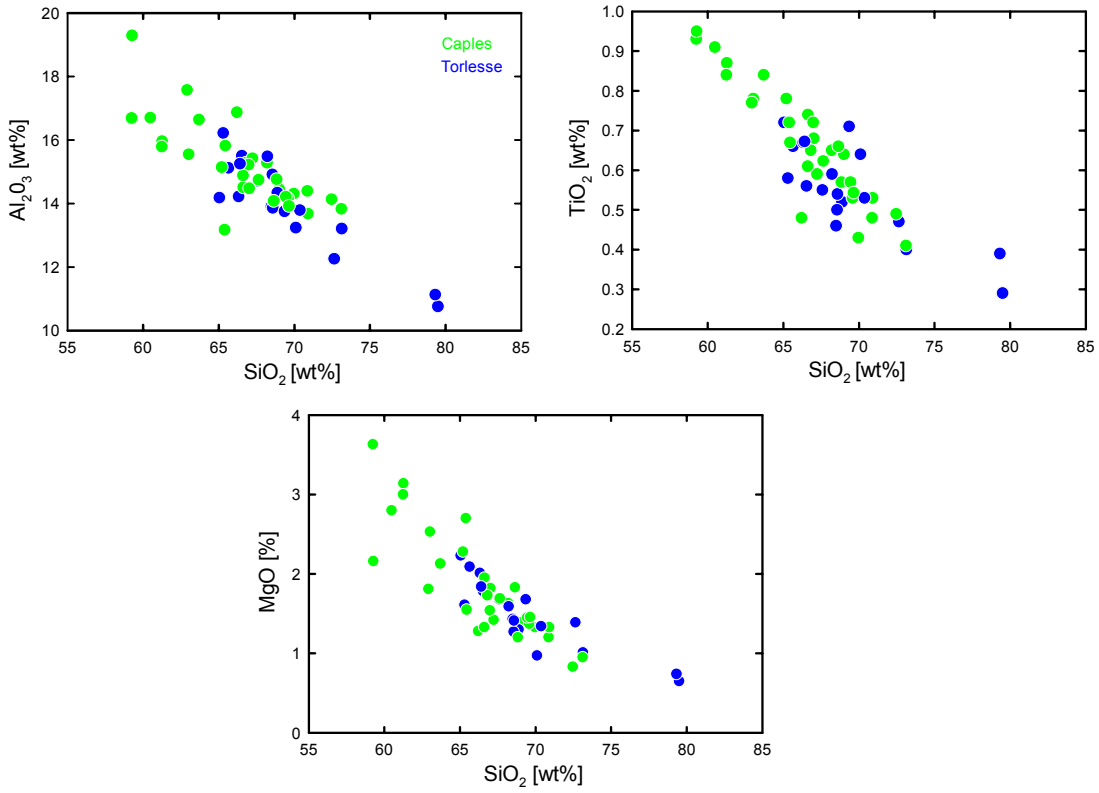

Fig. 4. Residual elements versus SiO_2 for Caples and Torlesse hand samples. Al_2O_3, TiO_2, and MgO correlate negatively with SiO_2.

A systematic relation of residual enrichment of TiO_2, MgO, and Al_2O_3 with volume loss is not apparent (Fig. 5). This may be due to the fact that the protolith is unknown. Compositional variations of protoliths caused by sedimentary sorting may obscure a relation to volume strain (see above), which is also indicated by the lack of correlation between volume strain and the amount of silica in single samples (Fig. 5). However, also different grain size might be responsible for different amounts of volume strain because pressure solution is a grain size sensitive deformation mechanism (Spiers et al. 1990).

The Zr-SiO_2 diagram can be used to address the problem that sedimentary sorting obscures fractionation effects caused by mass change, because Zr is basically stored in zircon. Zircon accumulates in coarse grained quartz-rich sediments (Ague 1997, Moss et al. 1995) but is nearly insoluble in common metamorphic fluids (Ague 1994, Ayers & Watson 1991). The differences in sedimentary sorting processes and dissolution behaviour makes Zr ideal for monitoring mass changes in pressure solved rocks.

Our results for hand samples show a vast scatter of Zr/SiO_2 ratios without any visible relationship to volume strain (Fig. 6). However, this is similar to Zr/SiO_2 ratios of hand specimens analysed by Breeding & Ague (2002). We did not measure enough samples in single outcrops to determine outcrop averages, but averages of all Caples and of all Torlesse samples plot within the 95% confidence level of the trend line defined by TZ 1 outcrop averages of Breeding & Ague (2002) (Fig. 3). The variation of average compositions in

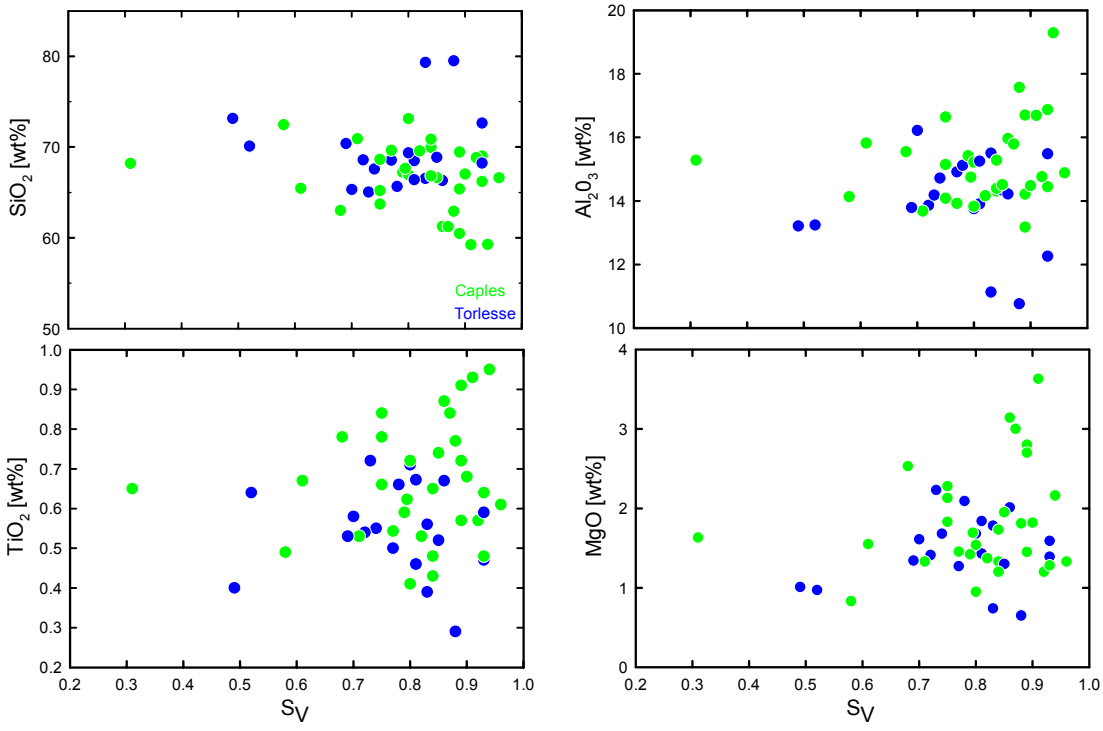

Fig. 5. Residual elements and SiO_2 versus volume strain. Element fractions and volume strain do not correlate in hand samples.

Torlesse and Caples sandstones can be explained by sedimentologic differences; Torlesse sandstones are more mature and therefore have higher amounts of Zr and SiO_2 compared to Caples sandstones, which had shorter sedimentary transport (Mortimer & Roser 1992).

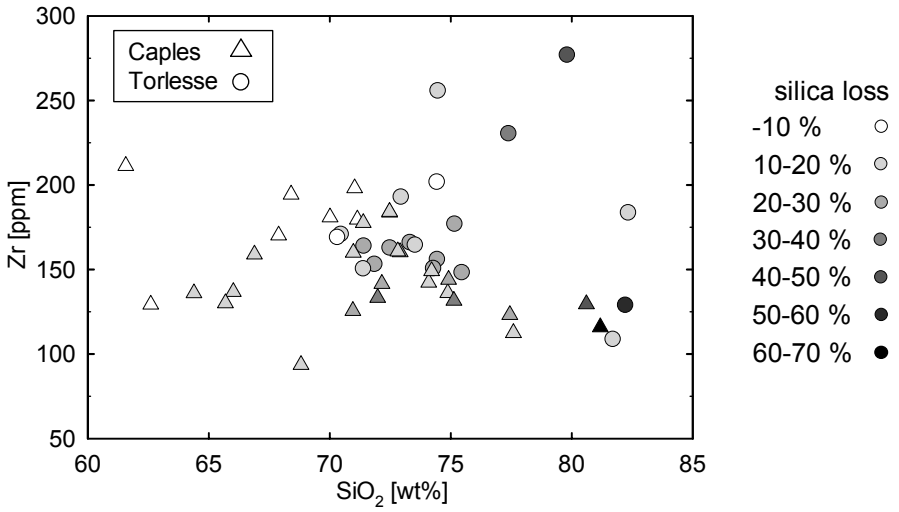

Fig. 6. Zr versus SiO_2 plot for hand samples. In contrast to outcrop averages discussed in Breeding & Ague (2002), there is no correlation of Zr/SiO_2 ratios with volume strain in hand specimens.

The difference in correlation of Zr and SiO_2 between hand samples and outcrop averages may result from the fact that a hand specimen is not big enough to be representative for a whole outcrop. Due to inhomogeneities the number of zircon grains may vary strongly between single samples and therefore produce an artificial scattering of data points. Al_2O_3, TiO_2, and MgO values of single samples show a positive correlation with SiO_2 suggesting that sedimentary sorting or different source regions are not responsible for the scatter in Zr versus SiO_2 data.

What is the protolith?

To estimate regional mass transfer, Breeding & Ague (2002) assumed that deformed and metamorphosed TZ 1 rocks in the Otago Schist did not undergo any mass changes and thus represent the protolith. If so, volume change can be estimated by the deviation of any analysed outcrop Zr/SiO_2 ratio from the reference protolith array that is defined by the compositions of low-grade textural outcrops (Fig. 3). However, the results of Rahl et al. (2003) show that low-grade rocks underwent pressure solution deformation and volume loss. Therefore, they cannot be regarded as protolith.

For determining the protolith we use a combination of our geochemical analyses and the corresponding volume strain data from Rahl et al. (2003). We follow Rahl et al. (2003)

who concluded that loss of silica caused the volume loss. This seems reasonable because of the relatively high solubility of SiO_2 in rocks under low-grade metamorphic conditions. In addition, except Al_2O_3, all other elements are not abundant enough to account for the measured volume strains in the examined sandstones. The positive correlation of Al_2O_3 and TiO_2 let infer that neither Al_2O_3 nor TiO_2 are dissolved, otherwise one of these elements would be residually enriched and Al_2O_3 versus TiO_2 ratios should show a negative correlation (Fig. 7). To backcalculate the protolith, volume loss is reversed by adding the amount of silica to the geochemical analysis that corresponds to volume strain (Table 2) (Fig. 2).

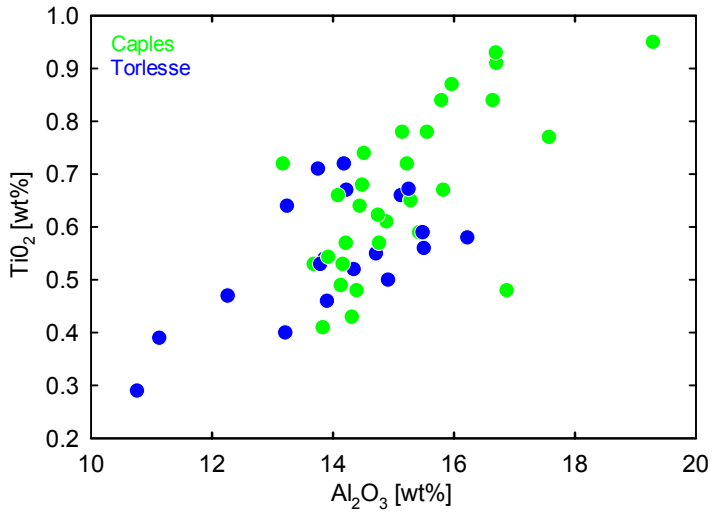

Fig. 7. Al_2O_3 versus TiO_2 plot of hand specimens. The positive correlation suggests that neither of the two residual elements were dissolved, otherwise one of the elements would be residually enriched causing a negative correlation.

Discussion

Two questions will be addressed: (1) Which geochemical fractionation processes affected the metamorphosed sandstones in the Torlesse accretionary wedge? (2) Is it possible to estimate regional mass transfer based on differences in geochemical compositions in the Torlesse wedge?

Geochemical fractionation

We have shown how volume strain affected the geochemical composition of the examined sandstones. SiO_2 was depleted while TiO_2, MgO, Al_2O_3, and Zr were residually enriched. The calculation of the protolith can be used to examine sedimentary sorting and whether the samples derived from the same source region. As Mortimer & Roser (1992) showed geochemical differences between Caples and Torlesse rocks, we distinguish between the two terranes. Reversing the effect of volume loss demonstrates that sedimentary sorting already

caused a geochemical fractionation of the sediments. TiO_2, MgO, and Al_2O_3 depict a negative correlation with SiO_2 in the protolith (Fig. 8). If only post-depositional metasomatism was responsible for fractionation, protolith compositions of single samples should plot in two points that represent the Caples and Torlesse terrane. The sedimentary fractionation in the protoliths is the reason for the obscured relationship between residual elements and volume strain (Fig. 5). The well-defined correlation between MgO, TiO_2 and Al_2O_3 with SiO_2 suggests that the protolith compositions within each of the two terranes were not influenced by different sources, otherwise data points should display a stronger scatter. This is a surprising result because single samples are derived from an area that comprises several thousands of square kilometres.

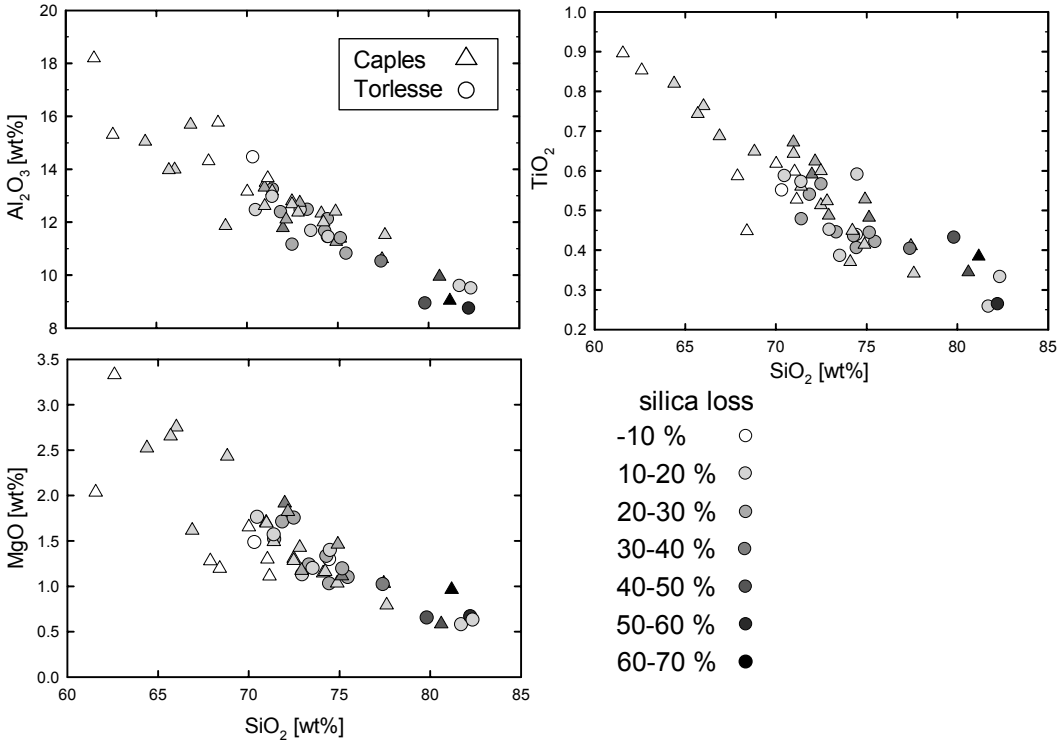

Fig. 8. Residual elements versus SiO_2 in protolith Caples and Torlesse hand samples. Despite the removal of volume loss residual elements still show a negative correlation with SiO_2. This implies that sedimentary sorting processes already fractionated the protolith before deformation-related volume strain became active.

We note that our backcalculated average protolith for the Caples and Torlesse rocks agree with the general composition of an active continental margin sandstone (e.g. Mortimer & Roser, 1992). This also suggests that our method of backcalculating the protolith chemistry is reasonable, because Caples and Torlesse are both assumed to be derived from an active margin (Mortimer & Roser 1992). The compositional variations between single hand samples is comparable to what can be expected in sandstones. The range of compositions is larger in

Caples rocks than in Torlesse rocks probably because Torlesse sandstones have higher maturity due to longer transport (Fig. 8).

Mass transfer in the Torlesse wedge

Breeding & Ague (2002) used systematic deviations of Zr/SiO_2 ratios from a compositional reference line to estimate regional volume changes. Average Zr/SiO_2 compositions for low-grade Torlesse and Caples rocks analysed in this study plot long this reference line (Fig. 3). However, in contrast to Breeding & Ague (2002) we attribute a volume strain of $S_V = 0.8$ to the TZ 1 reference line (instead of $S_V = 1.0$ as done by Breeding & Ague (2002)) (Fig. 9). Regional mass change can now be estimated using average outcrop compositions (Fig. 9).

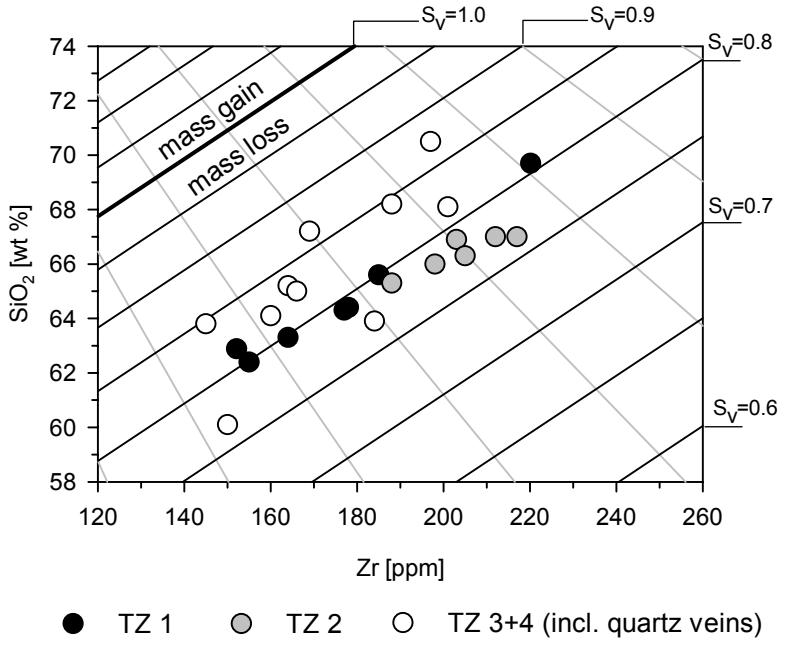

Fig. 9. Zr versus SiO_2 diagram for average compositions combining results of Breeding & Ague (2002) and this study. The reference line defined by compositions of low-grade outcrops is specified with a volume strain $S_V = 0.8$ (Rahl et al. 2003). This enables to determine volume strain in higher-grade outcrops that show volume loss of up to 15%.

The new specification of the geochemical reference line has significant consequences for mass transfer within the Torlesse accretionary wedge. Breeding & Ague (2002) assumed outcrop mass gains in TZ 3 and 4 rocks of up to 11%, which are thought to be derived from the subducted slab. Our recalculation, instead, indicate mass loss for those rocks of 9% to 15% (Fig. 9). This result is in line with other volume strain studies, which all demonstrate considerable volume loss in accretionary wedges (Feehan & Brandon 1999, Ring & Brandon 1999, Ring et al. 2001).

This result shows decreasing silica loss from lower- to higher-grade rocks. This may have two different reasons: (1) Rocks from all textural zones experienced the same initial deformation history and lost c. 20% of their initial volume at an early stage of deformation. Subsequently, the high-grade rocks were buried to greater depth and underwent mass addition of c. 5% from an external source. (2) High-grade rocks had a different deformation and accretion history than the low-grade rocks. Volume loss in low-grade rocks occurred at relatively shallow levels where there was still a reasonable amount of transient porosity. Furthermore, decomposition of organic materials may have produced organic acids which enhanced silica solubility (Hajash et al. 1998). Therefore, the ability of fluids to move through the rock combined with the presence of more corrosive pore fluids caused the high volume loss. Higher-grade textural rocks show evidence of both pressure-solution and intracrystalline deformation. Increased burial may have reduced porosity. As a result the dissolved material could not completely be removed and may largely be precipitated in local veins. The amount of veins combined with a total mass loss of c. 15% suggests that the material next to the veins has even suffered higher volume strain.

Fluids are assumed to dissolve silica in a direction of increasing temperatures while they tend to precipitate quartz as temperature decreases (Ague 1994, Ferry & Dipple 1991, Manning 1994). In normal geothermal gradients as postulated for accretionary wedges (Barr & Dahlen 1989, Peacock 1996) silica saturated fluids should rise up to shallower depth where SiO_2 may precipitate. If so, the vein material in high grade textural zones was not derived from dissolved silica in low textural zones. This raises the question where all the dissolved material has gone. Sinks for the deposition do not exist in the Torlesse wedge. We envision that the dissolved material moved in an open-system mass transfer out of the accretionary wedge.

Conclusions

The combination of chemical analysis with published volume strain data reveals that geochemical fractionation of sandstones in the Torlesse wedge was initially achieved by sedimentary sorting followed by deformation-related loss of silica. Removing the effects of volume strain shows that protoliths for Caples and Torlesse sandstones have similar active margin source regions.

Absolute strain measurements in rocks of the Torlesse wedge indicate a volume loss of 20% in low-grade textural zones. This together with Zr/SiO_2 systematics allows to constrain volume change in the higher-grade rocks. Despite the high abundance of 15 to 33% veins, high-grade rocks lost up to 15% of their original mass. The decrease of mass loss in higher textural zones might be explained by a lower transient porosity that hinders as high mass

fluxes as in lower textural zones. The remaining of the dissolved material and transport mechanisms for this mass transfer are unclear. Possible sinks are unknown in the Torlesse wedge. A removal out of the accretionary wedge seems likely.

References

Ague, J. 1994. Mass transfer during Barrovian metamorphism of pelites, south-central Connecticut: Channelized fluid flow and the growth of staurolite and kyanite. *American Journal of Science* 294, 1061-1134.

Ague, J. 1997. Compositional variations in metamorphosed sediments of the Littelton Formation, New Hampshire: Discussion. *American Journal of Science* 297, 440-449.

Austrheim, H., Erambert, M. & Engvik, A. K. 1997. Processing of crust in the root of the Caledonian continental collision zone: the role of eclogitization. *Tectonophysics* 273, 129-253.

Ayers, J. C. & Watson, E. B. 1991. Solubility of apatite, monazite, zircon, and rutile in supercritical aqueous fluids with implications for subduction zone geochemistry. *Royal Society of London Philosophical Transactions* 335, 365-375.

Barr, T. D. & Dahlen, F. A. 1989. Brittle frictional mountain builiding: 2. Thermal structure and heat budget. *Journal of Geophysical Reserach* 94, 3923-3947.

Bishop, D. G. 1972a. Progressive metamorphism from prehnite-pumpellyite to greenschist facies in the Dansey Pass area, Otago, New Zealand. *Geological Society of America Bulletin* 83, 3177-3198.

Bray, C. J. & Karig, D. E. 1985. Porosity of sediments in accretionary prisms and some implications for dewatering processes. *Journal of Geophysical Research* 90, 768-778.

Breeding, C. M. & Ague, J. J. 2002. Slab-derived fluids and quartz-vein formation in an accretionary prism, Otago Schist, New Zealand. *Geology* 30, 499-502.

Feehan, J. G. & Brandon, M. T. 1999. Contribution of ductile flow to exhumation of low-temperature, high pressure metamorphic rocks: San Juan-Cascade nappes, NW Washington State. *Journal of Geophysical Research* 104, 10883-10902.

Ferry, J. M. & Dipple, G. M. 1991. Fluid flow, mineral reactions, and metasomatism. *Geology* 19, 211-214.

Hajash, A., Carpenter, T. D. & Dewers, T. A. 1998. Dissolution and time-dependent compaction of albite sand: experiments at 100ºC and 160ºC in pH-buffered organic acids and distilled water. *Tectonophysics* 295, 93-115.

Hutton, C. O. & Turner, F. J. 1936. Metamorphic zones in north-west Otago. *Transactions of the Royal Society of New Zealand* 65, 405-406.

Korsch, R. J. & Wellman, H. W. 1988. The geological evolution of New Zealand and the New Zealand region. In: *The Ocean Basins and Margins* (edited by Nairn, A. E. M., Stehli, F. G. & Uyeda, S.) 7B. Plenum Publishing Corporation, 411-482.

MacKinnon, T. C. 1983. Origin of the Torlesse terrane and coeval rocks, South Island, New Zealand. *Geol.Soc.Am.Bull.* 94, 967-985.

Manning, C. E. 1994. The solubility of quartz in H_2O in the lower crust and upper mantle. *Geochimica et Cosmochemica Acta* 58, 4831-4839.

Mortimer, N. 2000. Metamorphic discontinuities in orogenic belts: example of the garnet-biotite-albite zone in the Otago Schist, New Zealand. *International Journal of Earth Sciences* 89, 295-306.

Mortimer, N. & Roser, B. P. 1992. Geochemical evidence for the position of the Caples-Torlese boundary in the Otago Schist, New Zealand. *J.Geol.Soc.London* 149, 967-977.

Mortimer, N. & Tulloch, A. J. 1996. The Mesozoic basement of New Zealand. *Geol.Soc.Australia Extended Abstracts* 43, 391-400.

Moss, B. E., Haskin, L. A. & Dymek, R. F. 1995. Compositional variations in metamorphosed sediments of the Littelton Formation, New Hampshire, and the Carrabasset Formation, Maine, at sub-hand specimen, outcrop, and regional scales. *American Journal of Science* 295, 473-505.

Newman, J. & Mitra, G. 1993. Lateral variations in mylonite zone thickness as influenced by fluid-rock interactions, Linville Falls Fault, North Carolina. *Journal of Structural Geology* 15, 849-863.

Paterson, S. R., Yu, H. & Oertel, G. 1995. Primary and tectonic fabric intensities in mudrocks. *Tectonophysics* 247, 105-119.

Peacock, S. M. 1996. Thermal and Petrologic Structure of Subduction Zones. In: *Subduction - Top to Bottom* (edited by Bebout, G. E., Scholl, D. W., Kirby, S. H. & Platt, J. P.). *Geophysical Monograph* 96. American Geophysical Union, Washington, 119-133.

Rahl, J. M., Deckert, H., Brandon, M. T., Mortimer, N. & Ring, U. 2003. Regional mass-transfer deformation and three-dimensional flow in a Mesozoic subduction wedge, Otago, New Zealand. *Journal of Structural Geology* to be submitted.

Ramsay, J. G. & Wood, D. S. 1973. The geometric effects of volume change during deformation processes. *Tectonophysics* 16, 263-277.

Ring, U. 1996. Volume strain, strain type and flow path in a narrow shear zone. Geol. Rundsch. 86, 786–801. *Geologische Rundschau* 86, 786-801.

Ring, U. & Brandon, M. T. 1999. Ductile deformation and mass loss in the Franciscan subduction complex: implications for exhumation processes in accretionary wedges. In: *Exhumation Processes: Normal faulting, ductile flow and erosion.* (edited by Ring, U., Brandon, M. T., Lister, G. S. & Willett, S. D.) 154. Special Publications of the Geological Society, London, 55-86.

Ring, U., Brandon, M. T. & Ramthun, A. 2001. Solution-mass transfer deformation adjacent to the Glarus thrust with implications for the tectonic evolution of the Alpine wedge in eastern Switzerland. *Journal of Structural Geology* 23, 1491-1505.

Roser, B. P. & Korsch, R. J. 1999. Geochemical characterization, evolution and source of a Mesozoic accretionary wedge: the Torlesse terrane, New Zealand. *Geological Magazine* 136, 493-512.

Roser, B. P., Mortimer, N., Turnbull, I. M. & Landis, C. A. 1993. Geology and geochemistry of the Caples Terrane, Otago, New Zealand: compositional variations near a Permo-Triassic arc margin. In: *South Pacific Sedimentary Basins* (edited by Ballance, P. F.) Sedimentary Basins of the World, 2, 3-19.

Spiers, C. J., Schutjens, P. M., Brzesowsky, R. H., Liezenberg, J. L. & Zwart, H. J. 1990. Experimental determination of constitutive parameters governing creep of rocksalt by pressure solution. In: *Deformation Mechanisms, Rheology and Tectonics* (edited by Knipe, R. J. & Rutter, E. H.) 54. Geological Society of London Special Publication, 215-227.

Steyrer, H. P. & Sturm, R. 2002. Stability of zircon in a low-grade ultramylonite and its utility for chemical mass balancing: the shear zone at Miéville, Switzerland. *Chemical Geology* 187, 1-19.

Turnbull, I. M., Mortimer, N. & Craw, D. 2001. Textural zones in the Haast Schist - a reappraisal. *New Zealand Journal of Geology & Geophysics* 44, 171-183.

Turnbull, I. M. c. 2000. Geology of the Wakatipu area. Institute of Geological & Nuclear Sciences, Lower Hutt, New Zealand.

Wright, T. O. & Henderson, J. R. 1992. Volume loss during cleavage formation in the Meguma Group, Nova Scotia, Canada. *Journal of Structural Geology* 14, 281-290.

Table 1:XRF analyses

Sample	Sv*	SiO_2 [%]	Al_2O_3 [%]	CaO [%]	MgO [%]	Na_2O [%]	K_2O [%]	Fe_2O_3 [%]	MnO [%]	TiO_2 [%]	P_2O_5 [%]	LOI [%]	Sum [%]	Rb	Sr	Y	Zr	Nb	Ba
000301-1A	0.93	71.03	13.50	1.95	1.30	4.16	1.93	4.03	0.07	0.60	0.08	1.50	100.15	70	228	23	198	7	507
000301-1B	0.84	74.09	12.34	1.66	1.15	3.25	2.12	2.48	0.04	0.37	0.05	1.55	99.11	76	175	18	142	4	357
000303-1	0.70	73.31	12.48	1.91	1.24	2.91	2.00	2.87	0.04	0.45	0.13	1.65	98.98	88	685	15	166	7	528
000303-4	0.85	72.93	12.47	2.01	1.13	3.09	1.87	2.94	0.04	0.45	0.12	1.78	98.83	77	562	15	193	7	374
000304-2	0.93	74.42	11.46	1.85	1.30	3.13	2.34	3.21	0.05	0.44	0.08	1.31	99.59	79	325	16	202	6	498
000304-4	0.81	73.51	11.68	2.10	1.20	2.93	2.20	2.93	0.04	0.39	0.08	1.81	98.88	84	371	16	165	7	522
000304-5	0.77	74.42	12.12	1.67	1.03	3.67	1.92	2.62	0.06	0.41	0.11	1.54	99.57	63	231	15	156	7	548
000305-4	0.74	74.27	11.67	3.48	1.33	2.91	0.91	3.14	0.05	0.44	0.12	1.47	99.80	41	469	17	151	3	266
000305-5	0.72	75.45	10.83	3.98	1.10	2.85	0.51	3.02	0.05	0.42	0.10	1.56	99.86	23	572	13	148	3	166
000305-7	0.78	71.84	12.39	2.61	1.71	3.09	1.48	3.79	0.05	0.54	0.12	1.64	99.26	67	434	20	153	4	393
000307-4	0.86	70.45	12.47	2.34	1.76	3.04	1.88	4.75	0.06	0.59	0.11	1.93	99.39	66	339	19	171	5	533
010309-4	0.83	71.39	13.25	2.01	1.52	3.33	2.07	3.55	0.06	0.48	0.13	1.71	99.50	80	454	21	164	6	497
99311-1	0.73	72.47	11.17	2.42	1.76	2.77	1.66	4.61	0.06	0.57	0.10	1.22	98.81	65	280	17	163	4	443
99311-6	0.80	74.46	11.46	1.71	1.40	3.00	0.95	3.98	0.07	0.59	0.10	1.75	99.47	43	209	21	256	7	233
99312-1	0.88	81.69	9.61	0.51	0.58	3.67	0.74	1.46	0.02	0.26	0.06	0.80	99.40	37	240	9	109	4	192
99319-6	0.84	74.88	12.41	0.61	1.03	3.81	2.38	2.73	0.03	0.41	0.07	1.34	99.71	83	108	12	136	4	403
99320-5	0.82	74.21	12.00	1.39	1.16	4.23	1.64	2.79	0.04	0.45	0.08	1.36	99.35	64	157	19	149	5	355
19-2-1	0.52	79.80	8.95	2.73	0.66	2.34	1.09	2.26	0.03	0.43	0.16	1.45	99.89	46	289	19	277	7	236
19-2-3	0.49	82.21	8.75	1.39	0.67	2.76	1.19	1.55	0.02	0.26	0.09	1.03	99.91	44	329	11	129	3	299
19-3-1	0.61	75.13	11.38	0.67	1.12	3.46	1.13	3.60	0.05	0.48	0.17	1.76	98.94	45	50	20	132	4	245
8-3-2b	0.68	71.98	11.78	2.81	1.92	3.08	1.41	4.48	0.08	0.59	0.14	1.44	99.70	52	360	13	133	3	345
22-3-2a	0.75	70.96	13.31	1.46	1.70	3.15	1.12	5.41	0.06	0.67	0.10	2.16	100.11	48	199	19	126	5	184
21-3-1	0.75	72.15	12.11	1.95	1.82	3.07	1.08	4.79	0.06	0.62	0.09	2.04	99.80	46	107	18	142	<2	212
22-3-1a	0.89	64.39	15.05	1.54	2.52	4.83	0.76	7.04	0.10	0.82	0.15	2.21	99.40	33	247	23	136	4	159
2C-6	0.85	70.97	12.62	1.38	1.70	3.49	1.16	5.02	0.07	0.64	0.09	1.96	99.09	48	207	23	160	4	223
CA 98-91	0.31	81.18	9.04	0.63	0.96	1.75	1.66	2.70	0.04	0.38	0.08	1.60	100.02	68	40	9	116	5	345
BB 99-51	0.71	77.44	10.60	0.84	1.03	2.77	1.30	3.05	0.33	0.41	0.05	2.05	99.89	53	82	18	123	4	266
BB 99-52	0.58	80.61	9.95	0.54	0.58	3.35	1.68	1.44	0.03	0.35	0.08	1.20	99.81	53	112	20	130	3	238
BB 99-53	0.80	77.59	11.53	0.36	0.79	3.72	2.17	1.83	0.03	0.34	0.06	1.08	99.48	76	93	10	113	6	363

Table 1 continued

Sample	Sv*	SiO2 [%]	Al2O3 [%]	CaO [%]	MgO [%]	Na2O [%]	K2O [%]	Fe2O3 [%]	MnO [%]	TiO2 [%]	P2O5 [%]	LOI [%]	Sum [%]	Rb	Sr	Y	Zr	Nb	Ba
AW 1-1	0.86	66.01	14.00	3.31	2.75	3.77	0.49	6.39	0.10	0.76	0.13	2.41	100.12	20	401	19	137	2	99
AW 1-2	0.87	65.69	13.97	3.35	2.65	3.91	0.52	6.19	0.10	0.74	0.13	2.52	99.80	22	350	17	130	<2	103
AW 2-1	0.91	62.60	15.31	2.97	3.33	3.62	1.10	7.32	0.10	0.85	0.13	2.75	100.09	44	207	23	129	4	185
AW 3-1	0.89	68.81	11.86	5.05	2.43	1.87	0.37	5.71	0.10	0.65	0.09	3.15	100.10	14	102	15	94	2	102
AW 4-1	0.92	71.14	13.67	1.70	1.11	4.05	2.07	3.29	0.06	0.53	0.07	1.71	99.40	80	166	20	180	5	523
AW 4-2	0.93	68.40	15.77	1.02	1.20	3.61	3.48	3.54	0.06	0.45	0.08	1.92	99.51	135	118	31	194	7	602
AW 5-1	0.94	61.57	18.20	1.37	2.04	3.37	2.83	6.74	0.10	0.90	0.16	2.78	100.05	123	142	52	211	8	452
AW 5-2	0.88	66.88	15.69	1.33	1.62	2.26	2.50	5.51	0.07	0.69	0.26	3.26	100.06	102	102	34	159	7	432
AW 6-1	0.89	72.47	12.80	1.98	1.31	3.65	2.18	3.49	0.06	0.51	0.08	1.49	100.02	84	140	24	184	5	489
AW 6-2	0.90	70.01	13.16	2.57	1.65	3.79	2.05	4.39	0.07	0.62	0.11	1.59	100.03	78	315	20	181	5	394
AW 7-1	0.84	71.39	13.17	1.14	1.49	4.27	1.89	3.86	0.07	0.56	0.08	1.59	99.51	67	200	18	178	6	428
AW 7-3	0.79	72.91	12.74	0.86	1.17	4.01	2.06	3.31	0.06	0.49	0.08	1.45	99.13	71	207	18	160	5	428
AW 7-4	0.80	72.48	12.68	1.43	1.28	4.33	1.63	3.88	0.07	0.60	0.08	1.42	99.88	55	306	18	184	6	343
AW 7-5	0.75	74.91	11.26	1.97	1.46	2.78	1.90	3.47	0.06	0.53	0.07	1.60	100.02	67	210	14	144	6	411
LP 99/20	0.69	77.37	10.53	1.54	1.02	2.75	1.92	2.67	0.04	0.40	0.09	1.15	99.49	69	357	18	231	5	471
NZ 97-1	0.83	82.32	9.51	0.81	0.63	3.13	1.04	1.38	0.02	0.33	0.07	0.85	100.11	44	297	14	184	3	270
NZ 97-3	0.96	67.88	14.31	1.99	1.28	4.02	2.41	4.22	0.06	0.59	0.10	2.12	98.97	84	245	21	170	6	423
NZ 97-5	0.93	70.30	14.47	1.63	1.49	2.66	2.57	3.47	0.07	0.55	0.12	2.10	99.43	124	391	23	169	9	499
Averages																			
total	0.79	72.82	12.37	1.84	1.43	3.31	1.65	3.76	0.06	0.52	0.10	1.74	99.60	64	260	19	161	5	353
Torlesse	0.77	75.14	11.40	2.04	1.20	3.00	1.57	3.01	0.05	0.44	0.11	1.49	99.45	63	380	17	177	5	387
Caples	0.81	71.37	12.97	1.72	1.57	3.50	1.69	4.23	0.07	0.57	0.10	1.90	99.70	64	185	20	151	5	332

Table 2: Geochemical composition normalised to S_V=1

Sample	Sv*	SiO_2 [%]	Al_2O_3 [%]	CaO [%]	MgO [%]	Na_2O [%]	K_2O [%]	Fe_2O_3 [%]	MnO [%]	TiO_2 [%]	P_2O_5 [%]	LOI [%]	Sum [%]	Rb	Sr	Y	Zr	Nb	Ba
000301-1A	0.93	71.03	13.50	1.95	1.30	4.16	1.93	4.03	0.07	0.60	0.08	1.50	100.15	70	228	23	198	7	507
000301-1B	0.84	74.09	12.34	1.66	1.15	3.25	2.12	2.48	0.04	0.37	0.05	1.55	99.11	76	175	18	142	4	357
000303-1	0.70	73.31	12.48	1.91	1.24	2.91	2.00	2.87	0.04	0.45	0.13	1.65	98.98	88	685	15	166	7	528
000303-4	0.85	72.93	12.47	2.01	1.13	3.09	1.87	2.94	0.04	0.45	0.12	1.78	98.83	77	562	15	193	7	374
000304-2	0.93	74.42	11.46	1.85	1.30	3.13	2.34	3.21	0.05	0.44	0.08	1.31	99.59	79	325	16	202	6	498
000304-4	0.81	73.51	11.68	2.10	1.20	2.93	2.20	2.93	0.04	0.39	0.08	1.81	98.88	84	371	16	165	7	522
000304-5	0.77	74.42	12.12	1.67	1.03	3.67	1.92	2.62	0.06	0.41	0.11	1.54	99.57	63	231	15	156	7	548
000305-4	0.74	74.27	11.67	3.48	1.33	2.91	0.91	3.14	0.05	0.44	0.12	1.47	99.80	41	469	17	151	3	266
000305-5	0.72	75.45	10.83	3.98	1.10	2.85	0.51	3.02	0.05	0.42	0.10	1.56	99.86	23	572	13	148	3	166
000305-7	0.78	71.84	12.39	2.61	1.71	3.09	1.48	3.79	0.05	0.54	0.12	1.64	99.26	67	434	20	153	4	393
000307-4	0.86	70.45	12.47	2.34	1.76	3.04	1.88	4.75	0.06	0.59	0.11	1.93	99.39	66	339	19	171	5	533
010309-4	0.83	71.39	13.25	2.01	1.52	3.33	2.07	3.55	0.06	0.48	0.13	1.71	99.50	80	454	21	164	6	497
99311-1	0.73	72.47	11.17	2.42	1.76	2.77	1.66	4.61	0.06	0.57	0.10	1.22	98.81	65	280	17	163	4	443
99311-6	0.80	74.46	11.46	1.71	1.40	3.00	0.95	3.98	0.07	0.59	0.10	1.75	99.47	43	209	21	256	7	233
99312-1	0.88	81.69	9.61	0.51	0.58	3.67	0.74	1.46	0.02	0.26	0.06	0.80	99.40	37	240	8.9	109	4	192
99319-6	0.84	74.88	12.41	0.61	1.03	3.81	2.38	2.73	0.03	0.41	0.07	1.34	99.71	83	108	12	136	4	403
99320-5	0.82	74.21	12.00	1.39	1.16	4.23	1.64	2.79	0.04	0.45	0.08	1.36	99.35	64	157	19	149	5	355
19-2-1	0.52	79.80	8.95	2.73	0.66	2.34	1.09	2.26	0.03	0.43	0.16	1.45	99.89	46	289	19	277	7	236
19-2-3	0.49	82.21	8.75	1.39	0.67	2.76	1.19	1.55	0.02	0.26	0.09	1.03	99.91	44	329	11	129	3	299
19-3-1	0.61	75.13	11.38	0.67	1.12	3.46	1.13	3.60	0.05	0.48	0.17	1.76	98.94	45	49.6	20	132	4	245
8-3-2b	0.68	71.98	11.78	2.81	1.92	3.08	1.41	4.48	0.08	0.59	0.14	1.44	99.70	52	360	13	133	3	345
22-3-2a	0.75	70.96	13.31	1.46	1.70	3.15	1.12	5.41	0.06	0.67	0.10	2.16	100.11	48	199	19	126	5	184
21-3-1	0.75	72.15	12.11	1.95	1.82	3.07	1.08	4.79	0.06	0.62	0.09	2.04	99.80	46	107	18	142	<2	212
22-3-1a	0.89	64.39	15.05	1.54	2.52	4.83	0.76	7.04	0.10	0.82	0.15	2.21	99.40	33	247	23	136	4	159
2C-6	0.85	70.97	12.62	1.38	1.70	3.49	1.16	5.02	0.07	0.64	0.09	1.96	99.09	48	207	23	160	4	223
CA 98-91	0.31	81.18	9.04	0.63	0.96	1.75	1.66	2.70	0.04	0.38	0.08	1.60	100.02	68	40.2	8.9	116	5	345
BB 99-51	0.71	77.44	10.60	0.84	1.03	2.77	1.30	3.05	0.33	0.41	0.05	2.05	99.89	53	82.2	18	123	4	266
BB 99-52	0.58	80.61	9.95	0.54	0.58	3.35	1.68	1.44	0.03	0.35	0.08	1.20	99.81	53	112	20	130	3	238
BB 99-53	0.80	77.59	11.53	0.36	0.79	3.72	2.17	1.83	0.03	0.34	0.06	1.08	99.48	76	92.5	10	113	6	363

Table 2 continued

Sample	Sv*	SiO2 [%]	Al2O3 [%]	CaO [%]	MgO [%]	Na2O [%]	K2O [%]	Fe2O3 [%]	MnO [%]	TiO2 [%]	P2O5 [%]	LOI [%]	Sum [%]	Rb	Sr	Y	Zr	Nb	Ba
AW 1-1	0.86	66.01	14.00	3.31	2.75	3.77	0.49	6.39	0.10	0.76	0.13	2.41	100.12	20	401	19	137	2	99.1
AW 1-2	0.87	65.69	13.97	3.35	2.65	3.91	0.52	6.19	0.10	0.74	0.13	2.52	99.80	22	350	17	130	<2	103
AW 2-1	0.91	62.60	15.31	2.97	3.33	3.62	1.10	7.32	0.10	0.85	0.13	2.75	100.09	44	207	23	129	4	185
AW 3-1	0.89	68.81	11.86	5.05	2.43	1.87	0.37	5.71	0.10	0.65	0.09	3.15	100.10	14	102	15	93.7	2	102
AW 4-1	0.92	71.14	13.67	1.70	1.11	4.05	2.07	3.29	0.06	0.53	0.07	1.71	99.40	80	166	20	180	5	523
AW 4-2	0.93	68.40	15.77	1.02	1.20	3.61	3.48	3.54	0.06	0.45	0.08	1.92	99.51	135	118	31	194	7	602
AW 5-1	0.94	61.57	18.20	1.37	2.04	3.37	2.83	6.74	0.10	0.90	0.16	2.78	100.05	123	142	52	211	8	452
AW 5-2	0.88	66.88	15.69	1.33	1.62	2.26	2.50	5.51	0.07	0.69	0.26	3.26	100.06	102	102	34	159	7	432
AW 6-1	0.89	72.47	12.80	1.98	1.31	3.65	2.18	3.49	0.06	0.51	0.08	1.49	100.02	84	140	24	184	5	489
AW 6-2	0.90	70.01	13.16	2.57	1.65	3.79	2.05	4.39	0.07	0.62	0.11	1.59	100.03	78	315	20	181	5	394
AW 7-1	0.84	71.39	13.17	1.14	1.49	4.27	1.89	3.86	0.07	0.56	0.08	1.59	99.51	67	200	18	178	6	428
AW 7-3	0.79	72.91	12.74	0.86	1.17	4.01	2.06	3.31	0.06	0.49	0.08	1.45	99.13	71	207	18	160	5	428
AW 7-4	0.80	72.48	12.68	1.43	1.28	4.33	1.63	3.88	0.07	0.60	0.08	1.42	99.88	55	306	18	184	6	343
AW 7-5	0.75	74.91	11.26	1.97	1.46	2.78	1.90	3.47	0.06	0.53	0.07	1.60	100.02	67	210	14	144	6	411
LP 99/20	0.69	77.37	10.53	1.54	1.02	2.75	1.92	2.67	0.04	0.40	0.09	1.15	99.49	69	357	18	231	5	471
NZ 97-1	0.83	82.32	9.51	0.81	0.63	3.13	1.04	1.38	0.02	0.33	0.07	0.85	100.11	44	297	14	184	3	270
NZ 97-3	0.96	67.88	14.31	1.99	1.28	4.02	2.41	4.22	0.06	0.59	0.10	2.12	98.97	84	245	21	170	6	423
NZ 97-5	0.93	70.30	14.47	1.63	1.49	2.66	2.57	3.47	0.07	0.55	0.12	2.10	99.43	124	391	23	169	9	499
Averages																			
total	0.79	72.82	12.37	1.84	1.43	3.31	1.65	3.76	0.06	0.52	0.10	1.74	99.60	64	260	19	161	5	353
Torlesse	0.77	75.14	11.40	2.04	1.20	3.00	1.57	3.01	0.05	0.44	0.11	1.49	99.45	63	380	17	177	5	387
Caples	0.81	71.37	12.97	1.72	1.57	3.50	1.69	4.23	0.07	0.57	0.10	1.90	99.70	64	185	20	151	5	332

Shear coupling at subduction zones – Implications from X-ray texture goniometry on phyllosilicate-rich rocks from the Torlesse subduction wedge, New Zealand

Hagen Deckert[a] & Mark T. Brandon[b]

[a] Institut für Geowissenschaften, Johannes Gutenberg-Universität, Becherweg 21, 55099 Mainz, Germany

[b] Kline Geology Laboratory, Yale University, P.O. Box 208109, 210 Whitney Avenue, New Haven, CT 06520-8109, U.S.A

This Chapter is identical to a manuscript submitted to the "Journal of Structural Geology" in April 2003 entitled "Shear coupling at subduction zones – Implications from X-ray texture goniometry on phyllosilicate-rich rocks from the Torlesse subduction wedge, New Zealand."

Abstract

The coupling between two converging plates in a subduction zone strongly influences the deformation within an accretionary wedge. How strong two plates might be actually coupled is still not specified. Finite deviatoric strain measurements obtained by X-ray texture goniometry in pelitic samples of the Torlesse subduction wedge, New Zealand, are used to evaluate the amount of shear strain recorded in the rocks that were exhumed from the base of the wedge after basal accretion. Shear strains range between $\gamma = 1.06$ and 3.16. We compare these values with theoretically expected shear strains, calculated by a simple geometric model that considers different plate convergence velocities and different exhumation rates. The model allows to comment on varying shear strains as a function of a coupling parameter α that may range between 0 for a decoupled and 1 for a fully coupled wedge. Maximum α value for the Torlesse is given with 0.15, clearly indicating a strong decoupling. Finite strains additionally suggest a regional plane strain deformation in the Torlesse with a strong vertical shortening component of 58% in the pelitic layers. No extension along the maximum stretching axis could be determined, suggesting that shortening was strongly compensated by volume loss along the maximum shortening axis.

Introduction

Accretionary wedges occur at subduction zones of two converging plates. The deformation and growths of the wedge is controlled by the flux of the accreted sediments and other crustal rocks into the wedge, either by frontal offscraping or by underplating. Moreover deformation and growth depend on the distribution of erosion on its surface (Brandon et al. 1998, England 1981), normal faulting in the upper parts (Platt 1986, Platt 1993) and ductile thinning within the deeper parts of the wedge, e.g. (Feehan & Brandon 1999, Ring & Brandon 1999, Selverstone 1985, Wallis et al. 1993) (Fig. 1). An additional important component that forces deformation, is the shear coupling between with the sediments of the subduction wedge and the down going plate (e.g., Moore 1979). This coupling is triggered by the shear stress that is transmitted across the subduction décollement. From the seismicity in subduction zones it is known, that most of the convergence occurs during large earthquakes by slip on the subduction thrust (e.g. Ruff & Kanamori, 1993). Nonetheless a certain amount of shear stress is transmitted across the subduction thrust and may be sufficient to drive flow within the more viscous part of the wedge where ductile deformation processes are active.

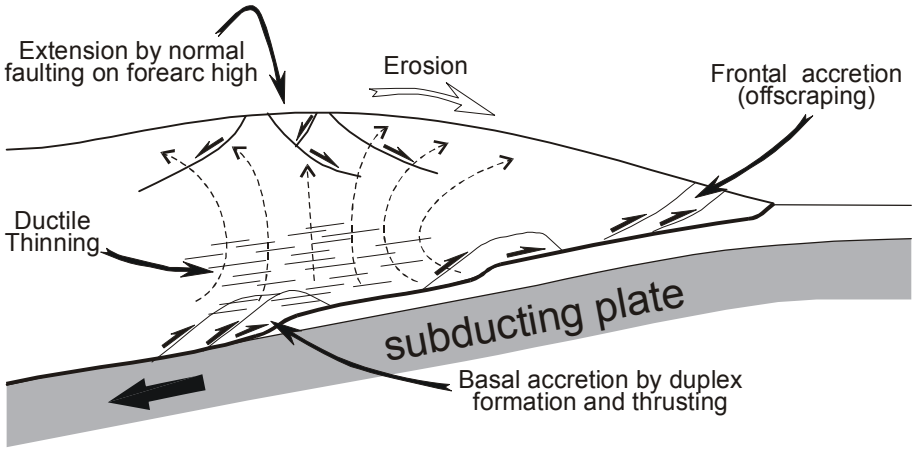

Fig. 1 Schematic cross section through an accretionary wedge (after (Feehan & Brandon 1999)). Deformation is controlled by flux of sediments in and out of the wedge.

A key question is, how much shear coupling occurs at typical subduction zone settings. The answer remains very difficult to constrain from both modern geophysical measurements and also from studies in ancient subduction zones. The focus of our paper is to use strain measurements from rocks exhumed from a large accretionary wedge to try to address this problem. As an example to study the shear coupling between two plates, we examine the Torlesse wedge in New Zealand's South Island, which represents a long-lived subduction wedge that formed above a south-westward-dipping subduction zone during Jurassic to Late Cretaceous convergence between the pacific oceanic plate and the east

Gondwana margin (Mortimer 2000) and references therein. The wedge grew in a fairly steady fashion accreting sedimentary materials and building outward , similar to the modern Barbados (lesser Antilles) or Makran (southern Iran) subduction wedges e.g. (Behrmann et al. 1988, Fisher & Hounslow 1990, Kukowski et al. 2001). The good preservation of the uplifted Otago Schist rocks, which have been barely effected by post-convergent deformation, provides the unique opportunity to get an insight in deformation processes operating within the deep interior of a subduction-related wedge.

We focus on strained rocks that are exposed in the Otago Schist uplift, which is interpreted as the former fore-arc high of the Torlesse wedge. These rocks represent the most deeply exhumed parts of the entire wedge setting coming from a depth of about 30 to 35 km (Mortimer 2000). The flat lying foliation in the Otago Schist suggests that these rocks were accreted by underplating in the deeper parts of the wedge (c.f. (Platt 1986, Platt 1993, Wallis et al. 1993)), implying that they traversed across the entire thickness of the subduction wedge and therefore should have integrated any coupling shear strain within the wedge during their ascent to the surface.

For strain determination in our samples we used a method called X-ray texture goniometry (XTG) which relates the preferred orientations of phyllosilicates to finite strains that have been recorded in the rocks. Due to their high amount of phyllosilicates, this technique is ideal for looking at strains in pelitic rocks, which should have been the weakest rocks during deformation and therefore the ones most suitable to record large amounts of this coupled shear strain. Under the assumption of a simple shear deformation maximum shear strains are estimated from the finite XTG strain data.

We interpret these shear strain results using a very simple shear zone kind of model where the accreted sedimentary materials migrate through this active shear zone within the wedge at a rate controlled approximately by the exhumation rate (Fig. 2). The modeled shear zone is not the subduction décollement itself, but a shear zone within the wedge which is caused by the shear stress transmitted across the subduction décollement. With this model it is possible to make predictions about what the shear strains should be, given different plate convergence velocities and different exhumation rates. Additionally it allows to comment on different shear strains as a function of the degree of coupling.

Besides the shear coupling as main issue of this paper, we also consider how the relative strain measurements obtained from XTG measurements might relate to absolute strains and involved volume strains recorded in the pelitic parts of this subduction wedge. This is an important issue in understanding the kinematic evolution of this wedge. Additionally, we consider the tectonic significance of these results both to the regional tectonic evolution of the Torlesse wedge and also in an understanding in general how thick sediment-rich subduction wedges might evolve.

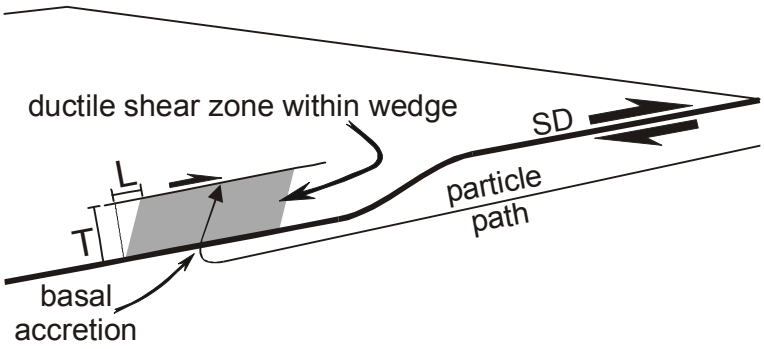

Fig.2. Shear zone model illustrating coupling between subducting plate and accretionary wedge. After basal accretion rocks enter a shear zone that is triggered by shear stresses transmitted from the subduction décollement. During their ascent to the surface caused by exhumational processes, rocks cross this shear zone recording shear strains that depend on exhumation rate, subduction velocity, and the degree of coupling. *T* represents thickness of the shear zone and the mechanically coupled area of the subduction déclomment. *L* is the translation distance within the shear zone. SD is the subduction décollement.

Geological setting

New Zealand´s South Island can be seen as an ancient convergent margin. In this tectonic setting, the Mesozoic Torlesse accretionary wedge, part of New Zealand's Eastern Province, established during the SW-directed subduction of the oceanic pacific plate underneath the NW-SE oriented eastern Gondwana margin between the Permian and the Late Cretaceous (e.g., Korsch & Wellman 1988, MacKinnon 1983, Mortimer & Campell 1996). The Gondwana margin on the South Island consists of the Cambrian to Devonian terranes of the Western Province (Fig. 3a). The subduction related magmatic arc is represented by the Median Batholith that separates the Western from the Eastern province (Mortimer et al. 1999).

The samples examined in this study are from the Otago Schist, a moderate pressure low temperature metamorphic belt (Mortimer 2000, Yardley 1982) that is interpreted as the former fore-arc high of the Torlesse accretionary prism. The Otago Schist itself consists of two metasedimentary terranes: the volcanogenic Caples terrane and the quartzofeldspathic Torlesse terrane, both dominated by psammitic and pelitic greyschist with subordinate greenschist bands (e.g., MacKinnon 1983, Mortimer 1993a, Mortimer 1993b).

The Otago Schist forms a 150 km-wide, NW trending two-sided arch that contains the deepest exhumed parts of the subduction wedge (Fig. 3b). The penetrative foliation across the Otago is moderately inclined in the periphery and flattens to subhorizontal towards the culmination axis. Such flat-lying foliations can be found in other orogens as well and are interpreted as an indicator of underplating (Platt 1986, Platt 1993, Wallis et al. 1993). Lineations strongly vary on the regional scale even if preferred orientations may exist in the local scale (Mortimer 1993b). Quartz U-Stage studies by Cooper (Cooper 1995) stated that

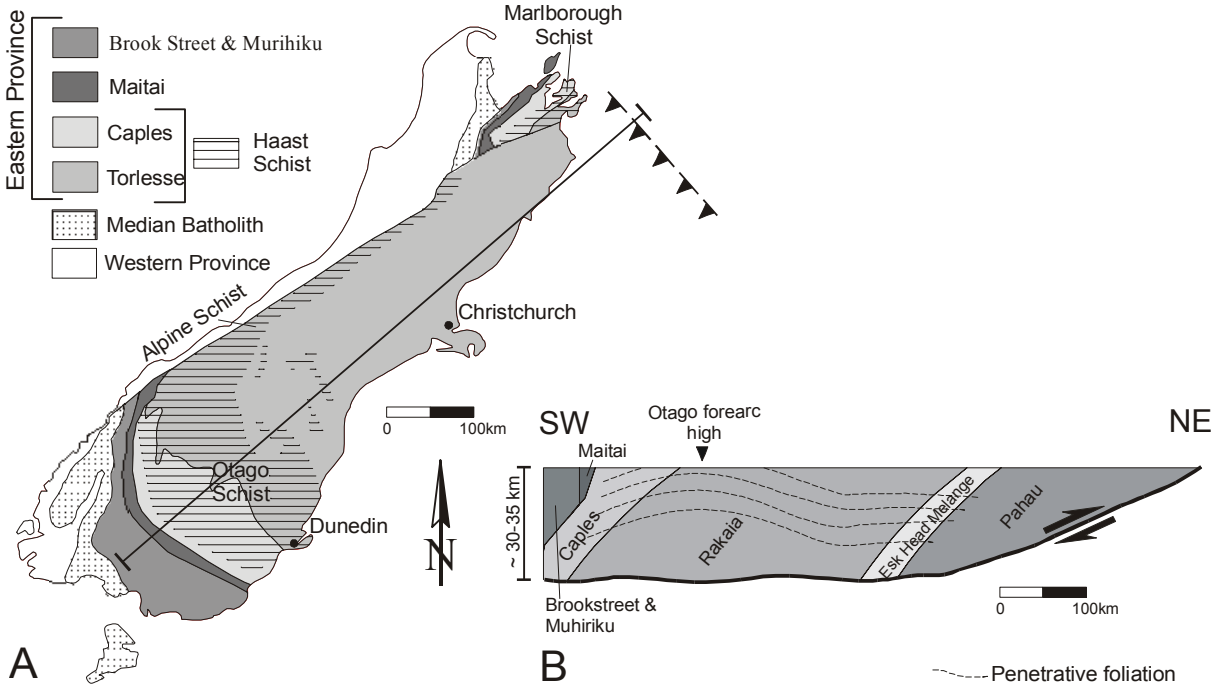

Fig. 3. (a) Simplified geological map of pre-Late Cretaceous basement, South Island, New Zealand (after Mortimer et al. 1999). Haast Schist belt is subdivided into Marlborough, Alpine, and Otago Schist. (b) Scematic cross section through theTorlesse accretionary wedge. Rakaia, Esk Head Melange, and Pahau are subterranes of the Torlesse (modified after Mortimer, 1993; Korsch & Wellman, 1988).

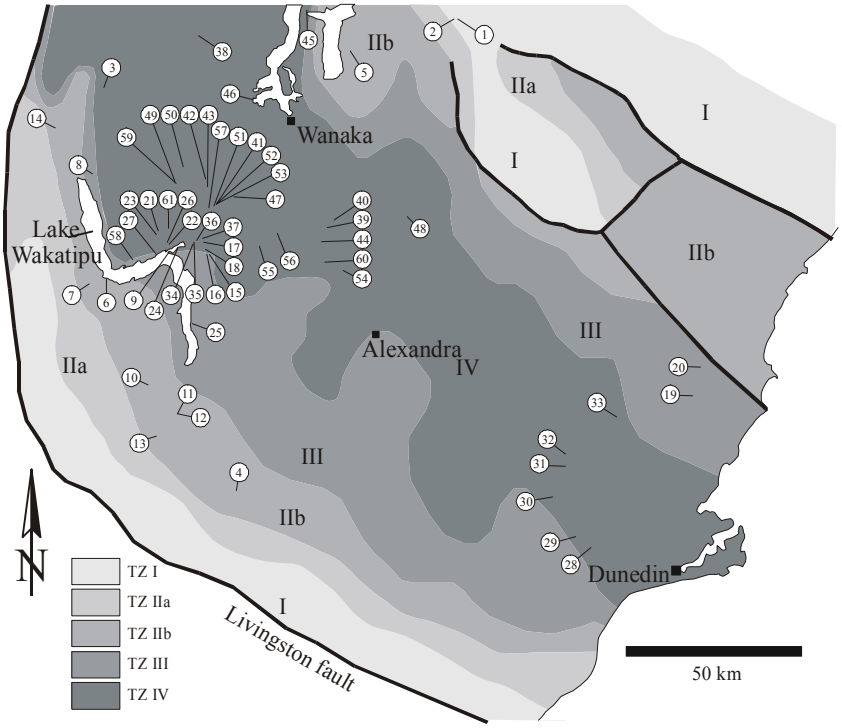

Fig. 4. Map of the Otago Schist showing different textural zones. Numbers depict localities of examined samples.

the mineral lineations parallel the finite maximum stretching axes.

To subdivide the monotonous rocks in the Otago Schist (Bishop 1972a, Hutton & Turner 1936, Turnbull et al. 2001) defined four different textural zones (TZ) based on meso- and micro structural changes in the metasedimentary rocks that could be correlated to increasing structural depth (Fig. 4). The zoning should primarily enable to identify post-metamorphic faults in the otherwise uniform rocks of the Schist belt, but strain work carried out by Norris & Bishop (1990) also postulated an amplification of strain with increasing TZ.

Metamorphic conditions in the Otago Schist range from prehnite-pumpellyite facies for the non-schistose rocks at the flanks to greenschist facies with peak metamorphic temperatures and pressures of 350-400°C and 8-10 kbar in the centre e.g. (Mortimer 2000, Turnbull 2000). This suggests a geothermal gradient of c. 11.5°C/km. Parallel to increasing metamorphism deformation increases towards the culmination axis of the Otago Schist as defined by the progressive development of fold generations and foliation transposition. The trace of the TZ also follow the strike of the metamorphic changes across the Otago culmination.

After peak metamorphism in the Middle Jurassic, the Otago Schist was exhumed to shallower crustal levels. There is a discussion if exhumation either occurred continuously at a slow rate of c. 0.2 km Ma-1 from 190-110 Ma (Adams & Gabites 1985, Adams & Robinson 1993) or was punctuated with rapid exhumation rates of 0.6-1.0 km Ma-1 after 135 Ma (Little et al. 1999). This demonstrates that the cooling history of the Otago Schist remains confusing

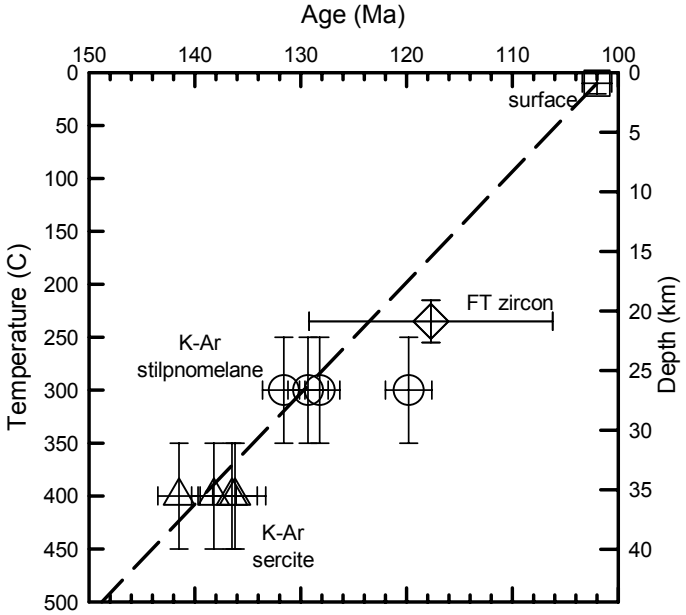

Fig. 5. Cooling history of the Otago Schist. Exhumation rate is estimated with c. 0.8km/Ma^{-1}. Closure temperatures are those cited by Hurford (1986) for biotite and muscovite. The 235° C closure temperature of Zircon fission tracks is from Brandon et al. (1998).

because of uncertainties about interpretation of various isotopic studies. In Fig. 5, we highlight some ages that can be used to provide more confident estimates of cooling and exhumation rates. Adams and Robinson (1993) dated brown (stilpnomelane and biotite) and white (sericite and phengite) mica separates from greenschists that directly underlie well dated Albian strata (102 Ma in Adams and Raine, 1988) within one of the middle Cretaceous half grabens south of Dunedin. Zircon fission track ages are from north of Queenstown. The relationship of the cooling ages to the unconformity age indicates a cooling rate of ~10 C°/Ma^{-1} and an erosion rate of 0.8 km/Ma^{-1}, using a thermal gradient of 12°C/km.

However rocks from the interior of the Torlesse wedge reached the surface at c. 102 Ma during a New Zealand wide initial rifting phase. This rifting phase caused the cessation of subduction processes at the Torlesse convergent margin and culminated in sea-floor spreading in the Tasman Sea at about 85 Ma (Kamp 1986 and references therein). During the early stages of rifting, post-accretionary major dextral shearing in the Mid-Cretaceous (118-100 Ma) bended the Gondwana continental margin and New Zealand's basement terranes in its now visible Z-shaped geometry (Bradshaw et al. 1996) (Fig. 6).

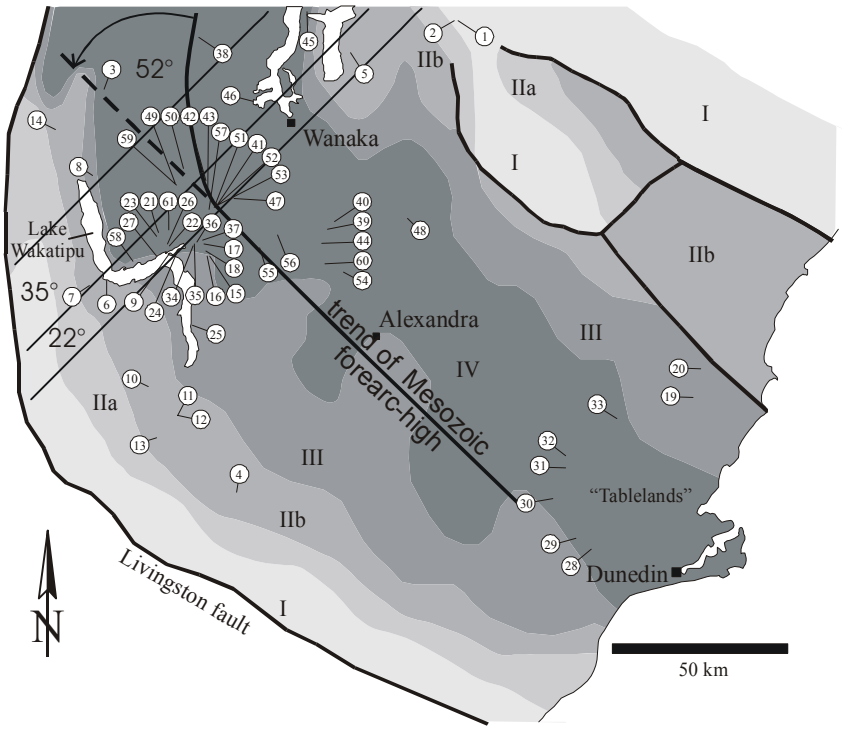

Fig. 6. Restoration of Mesozoic forearc high. Degree of post-Mesozoic rotation in central and western Otago is shown for three different sectors.

Subsequent widespread erosion of the Otago Schist between 102-85 Ma resulted in the establishment of the Waipounamu Erosion Surface (WES) and the peneplanation of much of the southern South Island (Bishop 1994, Crampton et al. 1999, LeMasurier & Landis 1996).

Miocene to Recent deformation, related to the formation of the Alpine Fault, folded the WES and gave Central and East Otago its present basin-and-range topography.

Basic strain concept

To fully describe finite strain in a rock, six independent variables are required. Three variables describe the orientation of the principal stretching directions *X,Y,Z,* where *X* represents the maximum stretching direction, *Y* the medium stretching direction, and *Z* the maximum shortening direction. The remaining three variables describe the magnitude of principal strain along those directions, represented by the absolute principal stretches S_X, S_Y, S_Z, where $S = l_f / l_i$, with l_i equal to initial length and l_f equal to final length. It always rules, that $S_X \geq S_Y \geq S_Z$. Another important invariant for the strain tensor is volume strain S_V. It is defined as $S_V = V_f / V_i$, where V_f is the final and V_i the initial volume of an elementary volume. Additionally the relationship between principal stretches and volume stretch is given with $S_V = S_X S_Y S_Z$. Relative principal strains normalized to a constant volume that is equal to one, are called principal deviatoric strains with $S'_X S'_Y S'_Z = 1$. The relationship between deviatoric and absolute strain is defined by

$$S' = S \; S_V^{1/3} \qquad (1).$$

Sometimes also the principal axial ratios R_{XZ} , R_{XY} , R_{YZ} are used to describe strain, where $R_{XZ} = S_X / S_Z$, $R_{XY} = S_X / S_Y$, and $R_{YZ} = S_Y / S_Z$.

Assuming a simple shear deformation, shear strain γ along a certain direction can be calculated by the given principal axial ratio *R* in this direction. Following (Ramsay 1967) the relationship is given with:

$$\gamma = \sqrt{(R-1)^2 / R} \qquad (2)$$

In particular γ_{XZ}, calculated from the maximum axial ratio R_{XZ}, is of interest, because it represents the maximum possible shear strain recorded in a rock. The conventional octahedral shear strain γ_{oct} can be used as a measure of the average distortion a sample suffered. It can be calculated by the amount of shear strain that is recorded by a material line and plane during deformation and is independent from strain geometry (for details see Brandon (1995)). It is defined as

$$\gamma_{oct} = \sqrt{R_{xy}^2 + 1/R_{xy}^2 + R_{yz}^2 + 1/R_{yz}^2 + R_{xz}^2 + 1/R_{xz}^2 - 6} \Big/ 3 \qquad (3)$$

Method

For strain determination in rocks of the Torlesse wedge X-ray texture goniometry combined with the March method (March 1932) was applied. In the following we start with a

description of the X-ray texture goniometer set-up, which was used to determine crystal preferred orientations. Then we will have detailed look on the March method, investigate its applicability, comment on critical assumptions, and discuss and verify the method by means of particular examples.

X-ray texture goniometry and sample preparation

The preferred orientation of phyllosilicates, necessary to calculate March strains, was determined by measuring the diffraction intensity of characteristic lattice planes with an X-ray texture goniometer (XTG). Samples were analysed at Yale University a Scintag-PadV X-ray diffractometer with a Cu-X-ray source (45 kV, 40 mA) and an energy-dispersive solid-state detector. Samples were analyzed using an asymmetric transmission mode configuration with the sample mounted in an auxilary stage with an azimuthal drive. This stage allowed the sample orientation to be varied azimuthally from 0 to 360 degrees. With the asymmetric geometry the stage and sample can be tilted relative to a constant two-theta diffraction geometry. The stage allows measurements with tilt angles up to 40 deg. For the sample preparation a c. 250 μm thin rock slab was cut perpendicular to the macroscopic foliation and mounted on a square aluminium holder with a circular hole through which the X-rays could pass. The region of interest is manually aligned by moving the sample holder relative to the X-ray beam. The irradiated area has a diameter of 1mm. After the sample was mounted on the X-ray pole-figure stage a 2Θ scan was made prior to the orientation measurements to get the exact diffraction angle for the minerals in a sample. For our purposes we measured the (002) planes of muscovite/Illite or the (002) planes of chlorite given with lattice spacings of 9.9 Å and 7.1 Å respectively. Subsequently the diffractometer was set to the correct diffraction angle and single intensities were measured over a 40° tilt with 6.67° intervals (7 steps) each over an azimuthal range of 360° again with 6.67° intervals (54 steps) giving a total of 378 stations. The intensity at each station was measured for 200 sec or alternatively until 200 counts were measured to ensure a specified lower level of precision for orientations with low diffraction intensities.

March strains

The March method is based on the theory of calculating finite strain from the preferred orientation of platy minerals, in common phyllosilicates, in a rock (March 1932). March neglected the real properties of crystals in rock matrix and instead treated the platy minerals in a rock as passive markers. These markers that can be simply seen as planes and lines are reoriented by a homogeneous strain that affects all components of a material. March (1932) recognised that to every possible strain a unique distribution of grain orientations is

associated. The relationship between strain and preferred orientation is given by March (1932) with:

$$S'_i = \rho_i^{-1/3} \qquad (4)$$

where S'_i is the principal deviatoric strain, and ρ_i is the principal pole density of the marker grains, divided by the average pole density for all orientations. The calculated strain data include the whole deformation history of the examined rock volume, i.e. deformation under metamorphic conditions as well as strain by compaction starting after the deposition of the minerals.

It is common to measure crystal preferred orientations of phyllosilicates by using an X-ray texture goniometer (XTG), which allows the rapid determination of a large number of mineral grains. Because the XTG does not measure single lattice planes, but diffraction intensities, pole intensities of eq. (4) are substituted by the measured diffraction intensity in a certain XTG-interval i_{net}, normalised by the uniform intensity i_{unif} of all intervals, i.e.

$$S'_i = (i_{net} / i_{unif})^{-1/3} \qquad (5).$$

March´s model requires several important assumptions. (1) The original distribution of the phyllosilicates has to be random and uniform. This assumption seems to be justified in fine grained, freshly deposited, and uncompacted sediments (Benett et al. 1981, Bowles et al. 1969, Moon 1972). And even if detrital phyllosilicate grains larger than 1mm are expected to deposit in a horizontal preferred orientation (Maltman 1981), bioturbation would create a random orientation immediately after deposition (Oertel 1985). (2) Phyllosilicate grains are reoriented as passive markers, i.e. grain to grain interactions are minor and grains can rotate in the matrix to reach their new orientation without being locked by neighbouring phyllosilicates. (3) Grains maintain their identity notwithstanding diagenetic and metamorphic phase changes during burial (e.g., Oertel 1985). Recrystallisation, if it has occurred, is by replacement of old phyllosilicate grains, rather than grows of new grains with new orientations. The original sheets of linked silica tetrahedra are probably preserved through phase transitions (Craig et al. 1982, Nicot 1981, Page 1980, Page & Wenk 1979).

In the last three decades further work on the March method has provided a more detailed understanding and an extensive discussion on its applicability (Lüneburg et al. 1999, Oertel 1970, Oertel 1983, Oertel 1985, Owens 1973, Tullis & Wood 1975, Wood & Oertel 1980) In particular tests have to be pointed out, that compare strain results obtained with the March model and other independent strain determination techniques in the same rock. The good consistency of March strains and results from other methods, like e.g. reduction spot measurements, give a positive justification of March´s theory (e.g . this study, Tullis & Wood 1975, Wood & Oertel 1980).

Estimates of the principal deviatoric stretches, both their magnitude and directions, were determined directly from the XTG data using a best-fit least-squares algorithm based on the March model. The inverse also accounting for changes in absorption and X-ray background with sample tilt. The fit to the X-ray intensity data is weighted using the standard errors for the intensities, as determined from count statistics. (The XTGFIT program, along with other programs used in this paper, are available, together with source code, at www.geology.yale.edu/~brandon.)

We applied several tests that demonstrate strains obtained from our XTG measurements are reasonable results of finite strain. One useful test is the degree of fit of the measured data to the best fit model. The XTG-Fit program, using routines of Press et al. (1986), iterates through a series of guesses to find the quadratic coefficients for the XTG data that match the observed measurements. Parameter errors are estimated from the parameter covariance matrix, which is scaled upward by the value of the reduced chi square when reduced chi square is greater than one. In many cases, we find that the phyllosilicate orientation density distribution is well fit by the predictions of the March model (Fig. 7a). In fact the degree of fit is comparable to the analytical errors in the XTG data. Observed counts and standard errors were compared to expected counts by applying chi-squared tests to verify the plausibility of our measurements at each single tilt step (Fig. 7b). Reduced chi-square results for each sample vary along one, indicating a good model for the calculation of March strains from measured XTG intensities.

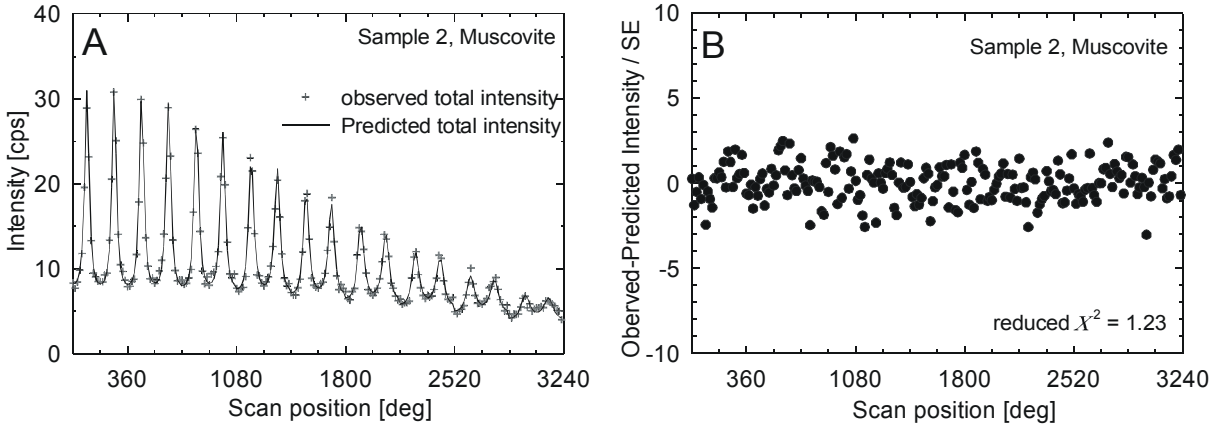

Fig. 7. XTG intensities of muscovite in sample 1. (a) Comparison of observed intensities and intensities predicted by a best-fit model. (b) Chi squared (X^2) statistic results for each single tilt-step.

Another test that should verify our results, was to measure the preferred distribution of two different phyllosilicate phases. They should be identical if they coexist in the same rock (c.f. Oertel 1983).Consecutively the orientation of muscovite and chlorite grains in a sample were determined without changing the position of the incident X-ray beam. Table 1 compares

strain geometry and uniform intensities of muscovite and chlorite in samples of different textural zones. The consistency of orientations and finite strain magnitudes of the two phases is striking.

The last test that should prove the validity of our results, is the comparison of the strain data acquired from our XTG measurements with other independent strain determination methods (e.g. Oertel 1985, Wood & Oertel 1980). For that purpose we measured the preferred orientation of white mica in Cambrian slate samples from Wales with known finite strains that were estimated by (Wood & Oertel 1980) using reduction spots. The calculated strain magnitudes match well with the finite strain from the reduction spots in the same sample (Fig. 8). Figs. 9a & 9b show again the good consistency between observed and predicted intensities.

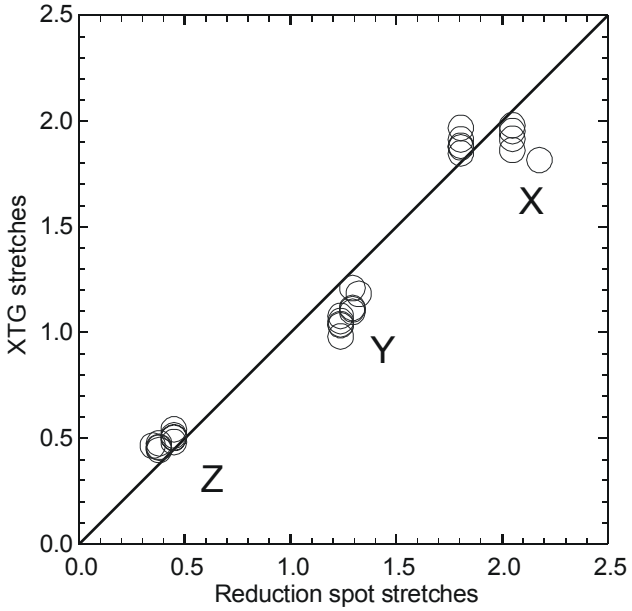

Fig. 8. Plot of principal stretches from X-ray texture goniometry against principal stretches measured from reduction spots in the same samples.

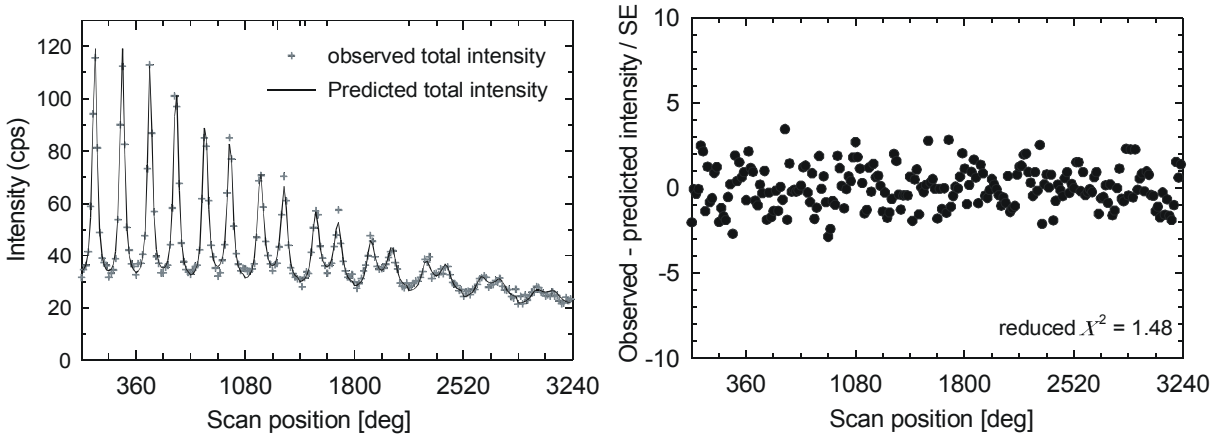

Fig. 9. XTG intensities of a welsh slate sample with the Yale XTG set-up. (a) Comparison of observed intensities and intensities predicted by a best-fit model. (b) Chi squared statistic results for each single tilt-step.

Results

We will now present the results of X-ray texture goniometry, including orientations of principal stretching directions, strain symmetry, and shear strain values of 61 oriented mudstone and mica schist samples from exposures of the Caples and Torlesse terranes in the Otago Schist (Fig. 4). The coverage of our samples comprises both the periphery and the deepest exhumed parts along the culmination axis of the Otago Schist, including all different metamorphic and textural zones. This widespread sampling also allows to investigate possible regional differences of finite strain. Moreover we will compare strain results obtained from XTG measurements with mesoscopic fabrics measured in the field. Finally, we calculated tensor averages that include all single strain measurements, to get an impression on the regional scale deformation in the Otago Schist.

Orientation and symmetry of finite strains

The full list of our deviatoric strain measurements is given in Table 2. Principal stretching directions are shown in Fig. 10. Maximum shortening directions of textural zones 2 to 4 cluster around a subvertical distribution maximum. The axis orientations do not differ with respect to different textural zones. Z directions for TZ 1 show unusual subhorizontal orientations, probably because the two samples were collected in a strongly cenozoic faulted region (sample 1 and 2 in Fig. 4) and orientations were possibly tilted (cf. Kumerics 2001). The X and Y directions are arranged in girdles perpendicular to the total Z maximum. A comparison of different textural zones again shows, that each of them has the same distribution pattern defining a subhorizontal great circle. The scattering of maximum stretching axes in the horizontal is similar to the diffuse horizontal orientation of the measured macroscopic stretching lineations (Table 2). No conspicuous pattern of maximum extension

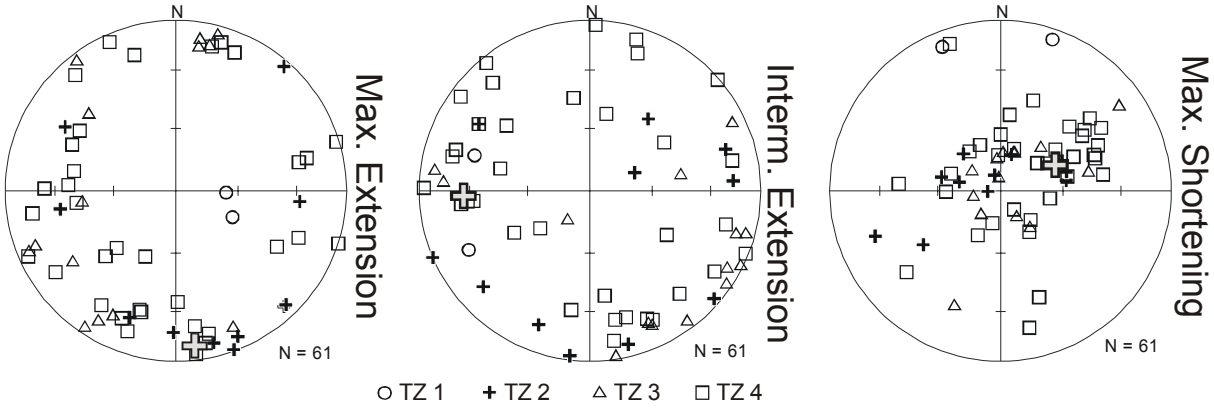

Fig. 10. Principal deviatoric stretching directions from XTG measurements. The grey cross represents the tensor average orientation of XTG samples.

axes across Otago can be identified, neither at the regional nor at the local scale, e.g. the Lake Wakatipu area (Fig. 11). This means that the scattering in the stereograms cannot be seen as a continuous change of the orientations from one region to another.

The symmetry of the single finite strains calculated by the March equation is shown in a logarithmic Nadai-Plot and Flinn diagram (Fig. 12a& 12b). Most of the samples are characterised by an oblate strain geometry. Differences in the distribution pattern between single textural zones cannot be identified.

Calculated maximum shear strains in the respective XZ-plane of each sample range between $\gamma_{XZ} = 3.16$ and $\gamma_{XZ} = 1.06$, assuming that strain would result solely by simple shear deformation. The mean for all data is given with $\gamma_{mean} = 1.85$. Again no variations concerning different textural zones are visible.

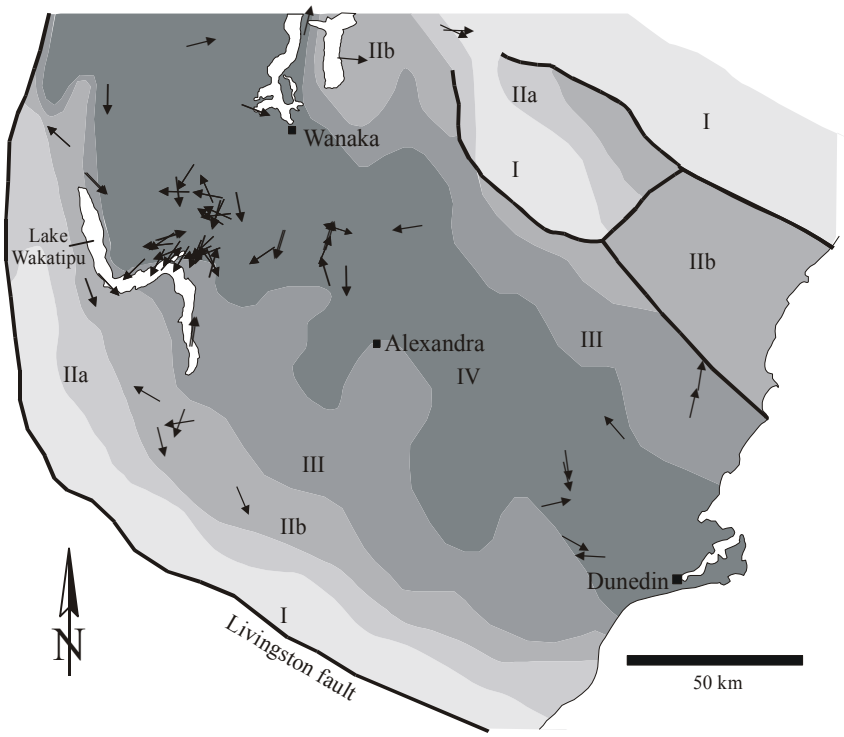

Fig. 11. Distribution and orientation of maximum principal stretching axes in the Otago Schist. No preferred orientation of S_X at the regional scale is visible.

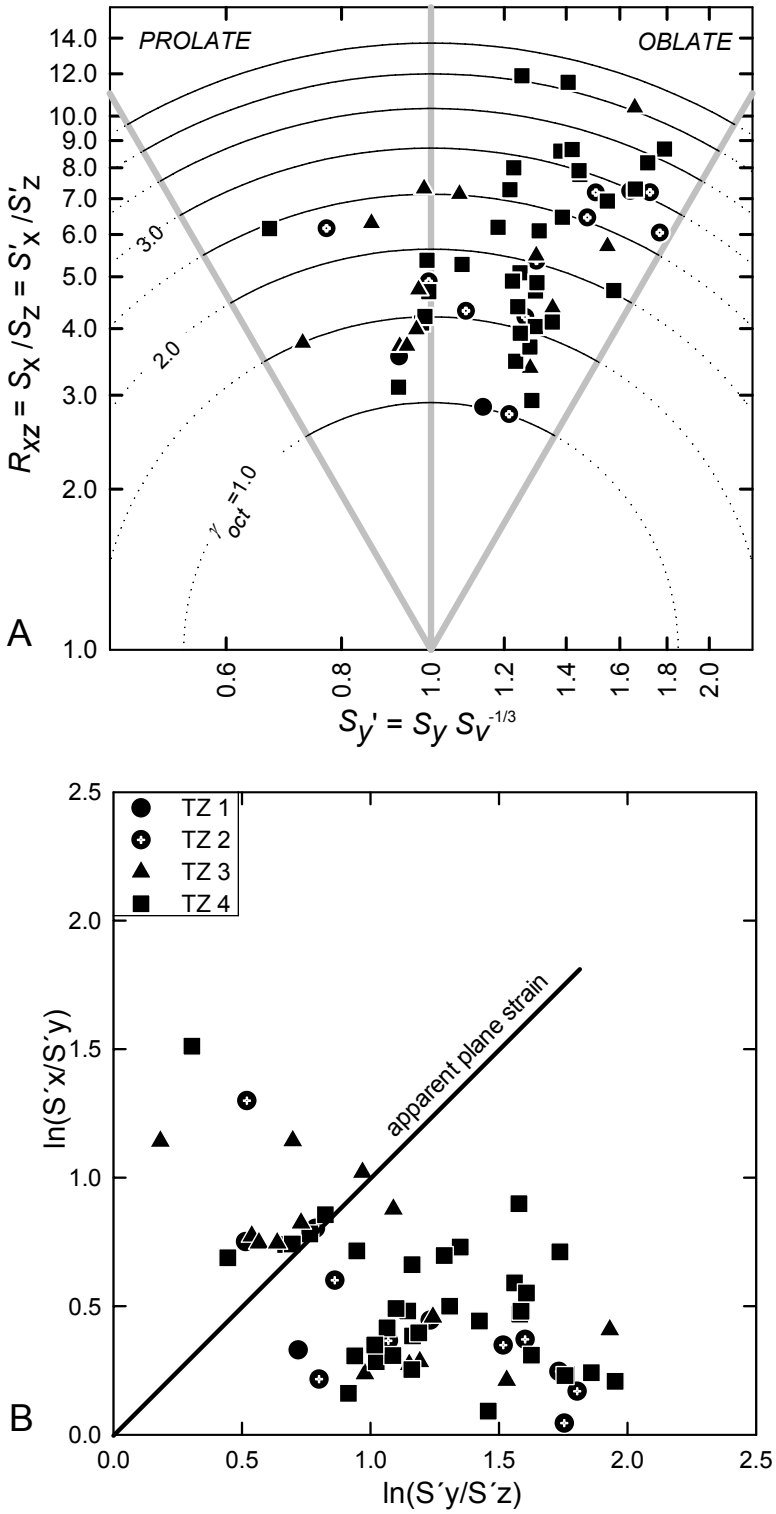

Fig. 12. Strain symmetry of examined deformed rocks distinguishing between different textural zones. (a) Nadai diagram. (b) Flinn diagram.

XTG strain vs. mesoscopic fabric

The measured maximum shortening directions parallel the orientations of the pole of the mesoscopic foliation (Fig. 13, Table 2). Both are expressions of finite strain and their consistency is another proof for the applicability of March strains. The relationship between X from XTG measurements and the mesoscopic lineation is poorer defined, even if more than 60% of the lineations enclose an angle smaller than 20° to S'_X (Fig.9). Some of the maximum stretching axes and mesoscopic lineations enclose large angles > 60°. In some of these samples this might be due to the similarity of S'_X and S'_Y magnitudes. The resulting low K-values cause a lower precision for XTG-measurements to distinguish between X and Y directions.

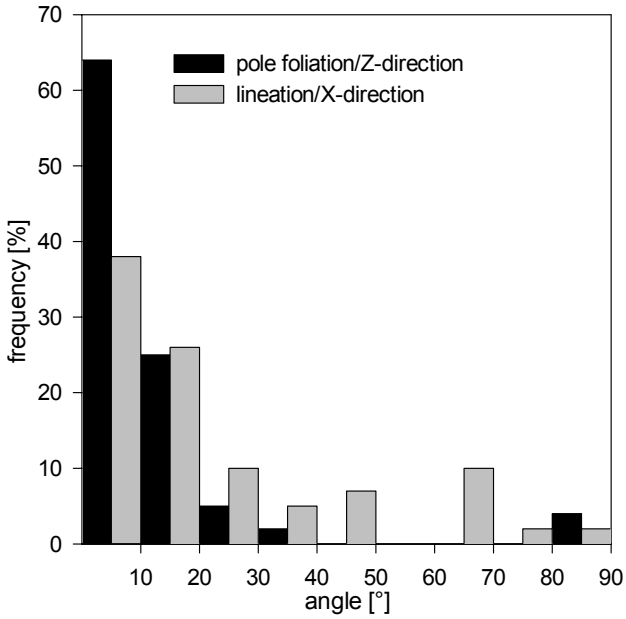

Fig. 13. Graph showing the angle between mesoscopic lineation and maximum stretching direction from XTG data, respectively pole of mesoscopic foliation and XTG shortening direction.

Tensor average calculations

To get an impression of the regional deformation in the Otago Schist, tensor averages of the single strain measurements have been calculated. For this purpose the program MEANDEF was applied that accounts strain data as tensors and calculates the tensor average for a given set of strain measurements using the Hencky-tensor method described in the appendix of (Brandon 1995).

To define the regional deformation during subduction it is necessary to restore the Mesozoic orientation of the single finite strain ellipsoids before the related tensor average can be calculated. Following (Bradshaw et al. 1996) the Gondwana margin was bended in the

mid-Cretaceous after the subduction of the pacific plate under Gondwana had stopped. If we assume that the fore-arc high of the Torlesse wedge was parallel to the Gondwana margin, the backrotation of its present trace into the original trend of the Gondwana margin of 135° (Bradshaw et al. 1996), can be used to restore the principal stretching directions of our strain measurements. The present trace of the fore-arc high is defined by the deepest exhumed rocks (Fig. 6), based on the Otago foliation thickness map of (Mortimer 2001). Because the mid-Cretaceous bending only affected the western parts of the Otago Schist and increased towards the west, we distinguished three zones in which rocks where differently rotated with respect to the orientation of the Mesozoic margin. Principal stretching directions of samples that are lying in one of these zones could now be back rotated with respect to the rotation angle given in Fig. 6 along a subvertical axis. Restored orientations are given in Table 3. A further later rotation of the stretching axes due to cenozoic basin-and range formation can be neglected (Deckert et al. 2002).

We determined two tensor averages from the complete strain data collection (Table 2). The first is based on the unrestored strain data, i.e. it is related to the present day geographic frame, the second is based on strain data corrected for mid-Cretaceous bending. There is no difference in strain magnitudes, only the azimuth direction of S'_X and S'_Y axes has changed about 20°.

In the following, we focus on the restored tensor average. It is characterised by a steeply inclined shortening direction. Stretch along S'_Z is given with 0.58. Average maximum and intermediate stretching axes are subhorizontally oriented. Their deviatoric magnitudes with $S'_X = 1.38$ and $S'_Y = 1.25$ are close together. This again can be related to the dispersion of the individual X and Y directions along a subhorizontal great circle (Fig. 10). Consequently, differences in X and Y are averaged out at the regional scale. Finally, strain at the regional scale can be seen as uniaxial shortening, even if single measurements can have other symmetries due to heterogeneous deformation at the local scale. A surprising result is that the restored tensor average X direction with an azimuth of 139° and a plunge of 5° matches perfectly to the orientation of the Mesozoic margin. The intermediate axis is oriented vertical and horizontal to the Gondwana margin.

A comparison of tensor averages of TZ2 to TZ 4 is used to verify if there are any changes of principal stretching directions or magnitudes with depth, show that the results are similar to the bulk average of all strain data (Table 2). A strong vertical shortening of around 45% can be seen in all TZ. Maximum stretching directions of TZ 2 and TZ4 averages differ less than 10° from the maximum stretching direction of all data and the Mesozoic margin. Only S'_X and S'_Y orientations of TZ3 tensor average do not fit to the dominant directions in Otago. This may be due to the fact, that most of the TZ3 samples are from an area around Lake Wakatipu (Fig. 4) and do not have the same widespread origin like samples from other

textural zones. Thus the tensor average might represent a more local phenomena and do not reflect the regional average deformation of the Otago Schist.

Discussion

Comparison with previous strain studies

Earlier strain work by Norris & Bishop (1990), who measured deviatoric strains in 28 deformed conglomerates ranging from TZ 1 to TZ 4, postulate a positive correlation between TZ and deformation intensity. This general trend gets obvious by examining γ_{oct} and R_{XZ} values for their individual samples (Table 4, Fig. 14). To address possible strain partitioning in different lithologies, Norris and Bishop (1990) additionally distinguished between strain recorded in lithic clasts or quartzitic pebbles. Distortion in the quartzitic pebbles is lower than in the lithic clasts, nevertheless in both fractions strain is increasing with higher TZ (Fig. 14).

Such a relation of increasing deformation with higher TZ, that is equal to increasing depth, can not be found in our XTG results. In contrast to Norris and Bishop data no systematic higher R_{XZ} or γ_{oct} values are indicated in the Nadai diagram of Fig. 12a. Mean γ_{oct} for each TZ indicate a jump from γ_{oct} = 1.1 in TZ 1 to γ_{oct} = 2.1 in TZ 2. But TZ 2, 3, and 4 show more or less the same amount of distortion.

It must be stressed that Norris and Bishop only measured one TZ 1 sample from each fraction and thus a statistical significance for TZ 1 is not given. This may explain the discrepancy in R_{XZ} or γ_{oct} values between their and TZ 1 values in this study. If TZ 1 values of Norris & Bishop represent reasonable results than the discrepancy could be also due to the fact that March strains in our samples also include compaction strain. In textural zones 1 and 2 γ_{oct} values of the quartzitic fraction are lower than XTG and lithic strain data. Norris & Bishop (1990) explain lower strains by strain partitioning between clasts and matrix. The lithic clasts consist of fine sandstone or siltstone and strongly resemble the matrix of the rocks and therefore take up higher strains. This is not surprising because temperatures in TZ 1 and TZ 2 rocks are not high enough to initiate intracrystalline deformation. Thus deformation is mainly restricted to pressure solution processes. The magnitude of pressure solution deformation also depends on grain sizes (Spiers et al. 1990). Therefore distortion in the meta mudstones with their small grain sizes has to be larger than in the quartzitic pebbles. A surprising result is the fact, that maximum shear strains γ_{XZ} do to not differ significantly neither comparing different TZ nor in Norris and Bishop (1990) and our samples (Fig. 15). Besides differences in the amount of distortion, strain data in both studies strongly resemble each other concerning their strain symmetry (Fig. 12a, Fig. 14). Bulk data plot in the apparent flattening field.

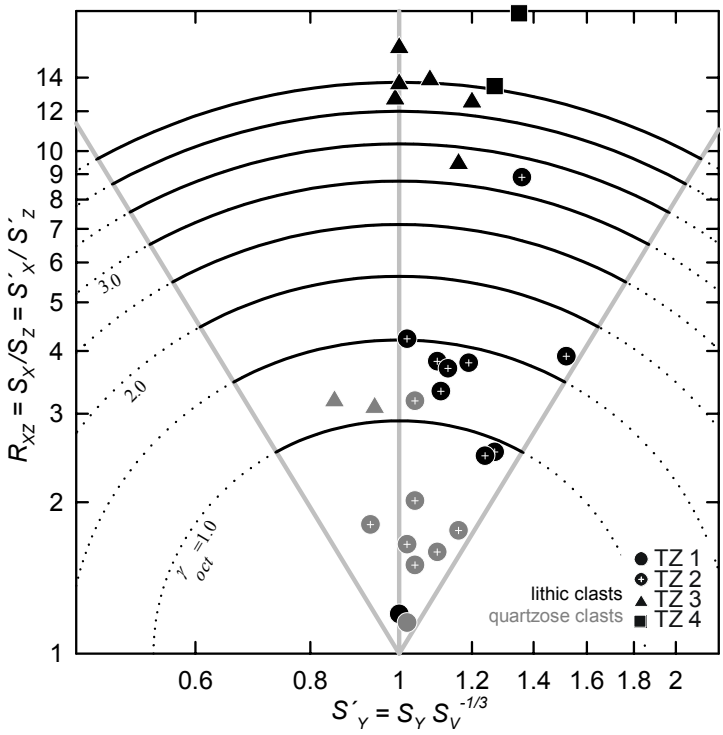

Fig. 14. Nadai diagram presenting strain symmetry of deformed conglomerates measured by Norris & Bishop (1990). Lithic and quartzose clasts show different deformation intensities with increasing textural zones.

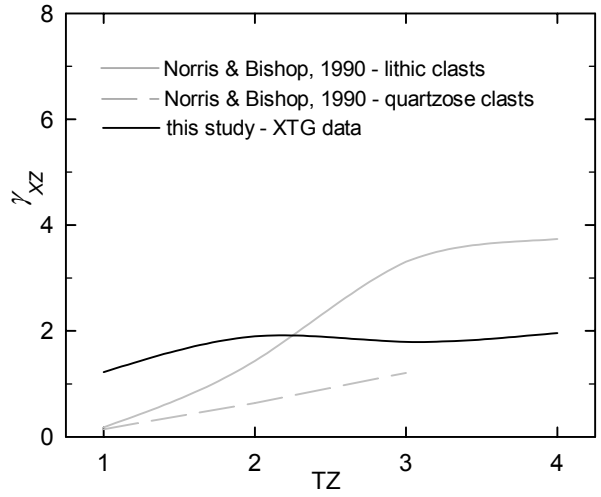

Fig. 15. Comparison of mean shear strains derived from this study and results of Norris & Bishop (1990).

Summarising, a significant relationship between deformation and different TZ is not given in the examined rocks of this study, contrasting to strain results from deformed conglomerates. Thus, we suggest that differences in distortion are due to different lithologies rather than to a general increasing deformation with depth. Compared to conglomerates the weaker pelitic layers do not comprise significant higher shear strains. Because Norris & Bishop did not record any strain directions, a comparison to results in this study could not be performed.

Shear coupling

Many studies assume that coupling of the wedge with the downgoing plate is strong (e.g. Moore, 1979; Cloos and Shreve, 1988). If true, then rocks, that were subducted and accreted to the base of an accretionary wedge, should have recorded high shear strains to mirror this strong coupling. As already outlined, this is because the coupling is responsible for transmitting shear stresses across the subduction décollement. The shear stresses will still effect the rocks even if they are, after accretion, now within the wedge. We use the Otago Schist as a case study to test the general assumption of strongly coupled plates. Therefore, we calculate theoretically expected shear strains in an accretionary wedge by using a simple geometric model and compare these results to our measured maximum shear strains in samples of the Otago Schist to see if they match the predicted results.

Our model is in geometric analogy to the model of (Moore 1979) but distinguishes in that way, that it is restricted to shear strains accumulated after accretion. The basic idea of the model is, that rocks are effected by shearing, while they cross a shear zone within the wedge during exhumation (Fig. 2).The shear zone thickness T represents the mechanically coupled area above the subduction décollement due to plate coupling. For a certain time (t), the shear strain rate $\dot{\gamma}$ is defined by the translation (L) in the shear zone divided by the thickness T of the shear zone, resulting in $\dot{\gamma} = L/Tt$. Because L/t is equal to the subduction velocity V_C, which can be seen as translation velocity in the shear zone,

$$\dot{\gamma} = V_C / T \qquad (6).$$

Finite shear strains can be obtained by multiplying equation (6) with the residence time (τ) of a particle within the shear zone, thus

$$\gamma = V_C \, \tau / T \qquad (7).$$

The residence time (τ) can be seen as the time the accreted material particle migrates through this shear zone at a rate controlled approximately by the exhumation rate ($\dot{\varepsilon}$). Therefore

$$\tau = T / \dot{\varepsilon} \qquad (8).$$

Inserting equation (8) in equation (7) shear strain can be calculated by

$$\gamma = V_C / \dot{\varepsilon} \qquad (9).$$

The thickness (T) of the shear zone is no longer relevant and shear strain is controlled only by the subduction velocity and the exhumation rate. Because the translation velocity in the shear zone is the same as in the subduction décollement itself, both given by V_C, equation (9) displays a fully coupled wedge with respect to the subduction décollement and thus, γ represents maximum values that might occur in a subduction wedge. Fig. 16 shows calculated shear strains in such a fully coupled Torlesse subduction wedge with different V_C and ε values.

No information about the Mesozoic subduction velocity of the Pacific plate under the East Gondwana margin is known, even if the low geothermal gradient of c. 112°C speaks for high subduction rates (Peacock 1996). Nevertheless, for our model we used the whole range of known worldwide, present-day convergence rates between 10 km/Ma^{-1} and 250 km/Ma^{-1}. Exhumation rates for the Otago Schist range between 0.2 km/Ma^{-1} (Adams & Gabites 1985, Adams & Robinson 1993) and c. 0.8 km/Ma^{-1} (Little et al. 1999, this study). It gets obvious that even at a high exhumation rate and lowest subduction rates of 10 km/Ma^{-1}, both minimizing γ-values, shear strains of 12.5 should be expected in a fully coupled Torlesse wedge. This differs in an order of magnitude from shear strains measured in our TZ 4 Otago Schist samples (Table 2), that represent the deepest exhumed rocks. They only provide mean shear strains of γ = 1.93. This discrepancy between calculated and actually measured shear strains suggests that the Torlesse wedge is not fully coupled to the down-going plate.

The question is, how much shear coupling actually occurs at a typical subduction zone and in particular at the Torlesse wedge. To answer this question, we provide the new coupling parameter (α), that includes information about the actual degree of coupling between two converging plates. α may range from zero to one, whereas one represents a fully coupled and zero a fully decoupled plate boundary. Inserting α in equation (9)

$$\gamma = \alpha V_C / \dot{\varepsilon} \qquad (10).$$

From equation (10) it gets clear that lower α-values reduce the translation velocity within the shear zone and thus produce lower shear strains, as expected in weaker coupled subduction zones. Fig. 17 displays this correlation. With the known mean shear strain of Otago´s TZ 4 rocks of γ = 1.93, α can be calculated for different subduction velocities and exhumation rates by using equation (10). The highest value, produced by the slowest subduction rate of 10km/Ma^{-1} and fastest exhumation rate of 0.8km Ma^{-1}, do not exceed α = 0.15 (Fig. 17), clearly confirming a strong decoupling of the two plates. Higher subduction rates, which are probable for the Mesozoic Torlesse wedge, as already outlined above, would result in an even stronger decoupling

.

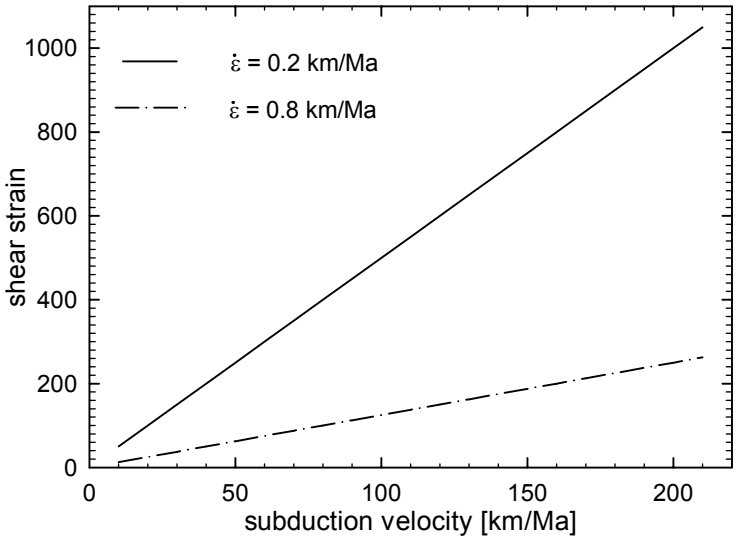

Fig. 16. Calculated shear strains expected in a fully coupled wedge, for different subduction velocities and exhumation rates.

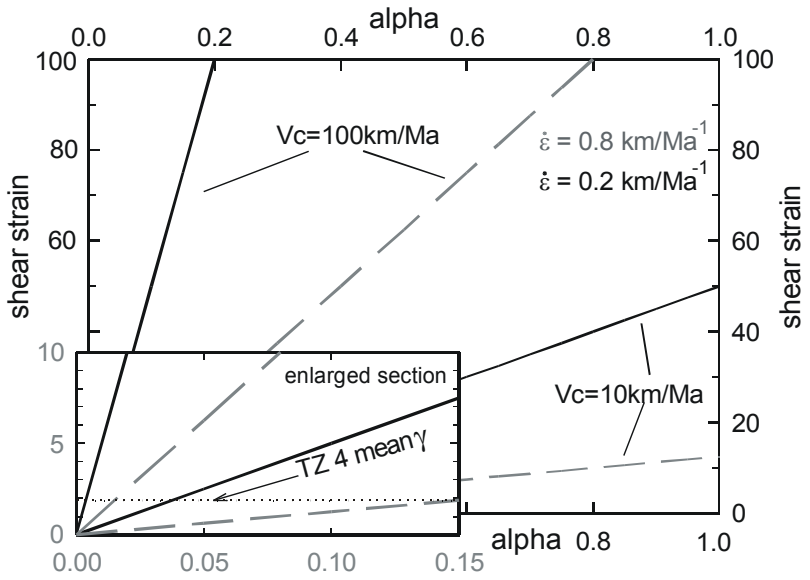

Fig. 17. Expected shear strains for different degrees of coupling. Mean shear strains for TZ 4 rocks in the Otago Schist predict a maximum coupling parameter (α) of 0.15, assuming slow subduction velocities and fast exhumation rates.

Additionally, it must be stressed that the calculated TZ 4 shear strains in Table 2 represent maximum values assuming that the strain symmetry recorded in a sample is solely a result of simple shear deformation. A general deformation or even a coaxial deformation, reasonable if looking at the regional deformation results of in the metasandstones, would actually reduce shear strains to values smaller than $\gamma = 1.93$. Lower shear strains would automatically result in even smaller α-values.

Summarising, the difference between modelled and actually measured shear strains and the low coupling parameters α for the Torlesse imply, that rocks of the Torlesse wedge, in the hanging wall of a weak subduction décollement, are characterised by regional coaxial deformation mainly driven by gravitational forces and erosional fluxes in and out of the wedge, without any or only small amounts of shear deformation due to plate coupling. This conclusion is consistent with vorticity estimates of Wk ~ 0.1 in meta sandstones of the Torlesse wedge (Maxelon et al. 1998) and the results of absolute strain studies in the Otago Schist by Rahl et al. (2003). Rahl et al. (2003) also claim a coaxial deformation because of the lack of systematic fold vergence at the regional scale. The high amount of uniaxial vertical thinning recorded in our strain data that produced the flat-lying macroscopic foliation is another hint for the strong gravitational forces that specifies deformation in the wedge and argues for a strong decoupling.

Estimation of absolute deformation in the Torlesse wedge

So far our results do not provide any information about absolute deformation in the Torlesse wedge, which is important to understand the kinematic evolution of the wedge. Therefore, we try to assess how relative strain measurements obtained from X-ray texture goniometry might relate to absolute strains recorded in the examined pelitic rocks of the subduction wedge. The additional advantage of absolute strains is, that they allow to comment on volume strains and associated mass transfer within the wedge.

In the following we explore a model that converts the deviatoric XTG data into absolute stretches. As outlined above the relationship between volume stretch S_V, deviatoric stretch S', and absolute stretch S is given in equation (1), i.e. if we would know volume strain in a sample we could easily determine absolute strains from the deviatoric stretches.

For the calculation of volume strain we have to make a fundamental assumption. We postulate that deformation in the wedge entirely approached plane strain at the regional scale, where one of the principal stretches is parallel to the margin and equal to one. This might be either the maximum or intermediate stretching direction. The plane strain assumption is a usual expectation for geologic deformation at the regional scale (Ramsay et al. 1983) and is even applicable in oblique convergence scenarios, because there the orogen-parallel

component of deformation is mostly compensated by large orogen-parallel shear zones. Examples for a postulated average plane strain deformation are orogens like the Franciscan Subduction Complex in California or the San Juan Cascade Wedge in Washington (Feehan & Brandon 1999, Ring & Brandon 1999). In these ancient accretionary wedges it was possible to determine absolute stretches directly. Tensor averages at the regional scale result in a plane strain deformation, whereas one of the principal stretching axes lies subhorizontal and parallel to the orogen strike and is characterised by no stretch, i.e. the stretch is one. Absolute strain data determined in meta sandstones of the Otago Schist also show no extension parallel to the orogen. There even a small, but negligible, amount of shortening was found (~ 5%). The maximum stretching direction of the restored XTG tensor averages (Table 2) matches perfectly the Mesozoic trend of the Gondwana margin given with 135°.

The plane strain assumption is used to calculate regional absolute and volume stretches in Otago on the basis of the deviatoric tensor average results. The maximum stretching axis is oriented parallel to the Gondwana margin. Thus, for the special pair of absolute and deviatoric stretches along this axis, equation (1) results in

$$S'_X = S_X S_V^{-1/3} \qquad (11)$$

The absolute stretch S_X is set equal to one to fulfil the plane strain assumption and equation (11) is simplified to

$$S_V = S'_X{}^{-3} \qquad (12)$$

Now S_V can be calculated from the deviatoric stretch S'_X. With $S'_X = 1.38$ average volume strain in Otago results in $S_V = 0.38$ or a volume loss of 62 %. Using equation (1) absolute strain magnitudes for each of the principal stretching directions give $S_X = 1$, $S_Y = 0.91$, and $S_Z = 0.42$.

The absolute strain data include important implications on the tectonic evolution of the Torlesse wedge. In many orogen wedges strong shortening strains are accommodated by a horizontal evasion of the material along the orogen strike (e.g. Tibet plateau, Eastern Alps). This might occur by ductile flow within deeper crustal levels and/or brittle escape structures along major strike-slip and detachment faults in higher crustal levels. Typically maximum stretching axes and mesoscopic lineations measured in such orogens show a preferred orientation parallel to the orogen. The situation in the Torlesse is different. Absolute strain data indicate strong shortening of 58% along a subvertical S_Z and slight shortening along S_Y that is oriented subhorizontal and normal to the Mesozoic margin. The fact that there is no stretch along S_X together with shortening along the other two principal stretches suggests to define the regional deformation as constrictional plane strain. Instead of an evasion parallel to the margin, the shortening in the Torlesse wedge seems to be accommodated by considerable volume loss. Another hint that speaks against orogen parallel extension is the fact that maximum stretching directions of the XTG results vary quite strong (Fig. 10 & 11) and do not

show a preferred orientation parallel to the orogen, similar to strain result of Rahl et al. (this issue). This is also documented in the scattering of mesoscopic stretching lineations across Otago in our data and in (Mortimer 1993b).

Volume strain

The above calculated total volume strain S_V of 62% has to be considered carefully. S_V is not equal to mass gain or loss, because it is a product of several different components and must be fully described as

$$S_{V.} = S_{V\,p}\, S_{V\,d}\, S_{V\,m} \qquad (13)$$

$S_{V\,p}$ contains the volume stretch due to porosity changes, i.e. S_{Vp} is the ratio of initial and final porosity. The biggest effect concerning $S_{V\,p}$ should be the compaction after the deposition of the sediments. $S_{V\,d}$ is the volume change caused by mineral density changes. It is defined by the proportion of initial to final average densities of the minerals in the sample. Given the metamorphic conditions in the Otago Schist $S_{V\,d}$ should be negligible. $S_{V\,m}$ is the volume stretch due to an open mass transfer. It could be quantified by the change of initial to final concentration of conserved elements in the rock.

XTG measurements for strain determination were done on phyllosilicate-rich rocks, like mudstones and mica-rich schists. The difficulty is to judge how the calculated local volume strains relate to outcrop-scale deformation. The mica-rich spot, only 1mm in diameter, represented by the XTG measurement may have a significant S_V even though mass transfer was only at a local sample or outcrop scale. One example to explain this problem is the development of the differentiation layering in TZ3 and TZ4 of the Otago Schist. This differentiation could develop by a mass migration over a scale of only 0.5 to 1 m resulting in alternating quartz (Q) and mica rich (P) layers. This would imply a volume loss for the mica rich layers while in a local scale that includes P and Q layers there would be no volume change. This is the reason why we have to distinguish between two components of mass transfer $S_{V\,m}$ in the rocks. Mass transfer that is associated with a "closed system" differentiation of mica and quartz rich layers and a component of mass transfer in an "open system" where material is really removed out of the system.

This shows that volume strain has to be treated critically. The amount of volume loss in our samples due to compaction S_{Vp} is unknown. Paterson et al. (Paterson et al. 1995) e.g. measured clay fabric orientations in rocks from ODP Hole 808c, located in the toe of the Nankai accretionary prism and from Deep Sea Core 174A from the distal Astoria Fan. The calculated volume loss, that is assumed to be entirely due to compaction, range between 3 to 58%. This variability partly seems to depend on different quartz-feldspar contents in the samples (Paterson et al. 1995). This explains how difficult it is to subtract porosity loss from

total volume strain to get the tectonic volume strain and associated mass transfer that affected the samples we measured in the Otago Schist. The problem is that March strains cannot be used directly to make a distinction between a reorientation of the phyllosilicate grains due to porosity loss or due to a solution mass transfer (SMT) of silica out of the examined area. Summarising, March strains in this study can be used to determine total volume strain and to describe the symmetry of finite strain. A predication about the composition of volume strain is so far not possible.

Using the calculated volume loss in the pelitic layers of our study to comment on mass transfer S_{Vm} within the Torlesse or out off the wedge, remains difficult because of the problems outlined above. S_V due to mass loss cannot be quantified due to the lack of information on porosity changes during compaction. Nonetheless, it is at least possible to make a vague estimate of S_{Vm}. Directed absolute strain measurements in meta sandstones of the Otago Schist indicate a volume stretch of $S_V = 0.8$ This volume loss of 20% is due to the loss of silica in the sandstones caused by pressure solution. It is therefore a direct measure of S_{Vm}. Pressure solution is a grain size sensitive deformation process (Spiers et al. 1990) also active in our examined pelitic rocks. Pressure Solution is enhanced in rocks with smaller grain size. Thus, compared to the coarser sandstones, a lower volume stretch of 0.38 determined in the pelitic rocks, seems reasonable. Assuming S_{Vm} in the meta sandstones as the minimum amount of mass transfer also in the pelitic rocks, would suggest S_{Vm} to range between 0.8 and 0.38. This range displays the unknown amount of volume change due to compaction. Unfortunately our data comprise no information to distinguish between open and closed-system mass transfer in the wedge.

Conclusion

This paper uses finite deviatoric strain measurements in phyllosilicate-rich rocks to comment on the shear coupling behaviour and tectonic evolution of the Torlesse subduction wedge. The Torlesse wedge is a common thick, sediment-rich subduction wedge and therefore results should also have general implications for other similar accretionary wedges.

The most important conclusion of this study is the strong decoupling between the Torlesse wedge and the down-going plate. Low shear strains measured in rocks accreted to the wedge by underplating, compared to theoretically expected shear strains, that are calculated by using a geometric shear zone model, do not justify a strong coupling. This result contrasts to models that assume strong shearing within tectonic wedges. The fact, that shear strains recorded in phyllosilicate-rich rocks were used to define the degree of coupling, prove the idea wrong, that shearing within a wedge should be accumulated in weaker mudstone

layers. This has been often postulated for accretionary wedges in which deformation examined in sandstone layers showed no significant prove of strong shearing.

Tensor average results of absolute strain data indicate no stretch along S_X, that is oriented parallel to the Gondwana margin. S_Y is characterised by slight shortening normal to the margin, while S_Z takes up strong subvertical shortening of 58%. Thus, deformation in the Torlesse wedge can be described as constrictional plane strain. The strong vertical contraction is accommodated by significant volume loss that hinders orogen-parallel extension. This contrasts to geodynamic models that suggest an orogen parallel evasion of material in convergent tectonic scenarios.

Average volume loss of up to 62% in the analysed samples is huge and certainly plays an important role in the deformation of the Torlesse wedge, as it compensates the strong vertical uniaxial contraction. The amount of volume strain related to compaction is not easy to determine and may range between c. 0-40%. Until now it is not possible to relate the results of single samples to a volume loss that is valid for the whole wedge. Material transport from phyllosilicate-rich layers to quartz dominated domains in higher grad rocks, or solution mass transfer into quartz veins are both processes that contribute to a strong volume loss in mudstones but do not essentially imply a total volume loss within the wedge. Future geochemical analysis should help to distinguish between “closed system” mass transfer and an “open system” movement of material out of an accretionary wedge.

References

Adams, C. J. & Gabites, J. E. 1985. Age of metamorphism and uplift of the Haast Schist Group at Haast Pass, Lake Wanaka and Lake Hawea, South Island, New Zealand. *New Zealand Journal of Geology and Geophysiscs* 28, 85-96.

Adams, C., and Raine, J., 1988, Age of Cretaceous silicic volcanism at Kyeburn, Central Otago, and Palmerston, eastern Otago, South Island, New Zealand: *New Zealand Journal of Geology and Geophysics* 31, 471-475.

Adams, C. J. & Robinson, P. 1993. Potassium-Argon age studies of metamorphism/ uplift/ cooling in Haast Schist coastal sections of Dunedin, Otago, New Zealand. *New Zealand Journal of Geology and Geophysiscs* 36, 317-325.

Behrmann, J., Brown, K., Moore, C., Mascle, A., Taylor, E., Alvarez, F., Andreieff, P., Barnes, R., Beck, C., Blanc-Gerard, Clark, M., Dolan, J. F., Fisher, A., Gieskes, J., Hounslow, M. W., McLellan, P., Moran, K., Ogawa, Y., Sakai, T., Schoonmaker, J., Vrolijk, P., Wilkens, R. H. & Williams, C. F. 1988. Evolution of structures and fabrics in the Barbados accretionary prism; insights from Leg 110 of the Ocean Drilling Program. *Journal of Structural Geology* 10, 577-591.

Benett, R. H., Bryant, W. R. & Keller, G. H. 1981. Clay fabrics of selected submarine sediments. *Journal of Sedimentary Petrology* 51, 217-231.

Bishop, D. G. 1972a. Progressive metamorphism from prehnite-pumpellyite to greenschist facies in the Dansey Pass area, Otago, New Zealand. *Geol.Soc.Am. Bull*. 83, 3177-3198.

Bishop, D. G. 1994. Extent and regional deformation of the Otago peneplain. Institute of Geological & Nuclear Sciences, Lower Hutt, New Zealand.

Bowles, F. A., Bryant, W. R. & Wallin, C. 1969. Microstructure of unconsolidated and consolidated marine structures. *Journal of Sedimentary Petrology* 39, 1546-1551.

Bradshaw, J., Weaver, S. & Muir, R. 1996. Mid Cretaceous oroclinal bending of New Zealand terranes. *New Zealand Journal of Geology and Geophysiscs* 39, 461-468.

Brandon, M. T. 1995. Analysis of geologic strain data in strain-magnitude space. J*ournal of Structural Geology* 17, 1375-1385.

Brandon, M. T., Roden-Tice, M. K. & Garver, J. I. 1998. Late Cenozoic exhumation of the Cascadia accretionary wedge in the Olympic Mountains, NW Washington State. *Geological Society of America Bulletin* 110, 985-1009.

Cooper, E. K. 1995. Petrofabric studies across the Caples/Torlesse terrane boundary, Otago Schist, New Zealand. Unpublished Master thesis, University of Canterbury.

Craig, J., Fitches, W. R. & Maltman, A. J. 1982. Chlorite-mica stacks in low-strain rocks from central Wales. *Geological Magazine* 119, 243-256.

Crampton, J., Schioler, P., King, P. & Field, B. 1999. Marine Expression of the complex Cretaceous Waipounamu erosion surface in the east coast region, New Zealand. *Geological Society of New Zealand Miscellaneous Publications* 107A, 34.

Deckert, H., Ring, U. & Mortimer, N. 2002. Tectonic significance of Cretaceous bivergent extensional shear zones in the Torlesse accretionary wedge, central Otago Schist, New Zealand. *New Zealand Journal of Geology and Geophysics* 45, 537-547.

England, P. C. 1981. Metamorphic pressure estimates and sediment volumes for the Alpine orogeny: an independent control on geobarometers? *Earth Planetary Sciences Letters* 56, 387-397.

Feehan, J. G. & Brandon, M. T. 1999. Contribution of ductile flow to exhumation of low-temperature, high pressure metamorphic rocks: San Juan-Cascade nappes, NW Washington State. *Journal of Geophysical Research* 104, 10883-10902.

Fisher, A. T. & Hounslow, M. W. 1990. Transient fluid flow through the toe of the Barbados accretionary complex; constraints from Ocean Drilling Program Leg 110 heat flow studies and simple models. *Journal of Geophysical Research* 95, 8845-8858.

Hurford, A.J., 1986. Cooling and uplift patterns in the Lepontine Alps, south central Switzerland, and an age of vertical movement on the Insubric fault line. C*ontributions to Mineralogy and Petrology* 92, 413-427.

Hutton, C. O. & Turner, F. J. 1936. Metamorphic zones in north-west Otago. *Transactions of the Royal Society of New Zealand* 65, 405-406.

Kamp, P. J. J. 1986. Late Cretaceous-Cenozoic tectonic development of the southwest Pacific region. *Tectonophysics* 121, 225-251.

Korsch, R. J. & Wellman, H. W. 1988. The geological evolution of New Zealand and the New Zealand region. In: The Ocean Basins and Margins (edited by Nairn, A. E. M., Stehli, F. G. & Uyeda, S.) 7B. Plenum Publishing Corporation, 411-482.

Kukowski, N., Schillhorn, T., Huhn, K., von Rad, U., Husen, S. & Flueh, E. 2001. Morphotectonics and mechanics of the central Makran accretionary wedge off Pakistan. *Marine Geology* 173, 1-19.

Kumerics, C. 2001. Verformungsanalyse an Metagrauwacken im Torlesse Terrane, Otago, Neuseeland. Unpublished diploma thesis, Universität Mainz.

LeMasurier, W. E. & Landis, C. A. 1996. Mantle-plume activity recorded by low-relief erosion surfaces in West Antarctica and New Zealand. *Geological Society of America Bulletin* 108, 1450-1466.

Little, T. A., Mortimer, N. & McWilliams, M. 1999. An episodic Cretaceous cooling model for the Otago-Marlborough Schist, New Zealand, based on 40 Ar/39Ar white mica ages. *New Zealand Journal of Geology and Geophysiscs* 42, 305-325.

Lüneburg, C. M., Lampert, S. A., Lebit, H. D., Hirt, A. M., Casey, M. & Lowrie, W. 1999. Magnetic anisotropy, rock fabrics and finite strain in deformed sediments of SW Sardinia (Italy). *Tectonophysics* 307, 51-74.

MacKinnon, T. C. 1983. Origin of the Torlesse terrane and coeval rocks, South Island, New Zealand. *Geol.Soc.Am.Bull*. 94, 967-985.

Maltman, A. J. 1981. Primary bedding-parallel fabrics in structural geology. *Journal Geological Society London* 138, 475-483.

March, A. 1932. Mathematische Theorie der Regelung nach der Korngestalt bei affiner Deformation. *Zeitschrift für Kristallographie* 81, 285-297.

Maxelon, M., Wohlers, A., Halama, R., Ring, U., Mortimer, N. & Brandon, M. T. 1998. Ductile strain in the Torlesse wedge, South Island, New Zealand. Eos 79(45), 889.

Moon, C. F. 1972. The microstructure of clay sediments. *Earth Science Review* 8, 303-321.

Moore, J. C. 1979. Variation in strain and strain rate during underthrusting of trench deposits. *Geology* 7, 185-188.

Mortimer, N. 1993a. Geology of the Otago Schist and adjacent rocks. Institute of Geological & Nuclear Sciences, Lower Hutt, New Zealand.

Mortimer, N. 1993b. Jurassic tectonic history of the Otago Schist, New Zealand. *Tectonics* 12, 237-244.

Mortimer, N. 2000. Metamorphic discontinuities in orogenic belts: example of the garnet-biotite-albite zone in the Otago Schist, New Zealand. *International Journal of Earth Sciences* 89, 295-306.

Mortimer, N. 2001. Foliation thickness and mica grain size: two new ways to subdivide the Otago Schist, New Zealand. In: *Proceedings of the 34th Annual Conference, Dunedin*. New Zealand Branch. Australasian Institute of Mining & Metallurgy, 43-49.

Mortimer, N. & Campell, H. J. 1996. Devonian to Jurassic rocks in New Zealand: classification, content and Gondwana context. In: *Gondwana Nine*. (edited by Guha, P. K. S., Sengupta, S., Ayyasami, K. & Gosh, R. N.). IBH Publishing, New Delhi, Oxford, 783-790.

Mortimer, N., Tulloch, A. J., Spark, R. N., Walker, N. W., Ladley, E., Allibone, A. & Kimbrough, D. C. 1999. Overview of the Median Batholith New Zealand: a new interpretation of the geology of the Median Tectonic Zone and adjacent rocks. *J.African.Earth Sci*. 29, 257-268.

Nicot, E. 1981. Les phyllosilicates des terrains précambriens du Nord-Ouest du Montana (USA) dans la transition anchizone-epizone. *Bulletin Mineralogie* 104, 615-624.

Norris, R. J. & Bishop, D. G. 1990. Deformed metaconglomerates and textural zones in the Otago Schists, South Island, New Zealand. *Tectonophysics* 174, 331-349.

Oertel, G. 1970. Deformation of a slaty, lapillar tuff in the Lake District, England. *Geological Society of America Bulletin* 81, 1173-1188.

Oertel, G. 1983. The relationship of strain and preferred orientation of phyllosilicate grains in rocks-a review. *Tectonophysics* 100, 413-447.

Oertel, G. 1985. Relationship of Strain and preferred orientation of phyllosilicates in rocks. In: Preferred orientation in metals and rocks. (edited by Wenk, H.-R.). Academic Press.

Oliver, P. J., Campell, J. D. & Spede, I. G. 1982. The stratigraphy of the Torlesse rocks of the Mt Somers area (S81) mid-Canterbury. *Journal of the Royal Society of New Zealand* 12, 243-271.

Owens, W. H. 1973. Strain modification of angular density distributions. *Tectonophysics* 16, 249-261.

Page, R. H. 1980. Partial interlay in phyllosilicates studied by transmission electron microscopy. *Contributions Mineralogy Petrology* 75(309-314).

Page, R. H. & Wenk, H. R. 1979. Phyllosilicate alteration of plagioclase studied by transmission electron microscopy. *Geology* 7, 393-391.

Paterson, S. R., Yu, H. & Oertel, G. 1995. Primary and tectonic fabric intensities in mudrocks. *Tectonophysics* 247, 105-119.

Peacock, S. M. 1996. Thermal and Petrologic Structure of Subduction Zones. In: Subduction - Top to Bottom (edited by Bebout, G. E., Scholl, D. W., Kirby, S. H. & Platt, J. P.). *Geophysical Monograph* 96. American Geophysical Union, Washington, 119-133.

Platt, J. P. 1986. Dynamics of orogenic wedges and the uplift of high-pressure metamorphic rocks. *Geological Society of America Bulletin* 97, 1037-1053.

Platt, J. P. 1993. Exhumation of high-pressure rocks: a review of concepts and processes. *Terra Nova* 5, 119-133.

Press, W.H., Flannery, B.P., Teukolsky, S.A., and Vetterling, W.T., 1986, Numerical recipes. Cambridge, England, Cambridge University Press 818 p.

Ramsay, J. G. 1967. Folding and fracturing of rocks. McGraw-Hill, New York.

Ramsay, J. G., Casey, M. & Kligfield, R. 1983. Role of shear in development of the Helvetic fold-thrust belt of Switzerland. *Geology* 11, 439-442.

Rahl, J. M., Deckert, H., Brandon, M. T., Mortimer, N. & Ring, U. 2003. Regional mass-transfer deformation and three-dimensional flow in a Mesozoic subduction wedge, Otago, New Zealand. *Journal of Structural Geology* to be submitted.

Ring, U. & Brandon, M. T. 1999. Ductile deformation and mass loss in the Franciscan subduction complex: implications for exhumation processes in accretionary wedges. In: Exhumation Processes: Normal faulting, ductile flow and erosion. (edited by Ring, U., Brandon, M. T., Lister, G. S. & Willett, S. D.) 154. *Special Publications of the Geological Society, London*, 55-86.

Selverstone, J. 1985. Petrologic constraints on imbrication, metamorphism and uplift in the SW Tauern Window, Eastern Alps. *Tectonics* 4, 687-704.

Spiers, C. J., Schutjens, P. M., Brzesowsky, R. H., Liezenberg, J. L. & Zwart, H. J. 1990. Experimental determination of constitutive parameters governing creep of rocksalt by pressure solution. In: Deformation Mechanisms, Rheology and Tectonics (edited by Knipe, R. J. & Rutter, E. H.) 54. Geological Society of London Special Publication, 215-227.

Tullis, T. E. & Wood, D. S. 1975. Correlation of finite strain from both reduction bodies and preferred orientation of mica in slate from Wales. *Tectonophysics* 78, 291-306.

Turnbull, I. M., Mortimer, N. & Craw, D. 2001. Textural zones in the Haast Schist - a reappraisal. *New Zealand Journal of Geology & Geophysics* 44, 171-183.

Turnbull, I. M. c. 2000. Geology of the Wakatipu area. Institute of Geological & Nuclear Sciences, Lower Hutt, New Zealand.

Wallis, S. R., Platt, J. P. & Knott, S. D. 1993. Recognition of syn-convergence extension in accretionary wedges with examples from the Calabrian arc and the Eastern Alps. *American Journal of Science* 293, 463-495.

Wood, D. S. & Oertel, G. 1980. Deformation in the Cambrian slate belt of Wales. *Journal of Geology* 88, 309-326.

Yardley, B. W. D. 1982. The early metamorphic history of the Haast Schists and related rocks of New Zealand. *Contributions Mineralogy Petrology* 81, 317-327.

Table 1. Comparison of Muscovite and Chlorite measurements

		Extension			Intermediate			Shortening				
No.		tr.	pl	S'_X	tr.	pl.	S'_Y	tr.	pl.	S'_Z	int.	TZ
2	muscovite	115	60	1.58	287	30	1.14	19	4	0.56	4.19	1
	chlorite	113	57	1.73	289	33	1.26	20	1	0.46	2.90	
5	muscovite	95	28	2.83	187	3	0.77	283	61	0.46	3.38	2
	chlorite	95	29	2.75	188	5	0.76	287	60	0.48	2.01	
37	muscovite	227	43	2.20	123	14	1.79	20	43	0.25	1.44	4
	chlorite	225	47	2.11	122	12	1.39	23	40	0.34	1.44	
58	muscovite	226	47	2.16	321	4	1.39	54	39	0.33	1.07	4
	chlorite	227	47	2.10	321	4	1.34	54	40	0.35	1.70	

tr. and pl. indicate trend and plunge. Int. is the uniform intensity [cps] and TZ marks the different textural zones.

Table 2. Principal stretches

	Extension			Intermediate			Shortening								Foliation		Lineation		Coordinates		
No.	tr.	pl	S'_X	tr.	pl.	S'_Y	tr.	pl.	S'_Z	γ_{oct}	TZ	R_{XZ}	γ_{XZ}	□	□ BA	tr.	pl.	tr.	pl.	Map	East	North
1	92	66	1.96	244	22	0.92	338	10	0.55	1.27	1	3.54	1.35		0	350	89	--	--	H39	501	328
2	115	60	1.58	287	30	1.14	19	7	0.56	1.01	1	2.85	1.10		0	200	89	--	--	G39	491	328
3	181	18	1.51	86	17	1.22	315	65	0.55	1.01	2	2.76	1.06		52	107	21	170	12	E40	487	110
4	157	8	2.19	247	0	1.51	339	82	0.30	2.85	2	7.19	2.31		0	105	8	119	7	F44	905	964
5	95	28	2.83	187	3	0.77	283	61	0.46	2.33	2	6.16	2.08		22	108	32	102	29	G39	192	237
6	137	8	2.10	39	45	1.64	235	44	0.29	2.99	2	7.24	2.32		22	68	47	128	27	E42	512	573
7	160	1	2.22	68	67	0.99	250	23	0.45	1.77	2	4.9	1.76		35	72	67	--	--	E42	462	545
8	136	8	2.04	228	17	1.73	17	72	0.28	3.07	2	7.19	2.31		52	202	22	291	2	E41	462	863
9	41	4	1.99	131	4	1.09	267	84	0.46	1.57	2	4.32	1.60		22	117	5	30	0	E41	686	652
10	300	26	2.03	201	17	1.30	81	58	0.38	2.04	2	5.36	1.88		0	--	--	--	--	E43	641	261
11	200	22	2.09	301	25	1.48	74	57	0.32	2.56	2	6.45	2.15		0	--	--	--	--	F43	726	184
12	261	32	1.85	166	8	1.77	64	57	0.31	2.71	2	6.05	2.05		0	--	--	--	--	F43	726	184
13	166	9	1.82	73	18	1.27	282	70	0.43	1.60	2	4.2	1.56		0	--	--	--	--	E43	670	119
	138	3	1.55	48	1	1.20	300	87	0.54							tensor average TZ2 (restored)						
14	312	32	2.70	79	45	0.86	202	29	0.43	2.31	3	6.3	2.11		52	34	65	317	26	E40	348	989
15	15	5	2.00	106	12	0.93	261	77	0.54	1.33	3	3.71	1.41		0	115	20	36	4	F41	804	641
16	157	15	2.73	64	8	0.98	307	73	0.37	2.64	3	7.32	2.34		0	156	15	--	--	F41	797	642
17	249	13	2.50	155	15	1.66	18	70	0.24	4.12	3	10.4	2.91		0	200	30	--	--	F41	788	675
18	323	4	2.28	219	73	0.73	54	15	0.61	1.50	3	3.76	1.42		0	22	13	32	11	F41	795	654
19	9	10	2.58	278	9	1.07	147	76	0.36	2.58	3	7.15	2.30		0	50	18	--	--	I42	216	346
20	13	13	1.99	105	6	0.94	221	76	0.54	1.33	3	3.71	1.41		0	44	19	--	--	I43	196	267
21	236	28	2.05	143	6	1.30	42	61	0.38	2.09	3	5.48	1.91		22	237	30	237	30	E41	652	692
22	214	5	2.03	124	4	0.96	354	83	0.51	1.43	3	3.99	1.50		22	155	15	212	8	E41	691	672
23	264	44	1.76	171	3	1.34	77	46	0.42	1.62	3	4.15	1.55		22	235	15	290	43	E41	653	693
24	211	13	1.92	119	9	1.55	354	74	0.34	2.36	3	5.71	1.97		0	180	13	213	11	F41	707	632
25	9	15	1.62	274	15	1.28	140	68	0.48	1.29	3	3.37	1.29		0	267	22	219	15	F42	756	444
26	248	8	2.21	156	17	0.97	4	71	0.47	1.71	3	4.73	1.72		22	182	23	243	12	E41	682	671
27	207	20	1.80	116	2	1.35	20	70	0.41	1.72	3	4.38	1.61		22	212	18	83	6	E41	650	641
	197	10	1.56	288	4	1.24	41	79	0.52							tensor average TZ3 (restored)						
28	273	37	3.04	57	47	0.67	168	19	0.49	2.47	4	6.16	2.08		0	340	64	--	--	I 44	915	829
29	119	33	1.91	350	44	1.30	229	28	0.41	1.80	4	4.7	1.71		0	58	62	--	--	H44	867	860
30	77	27	1.88	233	60	1.24	341	10	0.43	1.65	4	4.39	1.62		0	60	40	--	--	H44	803	972
31	167	15	2.17	265	29	0.99	53	57	0.46	1.69	4	4.69	1.70		0	239	35	--	--	H43	835	59
32	172	21	2.05	284	45	0.98	65	37	0.50	1.47	4	4.1	1.53		0	235	35	--	--	H43	839	95

	Principal Stretches														Foliation		Lineation		Coordinates		
	Extension			Intermediate			Shortening														
No.	tr.	pl	S'_X	tr.	pl.	S'_Y	tr.	pl.	S'_Z	γ_{oct}	TZ	R_{XZ}	γ_{XZ}	□	□ BA	tr.	pl.	tr.	pl.	Map	East	North
33	319	11	2.07	49	1	0.99	144	79	0.49	1.52	4	4.21	1.57		0	274	4	--	--	I43	976	199
34	203	20	2.49	112	2	1.38	18	69	0.29	3.23	4	8.6	2.59		0	165	16	242	3	F41	758	670
35	246	6	2.33	154	17	0.99	356	73	0.43	1.95	4	5.37	1.89		0	185	21	242	11	F41	762	674
36	199	14	2.16	104	19	1.31	322	66	0.35	2.31	4	6.1	2.06		0	145	20	--	--	F41	768	680
37	227	43	2.20	123	14	1.79	20	43	0.25	3.67	4	8.67	2.61		0	202	49	272	20	F41	782	687
38	76	22	2.02	171	12	1.25	289	65	0.40	1.91	4	5.09	1.81		52	120	25	80	20	F39	754	268
39	17	10	2.55	284	18	1.23	134	70	0.32	2.93	4	8	2.47		0	320	19	1	9	G41	143	728
40	108	0	3.08	19	16	1.25	194	74	0.26	4.29	4	11.9	3.16		0	212	13	290	1	G41	160	754
41	263	41	1.51	156	19	1.29	47	44	0.52	1.12	4	2.93	1.13		22	236	45	255	43	F41	820	786
42	336	5	2.18	241	48	1.71	71	41	0.27	3.40	4	8.17	2.51		22	251	45	274	42	F41	788	855
43	281	39	1.68	169	24	1.24	56	42	0.48	1.30	4	3.47	1.33		22	241	45	241	45	F41	793	831
44	23	13	1.70	287	19	1.28	145	66	0.46	1.41	4	3.69	1.40		0	334	29	23	19	G41	127	686
45	14	14	2.21	120	47	1.08	274	40	0.42	1.92	4	5.27	1.86		35	86	50	8	15	F39	63	348
46	111	24	2.29	17	8	1.18	269	64	0.37	2.28	4	6.19	2.09		35	68	30	38	26	F40	920	87
47	169	10	1.76	264	25	1.30	60	64	0.44	1.55	4	4.04	1.51		0	207	12	169	10	F41	869	805
48	261	16	1.84	12	52	0.92	160	34	0.59	1.10	4	3.1	1.19		0	312	38	240	14	G41	367	764
49	271	24	2.32	2	3	1.45	99	66	0.30	2.99	4	7.77	2.43		35	275	19	282	18	E41	696	845
50	213	21	2.11	306	7	1.55	53	68	0.31	2.79	4	6.93	2.25		35	230	11	228	11	F41	720	888
51	196	27	2.34	308	38	1.45	81	39	0.30	3.05	4	7.9	2.45		22	263	60	300	52	F41	815	782
52	205	55	1.77	318	16	1.25	58	31	0.45	1.48	4	3.92	1.47		22	237	51	200	45	F41	820	786
53	294	34	1.74	172	38	1.35	51	33	0.42	1.62	4	4.11	1.54		22	231	52	276	42	F41	820	786
54	179	35	2.87	271	3	1.41	7	53	0.25	4.28	4	11.6	3.11		0	190	32	194	30	G41	188	607
55	236	16	2.45	139	21	1.22	0	63	0.34	2.68	4	7.28	2.33		0	188	31	234	23	F41	948	669
56	197	28	1.94	301	25	1.30	65	51	0.40	1.87	4	4.87	1.75		0	245	35	195	15	F41	998	707
57	302	34	2.00	189	30	1.23	69	41	0.41	1.84	4	4.91	1.76		22	250	50	297	39	F41	802	775
58	226	50	2.16	321	4	1.39	54	39	0.33	2.50	4	6.47	2.15		22	256	54	--	--	E41	583	620
59	173	4	1.73	265	32	1.58	78	57	0.37	2.02	4	4.71	1.71		35	272	30	258	28	E41	696	845
60	343	18	2.47	78	16	1.42	207	66	0.29	3.28	4	8.66	2.60		0	42	22	347	13	G41	135	628
61	73	2	2.09	164	24	1.66	336	66	0.29	3.04	4	7.3	2.33		22	167	11	244	3	E41	683	716
	127	1	1.40	217	23	1.27	36	67	0.56							tensor average TZ4 (restored)						
	159	7	1.40	251	15	1.24	46	74	0.58							tensor average unrestored (all data)						
	139	5	1.38	231	15	1.25	33	74	0.58							tensor average restored (all data)						

tr. and pl. indicate trend and plunge. γ_{oct} is the conventional octahedral shear strain, TZ marks the different textural zones. BA bending angle, ie. amount of rotation due to Mid-Cretaceous bending (see text).

Table 3. Restored Mesozoic stretching directions

	Extension		Intermediate		Shortening	
#	tr.	pl.	tr.	pl.	tr.	pl.
1	92	66	244	22	338	10
2	115	60	287	30	19	7
3	129	18	34	17	263	65
4	157	8	247	0	339	82
5	73	28	165	3	261	61
6	115	8	17	45	213	44
7	125	1	33	67	215	23
8	84	8	176	17	325	72
9	19	4	109	4	244	84
10	300	26	201	17	81	58
11	200	22	301	25	74	57
12	261	32	166	8	64	57
13	166	9	73	18	282	70
14	260	32	27	45	150	29
15	15	5	106	12	261	77
16	157	15	64	8	307	73
17	249	13	155	15	18	70
18	323	4	219	73	54	15
19	9	10	278	9	147	76
20	13	13	105	6	221	76
21	214	28	121	6	20	61
22	192	5	102	4	332	83
23	242	44	148	3	55	46
24	211	13	119	9	354	74
25	9	15	274	15	140	68
26	226	8	134	17	342	71
27	185	20	94	2	358	70
28	273	37	57	47	168	19
29	119	33	350	44	229	28
30	77	27	233	60	341	10
31	167	15	265	29	53	57
32	172	21	284	45	65	37
33	319	11	49	1	144	79
34	203	20	112	2	18	69
35	246	6	154	17	356	73
36	199	14	104	19	322	66
37	227	43	123	14	20	43
38	24	22	119	12	237	65
39	17	10	284	18	134	70
40	108	0	19	16	194	74
41	241	41	134	19	25	44
42	314	5	219	48	49	41
43	259	39	147	24	34	42
44	23	13	287	19	145	66
45	339	14	85	47	239	40
46	76	24	342	8	234	64
47	169	10	264	25	60	64
48	261	16	12	52	160	34
49	236	24	327	3	64	66
50	178	21	271	7	18	68
51	174	27	286	38	59	39
52	183	55	296	16	36	31
53	272	34	150	38	29	33
54	179	35	271	3	7	53
55	236	16	139	21	0	63
56	197	28	301	25	65	51
57	280	34	167	30	47	41
58	204	50	299	4	35	39
59	138	4	230	32	43	57
60	343	18	78	16	207	66
61	51	2	142	24	314	66

Table 4: Strain data of Norris & Bishop (1990) assuming isochoric flow.

	Deviatoric stretches						
Sample	S'_X	S'_Y	S'_Z	R_{XZ}	γ_{oct}	TZ	clast
OU51976	1.09	1.00	0.91	0.91	1.20	1	lithic
OU51976	1.06	1.02	0.92	0.47	1.15	1	quartzose
OU51979	1.41	1.27	0.56	0.13	2.50	2	lithic
OU51979	1.21	1.10	0.76	0.26	1.60	2	quartzose
OU51981	1.41	1.24	0.57	0.17	2.45	2	lithic
OU51981	1.20	1.04	0.80	0.55	1.50	2	quartzose
OU51982	1.73	1.11	0.52	0.58	3.34	2	lithic
OU51983	1.87	1.10	0.49	0.66	3.85	2	lithic
OU51983	1.27	1.02	0.77	0.80	1.65	2	quartzose
OU51985	2.03	1.02	0.48	0.93	4.20	2	lithic
OU51985	1.39	0.93	0.77	2.22	1.80	2	quartzose
OU51986	1.60	1.52	0.41	0.04	3.90	2	lithic
OU51986	1.23	1.16	0.70	0.12	1.75	2	quartzose
OU51987	1.78	1.19	0.47	0.44	3.75	2	lithic
OU51987	1.39	1.04	0.69	0.71	2.00	2	quartzose
OU51991	1.81	1.13	0.49	0.57	3.70	2	lithic
OU51988	2.57	1.36	0.29	0.41	9.00	2	lithic
OU51988	1.75	1.04	0.55	0.81	3.20	2	quartzose
OU51989	3.55	0.99	0.28	1.02	12.50	3	lithic
OU51989	1.94	0.85	0.61	2.46	3.20	3	quartzose
OU51993	3.25	1.20	0.26	0.64	12.70	3	lithic
OU51994	3.67	1.00	0.27	0.99	13.50	3	lithic
Hw	4.01	1.00	0.25	1.00	16.10	3	lithic
OU51978	3.60	1.08	0.26	0.84	14.00	3	lithic
OU51980	2.83	1.16	0.30	0.67	9.30	3	lithic
OU51980	1.82	0.94	0.59	1.41	3.10	3	quartzose
OU51990	3.23	1.27	0.24	0.56	13.30	4	lithic
OU51992	3.76	1.35	0.20	0.54	19.00	4	lithic

Tectonic significance of Cretaceous bivergent extensional shear zones in the Torlesse accretionary wedge, central Otago Schist, New Zealand

Hagen Deckert[a], Uwe Ring[a] & Nick Mortimer[b]

[a] Institut für Geowissenschaften, Johannes Gutenberg-Universität, 55099 Mainz, Germany
[b] Institute of Geological and Nuclear Sciences, Private Bag 1930, Dunedin, New Zealand

This chapter is identical with a manuscript published in December 2002. "Deckert, H, Ring, U. & Mortimer, N. 2002. Tectonic significance of Cretaceous bivergent extensional shear zones in the Torlesse accretionary wedge, Central Otago Schist, New Zealand. *New Zealand Journal of Geology and Geophysics* 45, 537-54."

Abstract We describe two shear zones in the Otago Schist of the Torlesse accretionary wedge, South Island, New Zealand: the north-dipping Rise-and-Shine Shear Zone (RSSZ) and the south-dipping Cromwell Gorge Shear Zone (CGSZ). Kinematic indicators (shear bands and asymmetric folds) indicate top-north movement for the RSSZ and top-south transport for the CGSZ. Backrotation of the shear zones into their Late Cretaceous orientation and consideration of the relationship of the shear zones to arching of the Otago Schist shows that both shear zones are extensional. Offset of textural zones suggests up to 15 km of dip-slip displacement on the RSSZ and probably a similar amount of slip for the CGSZ. We speculate that the gold-mineralised RSSZ may be the western continuation of the Late Mesozoic gold-bearing Hyde-Macraes Shear Zone in eastern Otago forming a c. 100 km long extensional shear zone on the northern flank of the Otago Schist. Age constraints suggest that shear zone formation took place between 135 and 105 Ma. The shear zones aided the final exhumation of the deeper parts of the Otago Schist. We discuss whether normal shearing is related to syn-orogenic supercritical tapering of the Torlesse wedge, or due to post-orogenic New Zealand-wide Albian rifting.

Introduction

The role of syn-orogenic normal faulting in ancient and modern accretionary wedges related to ocean-continent subduction remains a controversial topic. The Hikurangi subduction zone in the North Island of New Zealand is an example where orogen-parallel extensional faults occur in the forearc (Pettinga 1982; Walcott 1987). However, the magnitude of extension accommodated by the listric normal faults is only 1-5% (Cashman & Kelsey 1990). Syn-orogenic normal faulting has also been proposed along the so-called Coast Range fault of the Franciscan subduction complex (Platt 1986; Harms et al. 1992). The tectonic juxtaposition of low-grade rocks above higher grade rocks was used as the major evidence for normal faulting. But subsequent work by Wheeler & Butler (1994), Ring & Brandon (1994) and Ring (1995) showed that this evidence is not conclusive, and Ring & Brandon (1994, 1999), and Bolhar & Ring (2001) showed that the Coast Range fault is an out-of-sequence thrust. Other well-studied accretionary wedges such as the Olympic subduction complex at the North American west coast also show no evidence for normal faulting (Brandon et al. 1998).

Frontal accretion and erosion both tend to promote horizontal contraction across an orogen. This case is well illustrated by the strain calculations in Dahlen & Suppe (1988). Horizontal extension may occur in the rear part of an accretionary wedge thickened by underplating (Platt 1986). But horizontal extension need not necessarily be expressed by normal faulting in the upper rear part of the wedge; it may also be accommodated by vertical ductile thinning related to a subhorizontal foliation. Thus a large amount of vertical ductile thinning tends to suppress normal faulting. Flow fields that give rise to horizontal extension in the rear of accretionary wedges develop when the rate of frontal accretion and erosion at the rear of the wedge are small, and when the rate of underplating is dominantly controlling the flow field in the wedge (Platt 1986, 1993; Brandon & Fletcher 1998).

Before c. 105 Ma, the New Zealand part of the south Gondwana margin was a subduction zone along which continental growth took place by terrane accretion and arc-related magmatism (Mortimer et al. 1999) (Fig. 1A). The older Torlesse (Rakaia) Terrane and the Caples Terrane comprise greywacke of Permian-Triassic stratigraphic age and are thought to have been deformed in a Jurassic-Cretaceous accretionary wedge (MacKinnon 1983; Korsch & Wellman 1988). Albian (c. 105 Ma) graben development (Ballance 1993; Laird 1993) is related to the separation of New Zealand from Australia and Antarctica. This post-subduction rifting phase culminated in seafloor spreading in the Tasman Sea at c. 85 Ma (e.g. Korsch & Wellman 1988).

In this paper we present new field and petrographic data from the Rise-and-Shine and Cromwell Gorge Shear Zones (RSSZ, CGSZ) in the Torlesse accretionary wedge of central Otago. The RSSZ and also the Hyde-Macraes Shear Zone of eastern Otago (Fig. 1B) have

previously been regarded as late subduction-related thrusts (e.g., Teagle et al. 1990; Winsor 1991). Nonetheless, our data show that the RSSZ and the CGSZ are net normal-sense shear zones. The age of shear zone formation is not well constrained, which makes it speculative to relate normal shearing to either late-accretionary destabilisation of the Torlesse wedge during ongoing convergence or to post-accretionary rifting.

Geological setting

The terranes of the South Island of New Zealand can be divided into two major provinces (Fig. 1A). (1) The Western Province, consisting of Cambrian-Devonian terranes with local Permian-Triassic sedimentary cover, are considered to have been part of Gondwana since the mid-Paleozoic (Mortimer & Campbell 1996). (2) The Eastern Province, consisting of Carboniferous-Cretaceous terranes, is interpreted to have been accreted to the Gondwana margin from the Triassic through the Cretaceous (e.g. MacKinnon 1983; Korsch & Wellman 1988; Mortimer & Campbell 1996). The two provinces are separated by the Median Batholith (Mortimer et al. 1999; Turnbull 2000), a Cordilleran-type magmatic arc that represents the major locus of Carboniferous to Early Cretaceous magmatism in New Zealand. Magmatic

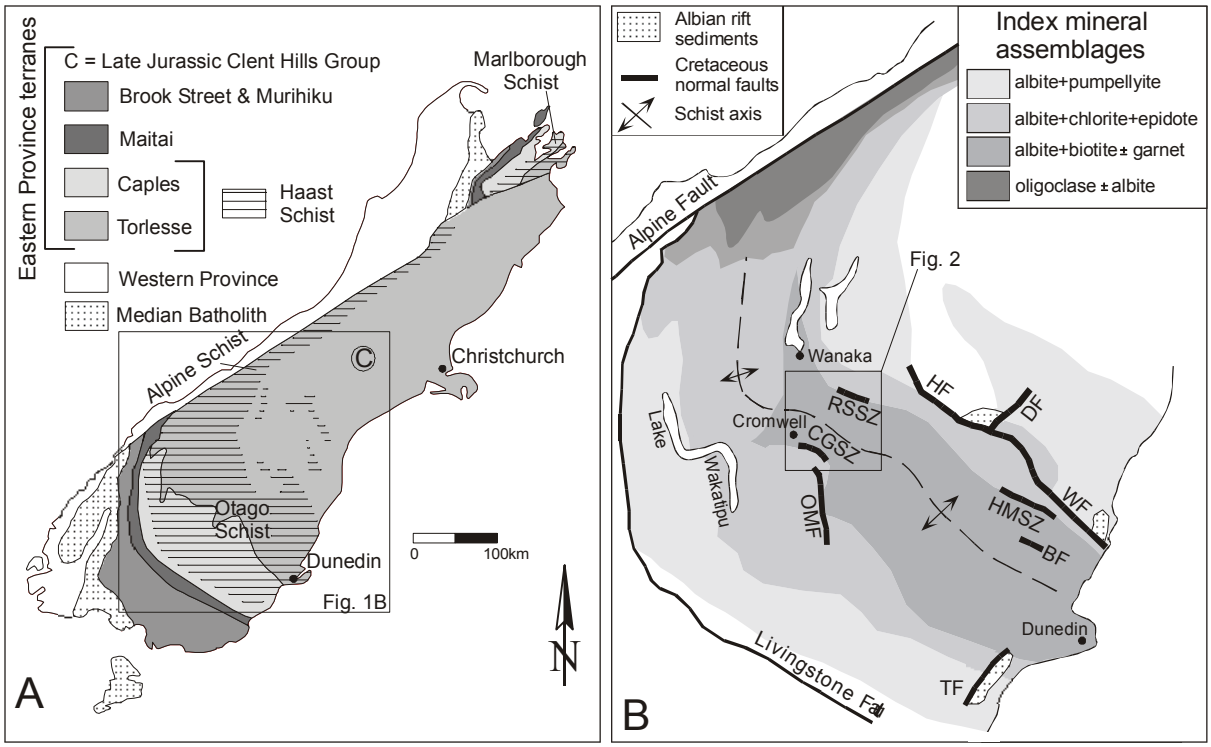

Fig. 1. A. Simplified geological map of pre-Late Cretaceous basement, South Island, New Zealand (after Mortimer et al. 1999). Haast Schist belt is subdivided into Marlborough, Alpine, and Otago Schist. B. Map of the Otago Schist showing metamorphic grade, Cretaceous normal faults and shear zones, and Albian graben sediments (after Mutch & Wilson 1952; Bishop & Laird 1976; Mortimer 1993, 2000). HF: Hawkdun Fault, DF: Dansey Pass Fault, WF Waihemo Fault, BF: Barewood Fault System, TF: Titri Fault, OMF: Old-Man Fault, HMSZ: Hyde-Macraes Shear Zone, CGSZ: Cromwell-Gorge Shear Zone, RSSZ: Rise-and-Shine Shear Zone.

pulses in the Median Batholith can be related to subduction of the oceanic Pacific plate underneath southern Gondwana (Mortimer et al. 1999).

The Haast Schist in New Zealand's South Island is subdivided into the Otago, Alpine, and Marlborough Schist (Fig. 1A). The Otago Schist is a moderately high-pressure metamorphic belt (Yardley 1982; Mortimer 2000), which formed by amalgamation of the Eastern Province Caples and Torlesse Terranes during the "Rangitata I" Orogeny in the Early-Middle Jurassic (Bradshaw et al. 1981; Adams & Robinson 1993; Little et al. 1999). The Otago Schist provides a view into the deeper part of the Torlesse accretionary wedge and forms a c. 150 km wide, two-sided arch. Metamorphism increases from prehnite-pumpellyite facies in the non-schistose rocks at the periphery of the arch to greenschist facies with peak metamorphic temperatures and pressures of 350-400°C and 8-10 kbar near the culmination axis in the deepest level of present exposure (Mortimer 2000) (Fig. 1B). Accompanying increasing metamorphism, there is an increase in deformation towards the centre of the Otago Schist as defined by the progressive development of fold generations and foliation transposition. Hutton & Turner (1936), Bishop (1972), Turnbull (2000), Forsyth (2001) and Turnbull et al. (2001) used meso- and microscale textural changes in the schist to define up to six different textural zones (TZs), which parallel the metamorphic and deformational changes across the Otago culmination. Textural zone discontinuities are the best indicators of postmetamorphic faults in the otherwise monotonous rocks of the Otago Schist (Craw 1998).

Exhumation of the Otago Schist either occurred very slowly and continuously at a rate of c. 0.2 km/m.y. from 190 to 110 Ma (Adams et al. 1985; Adams & Robinson 1993) or was punctuated by a phase of more rapid exhumation at rates of 0.6-1.0 km/m.y. after 135 Ma (Little et al. 1999). Deeply buried rocks in the Torlesse wedge reached the surface at c. 105 Ma during the initial rifting phase. This is indicated by the first appearance of schist fragments in the Kyeburn Formation (Korsch & Wellman 1988; Adams & Raine 1988). The Kyeburn Formation, together with the Horse Range Formation and the Henley Breccia, was deposited in Albian rift-related graben on the Otago Schist(Fig. 1B); similar graben are found throughout the New Zealand terranes (Ballance 1993; Laird 1993). Rifting is manifested as half graben in the Eastern Province terranes and magmatism and metamorphic core complex development in the Western Province (Tulloch & Kimbrough 1989). This deformation has been referred to as "Rangitata II" Orogeny (Bradshaw et al. 1981) and arguably is the oldest geological event common to all New Zealand basement terranes.

Widespread erosion of the Otago Schist and also the Albian graben sediments resulted in peneplanation of much of the southern South Island. The Waipounamu Erosion Surface is probably composite and time-transgressive (Bishop 1994; LeMasurier & Landis 1996). A prominent unconformity at the base of Haumurian (c. 85 Ma) sediments in northern and

offshore South Island is thought to be a lateral equivalent of the Waipounamu Erosion Surface (Crampton et al. 1999), and can be used to date the initial formation of the erosion surface between 105-85 Ma. Miocene - Recent deformation related to formation of the Alpine Fault folded the Waipounamu Erosion Surface and gave central and east Otago its present basin-and-range topography (Cotton 1917; Bishop 1994; Jackson et al. 1996; Turnbull 2000; Forsyth 2001) (Fig. 2).

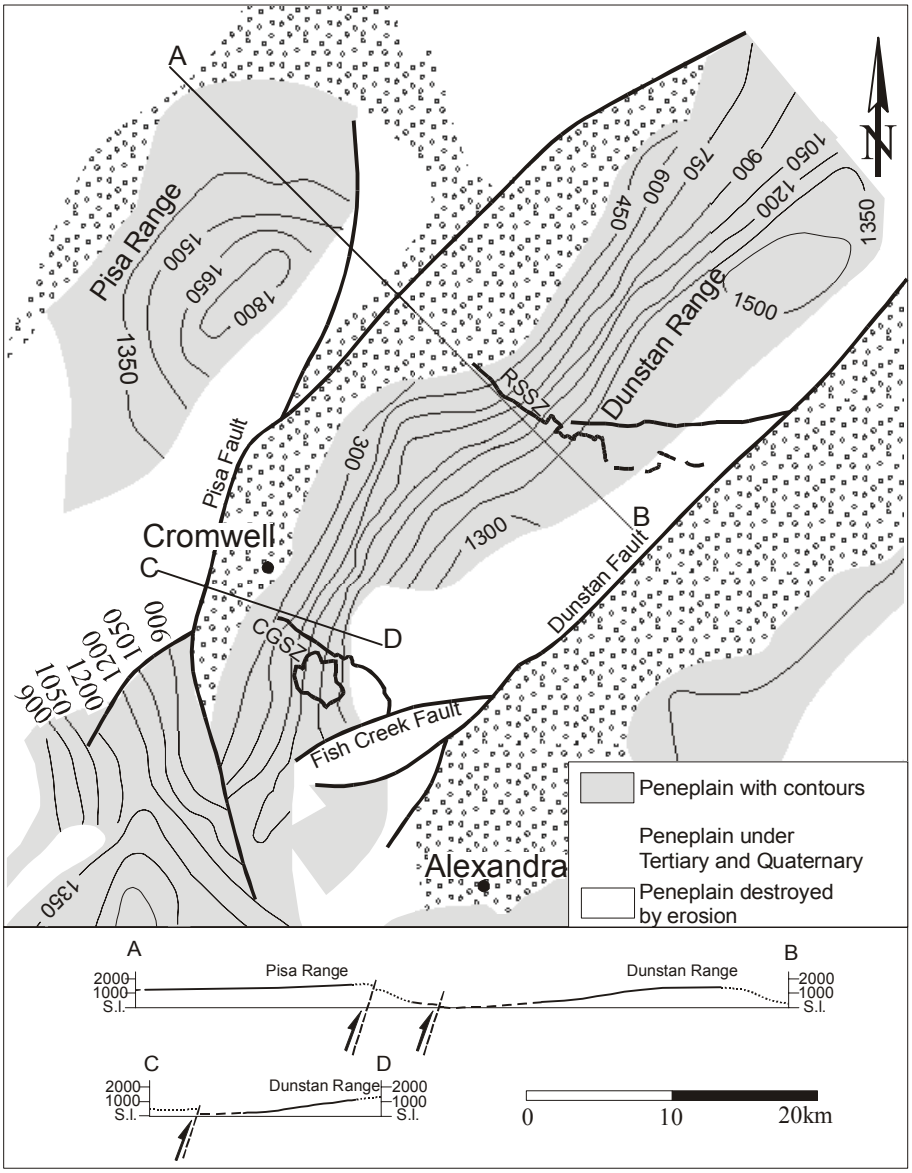

Fig. 2. Map showing Otago peneplain with contours in Dunstan Mountains (modified after Bishop 1994 and Turnbull 2000). Cross sections show Neogene deformation of peneplain.

Postmetamorphic shear zones in the Otago Schist

Postmetamorphic shear zones in the Otago Schist are of interest for two main reasons: (1) as hosts of gold mineralisation (e.g., Winsor 1991); (2) as structures that might shed light on the exhumation history of the Torlesse accretionary wedge. The best-studied low-angle shear zone in the schist is the northeast-dipping, gold-mineralised Hyde-Macraes Shear Zone in east Otago (Fig. 1B) (Teagle et al. 1990; Winsor 1991; Craw et al. 1999; De Ronde et al. 2000; Forsyth 2001). Kinematic studies of the shear zone have shown that late- to postmetamorphic thrusting was followed by a period of normal faulting (Teagle et al. 1990; Angus 1992). The gold mineralisation in the Hyde-Macraes Shear Zone took place between 132 and 158 Ma (Adams & Graham 1997).

The large-scale structure of the Otago Schist in the southern Dunstan Range (Fig. 3, 4) is dominated by a subhorizontal regional foliation which is folded about the c. north-south trending, broad, open, doubly plunging Miocene-Recent Leaning Rock Antiform (Turnbull 1987, 2000; Mortimer 1993). Before the development of the Leaning Rock Antiform the regional foliation was folded by the Bendigo fold nappe and minor related folds that are regionally classified as F3 (Craw 1985). The gold-bearing brittle-ductile RSSZ in the northern part of the Dunstan Range in central Otago is c. 10-50 m in thickness and was previously mapped in detail by Corner (1988) and Grieve (1997), and at 1:250 000 scale by Turnbull (2000). The brittle-ductile CGSZ in the Cairnmuir Mountains is a southwest dipping, >400 m wide system of faults on the southern side of Cromwell Gorge (Fig. 3, 4) (Turnbull 1987). The CGSZ and RSSZ are strongly localised features in the Otago Schist and crosscut older ductile F3 folds and the regional foliation. Thus, the two shear zones are not related to the general strain field in the Otago Schist, which is characterised by strong vertical shortening and the development of the subhorizontal foliation. Relative finite-strain work in conglomerate, sandstone, and mudstone indicates up to 70% of vertical shortening in the Otago Schist resulting in a generally oblate strain symmetry (Norris & Bishop 1990; Maxelon et al. 1998; Deckert et al. 2002).

Our structure contour data for the RSSZ indicate an average shear zone orientation of 025/15 (dip direction and dip) (Fig. 4). The constant orientation of the RSSZ across the projection of the Leaning Rock Antiform suggests a planar geometry. The shallowly south-dipping foliation in the immediate footwall of the RSSZ might be explained by an antithetic rotation of the foliation.

The CGSZ is mainly characterised by a c. 10 km long fault (lower CGSZ), which changes dip from subhorizontal in the east to c. 60° south dipping in the western part. A listric shape of the CGSZ is suggested by the fact that if the eastern part of the CGSZ is a non-listric fault it should reappear in the higher Dunstan Mountains to the north of the Cromwell Gorge

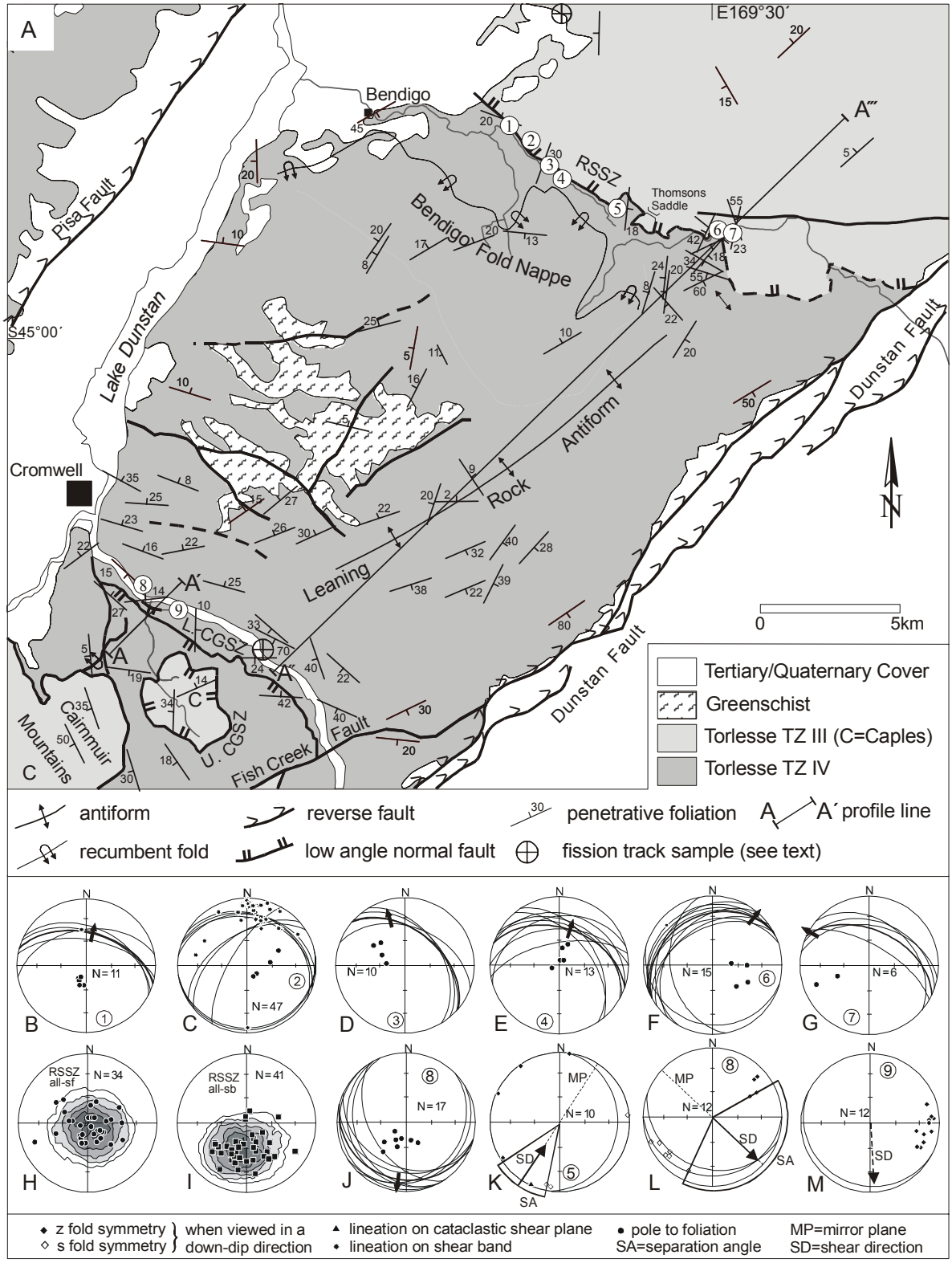

Fig. 3. Penetrative foliation, shear bands, and asymmetric folds along the Cromwell-Gorge and Rise-and-Shine shear zones (CGSZ and RSSZ). A, Geological map of the Dunstan Range area showing Cretaceous to Neogene fault pattern and textural zones (modified after Turnbull 1987, 2000; Mortimer 1993) and zircon and apatite fission track samples (Tippett & Kamp 1993). B-G and J, Stereograms showing shear bands (great circles), foliation (dots), the calculated mean direction of all shear bands measured in an outcrop (bold great circles) and the calculated mean displacement direction of the hanging wall (arrows) (equal area, lower hemisphere projections, corresponding to localities 1-4 and 6-8 on map). H and I, Contouring (Kamb method) of foliations and shear bands at the RSSZ. K-M Stereographic projection of fold axes from asymmetric folds along the RSSZ and CGSZ (localities 5, 8, 9); great circles represent measured fault planes.

due to its planar geometry. However, this is not the case (Fig. 3). The lower CGSZ cuts a subhorizontal subsidiary shear zone in its footwall, which also belongs to the CGSZ system. In this subsidiary shear zone kinematic indicators such as asymmetric folds and shear bands were mapped (Fig. 3).

The foliation within the CGSZ system dips shallowly to the north (Fig. 4). Steeply south-dipping synthetic branch faults are responsible for the antithetic rotation of the foliation to the north (Fig. 5A). About 400 m above the lower CGSZ there is the flat-lying upper CGSZ fault that underlies a klippe of Caples Terrane schist. We suggest that the whole CGSZ system comprises a set of several listric normal faults (Fig. 4).

The lack of suitable marker horizons has hindered an estimation of the displacement across intra-schist faults. Mortimer (2000) suggested that the RSSZ, CGSZ, and Hyde-Macraes Shear Zone could all be significant metamorphic discontinuities, with garnet-biotite-albite-zone rocks in their footwalls and chlorite-zone rocks in their hanging walls (Fig. 1B).

Displacement estimates

We studied the RSSZ for 15 km along strike. Our observations indicate that there is a textural zone break from TZ III to TZ IV across the RSSZ (Turnbull 2001; for photomicrographs see Mortimer 2001, fig. 3). Three TZ III rocks collected from the hanging wall have an average white-mica grain thickness of c. 20 μm, pelitic schist segregation thickness of c. 1 mm, and a psammite-pelite layering still visible as sharply-bounded grey and black bands. In contrast, three footwall rocks along the RSSZ are TZ IV with an average white-mica grain thickness of c. 40 μm, a pelitic schist segregation thickness of 5-10 mm and psammite-pelite differences blurred into gradational massive and layered schist. A recent review and revision of textural zones in Otago by Turnbull et al. (2001) has emphasised the progressive, irreversible five-fold increase in white-mica grain size between TZIIA and TZIV schist. Mortimer (2001) has provisionally correlated the grain size increase with a relative structural depth parameter in the Otago Schist. Based on this relationship, and assuming horizontal isotects in the Dunstan Mountains (Mortimer 1993), the observed differences of 20 μm in white mica grain size (textural grade) suggest net excision of at least c. 2 km and possibly up to c. 4 km of schist section across the RSSZ. Dip-slip movement on a 15°-dipping fault (Fig. 4, see below) yields a total net displacement of c. 8-15 km for the RSSZ.

A textural zone break from TZ III to TZ IV was also mapped across the upper CGSZ by Turnbull (1987). Therefore, we suggest a similar excision for the CGSZ as for the RSSZ, but because of the different dips of the individual CGSZ structures, the net displacement across the whole shear zone cannot be estimated.

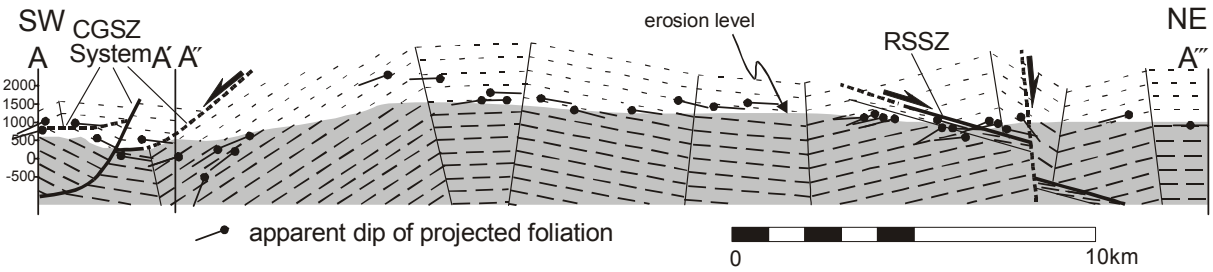

Fig. 4. Cross section through the Dunstan Range along the Leaning Rock Antiform based on a kink band model using foliation planes shown in Fig. 3A (only data near the section line were used). All used foliation planes were projected onto the section plane except the foliations from the Caples klippe in the south. Thin solid lines represent axial-plane orientations which separate different dip domains; dashed lines show projected trace of foliation above erosion level. Change of dip direction directly in the footwall of the RSSZ is due to drag of foliation into the shear zone.

Kinematics of the shear zones

Shear bands

We use the term shear band in the sense of C´-type shear bands of Berthé et al. (1979) and extensional crenulation cleavage according to Platt & Vissers (1980). In contrast to C-type shear bands, which are parallel to the shear zone, C´-type shear bands enclose an angle of 15-35° to the shear zone boundaries (Passchier & Trouw 1996). Shear-band orientations were collected from six outcrops of strongly foliated TZ IV metapelites and psammites in the footwall of the RSSZ (Fig. 3A). One outcrop was studied in the CGSZ. The shear bands only occur in the shear zones and crosscut the foliation at relatively steep angles of 30°-40° (Fig. 5B-D). At each locality, we measured the orientation of shear bands and foliations. If possible, the lineation on a shear band, which is assumed to trace the slip direction, was also recorded. The lineation measured in the outcrops is defined by stretched pre-existing grains. In pelitic layers no lineations were found. This can be explained by the initial fine grain size of the parent rocks that hinders the development of stretching lineations during deformation (Piazolo & Passchier 2002). In this case the shear direction was assumed to be the intersection lineation between the great circle of the shear band and a constructed great circle that is defined by the pole of the shear band and the pole of the regional foliation. The sense of shear was deduced by the offset across the shear bands.

We can rule out significant later rotation and reorientation of shear bands and foliation in the studied shear zones because all post-shear-zone deformation resulted in strongly localised brittle faulting at the range fronts and large-scale warping of the Otago Schist.

Almost all measured shear bands along the north-dipping RSSZ dip at c. 45° to the north. The shear directions vary from 300° to 040° and indicate a top-north movement at the RSSZ (Fig. 3B-G). The contouring of all data at the RSSZ shows that the modal foliation is subhorizontal and the shear band mode dips at 45° to the north (Fig. 3H, I).

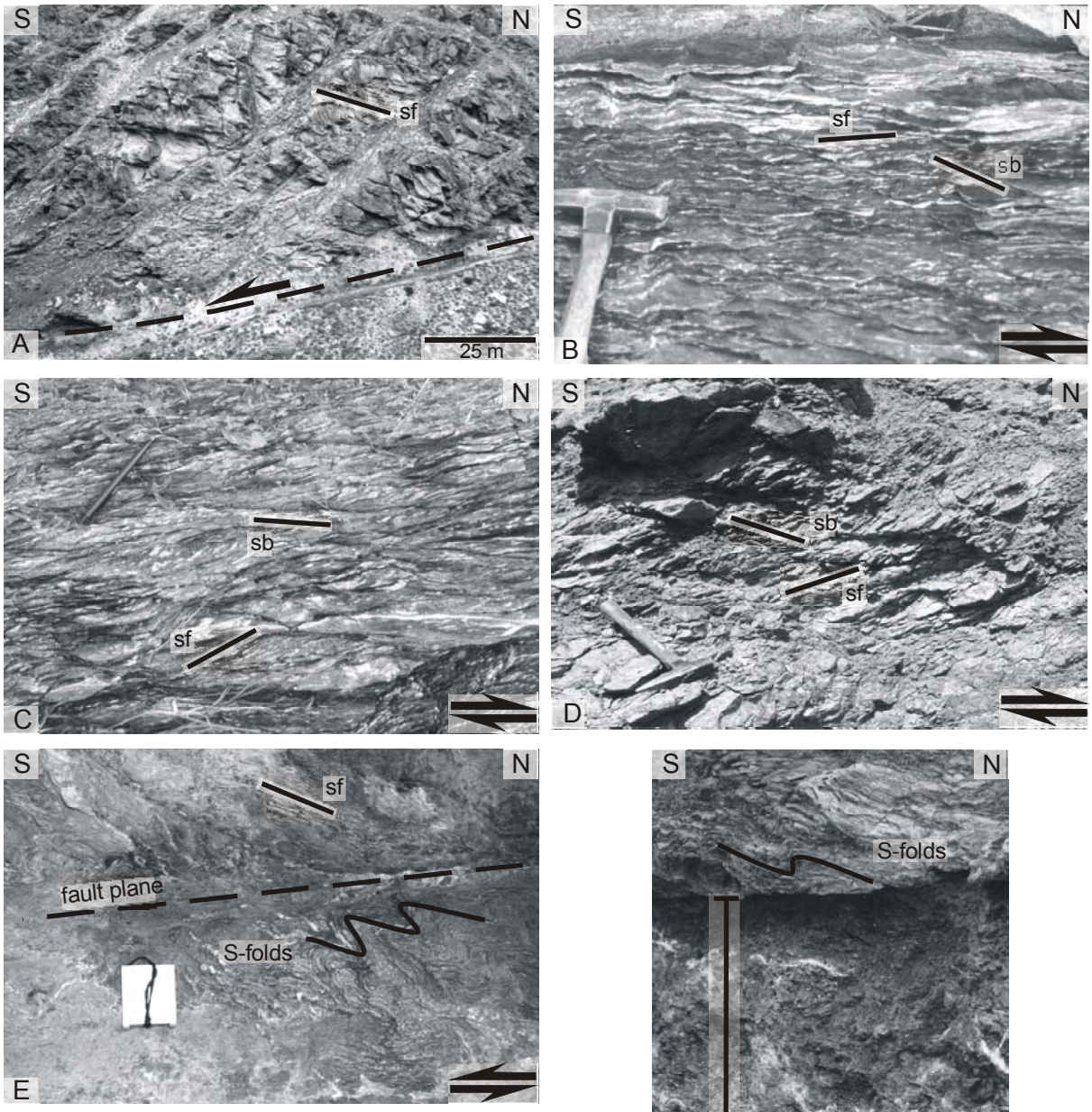

Fig. 5. Structures documenting opposite shear sense along the RSSZ and CGSZ. A, Shallowly dipping brittle shear zone in the CGSZ with top-to-south shear sense and c. 45° to the south south-dipping synthetic branch faults (from upper right to lower left) curving into the major fault. Foliation is dipping towards the north due to antithetic rotation during faulting; photograph has been taken at locality 9 in Fig. 3. B-D, Mesoscale shear bands in pelitic and psammitic outcrops at in the RSSZ, foliation (sf) curves into the shear bands (sb) indicating top-north displacement; photographs in B and C have been taken at locality 6 and the photograph in D at locality 2 in Fig. 3. E-F, Cataclastic shear zones at in the CGSZ; asymmetric folds (here S-shaped) show top-south shear; photographs have been taken at localities 2 and 8, respectively; bar in F marks a c. 50cm thick gouge layer.

In the studied outcrop of the south-dipping CGSZ, all shear bands are shallowly south dipping (Fig. 3J). The shear bands again have an angle of c. 45° to the moderately north-dipping regional foliation. The geometric relationship between foliation and shear-band orientations suggests a top-south shear sense, which is opposite to that of the RSSZ.

Asymmetric folds

Both shear zones contain several zones of fault gouge up to 50 cm thick. Within a distance of up to 1 m from the gouge layers, the schist is folded into asymmetric tight to semi-open folds with amplitudes ranging from a few centimetres to a few decimetres (Fig. 5E, F). The angular profiles of the folds and their spatial relationship to the shear zones distinguish them from the rounded F3 folds outside the shear zones. The shear zones and related fault gouges cut F3 folds and therefore provide robust crosscutting relationships.

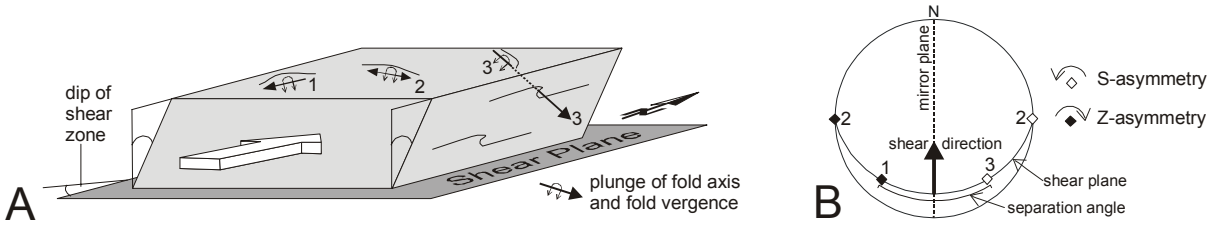

Fig. 6. Diagram illustrating relationship between asymmetric folds and shear direction (after Cowan & Brandon 1994). A, Material deformed in a ductile shear zone under progressive simple shear. Hinge lines of asymmetric folds are generally parallel to the shear plane, but may have different orientation within that plane. B, Hinge lines 1 to 3 from Fig. 6A are plotted in a lower hemisphere stereogram. The sense of asymmetry is assigned on the form of a fold when viewed in a down-plunge direction. Fold axes lie on a great circle that parallels the shear plane. Fold axes plot as two distinct groups, with Z-folds in one group and S-folds in the other. The separation angle is defined by the gap between these groups. The shear direction lies within the separation angle. See text for further information.

The method of Hansen (1971) (or internal-rotation-axis method of Cowan & Brandon 1994) was used to deduce the average direction and sense of shear from the asymmetric shear-zone-related folds. The method is based on the fact that layers in sheared rocks may form asymmetric folds, which reflect the sense of shear during deformation (Fig. 6A). The sense of asymmetry is used to distinguish between clockwise and anticlockwise asymmetry, or a Z and S shape of the fold, when viewed in the down-plunge direction of the fold axis. The axes of the S- and Z-folds are expected to lie on a great circle representing the shear plane in which they formed, and are distributed in two groups, separated from each other by the separation angle and a related mirror plane (Fig. 6B). The shear direction can be determined from the intersection of the shear plane (average girdle of S and Z axes) and the mirror plane. An important assumption is that the final deformation fabric has a monoclinic symmetry, defined by the mirror plane (Cowan & Brandon 1994). The slip vector is

interpreted to indicate the average direction and sense of tectonic transport of the hanging wall relative to a fixed footwall (Cowan & Brandon 1994).

In the RSSZ, one outcrop with shear-zone-related S- and Z-folds with subhorizontal axes was analysed (Fig. 3K). The separation angle lies between 190 and 235°, which is supported by one measurement of a stretching lineation at this locality. Fold asymmetries indicate a top-north shear. In the CGSZ, two outcrops were analysed (Fig. 3L, M). At locality 8 (in Fig. 3A), northeast-plunging axes of Z-folds and southwest-plunging axes of S-folds define a shear plane which parallels the shear-zone boundaries and supply a top-southeast sense of shear. At locality 9 (in Fig. 3A), only Z-folds are present. Therefore, a determination of the shear direction is not possible. If a 90° angle between the fold axes and the transport direction is assumed, top-south shear would be implied. It is possible that the fold axes are somewhat rotated into the shear direction, which would imply a more southeasterly shear direction, as has been deduced at locality 8.

Discussion

Thrusting versus normal faulting

The structural data show a consistent top-north shear sense for the north-dipping RSSZ and a top-south/southeast shear sense for the south-dipping CGSZ. However, to attribute the data to thrusting or normal faulting, the orientation of the shear zones and the related shear bands relative to the Earth's surface at the time of shearing has to be established (cf. Wheeler & Butler 1994).

It is not clear if the shear zones formed before, during or after folding of the Otago Schist into the 150 km wide regional arch. A pre- to syn-arching formation implies a modification of the dip of the shear zones by arching. Foliation thickness isopachs (Mortimer 2001) can be used as markers of folding. Their unfolding along the east-west trending anticlinorium axis that lies between the RSSZ and the CGSZ suggests a rotation of the shear zones of c. 5° to the north in the northern part, and to the south in the southern part of the Dunstan Mountains. Backrotation does not change the dip direction of the RSSZ, i.e. it remains a normal fault. The subhorizontal eastern part of the CGSZ would be slightly tilted (≤ 5°) to the north resulting in a top-south thrust geometry. However, thrust faulting is in contrast to the observed synthetic high-angle normal faults that merge into the CGSZ (Fig. 3, 5A).

Thus, we favour post-arching formation of the shear zones. If so, the shear zones cut across arched isotects and isograds. This would render our assumption of horizontal isotects (see section on displacement estimates) wrong. However as shown above, arching only caused c. 5° of rotation and in the Dunstan Range therefore our estimates are not significantly affected by this small rotation.

Nonetheless, later rotation caused by Cenozoic deformation must be taken into account. The Waipounamu Erosion Surface can be used as a proxy for pre-Miocene (and possibly pre-Cenozoic) paleohorizontal. The dip of the peneplain is c. 7° to the WNW in the Dunstan Range (Turnbull 2000; Fig. 2). Rotation of the shear zones and related shear bands by 7° about a NNE-trending axis does not change their orientations significantly and shows that both the RSSZ and CGSZ remain low-angle normal faults rather than tilted thrust faults. This is compatible with the observed map pattern of texturally and metamorphically low-grade rocks structurally above higher grade rocks. We found no unequivocal evidence for an earlier thrusting event along the two studied shear zones as has been postulated for the Hyde-Macraes Shear Zone.

Correlation of extensional shear zones in the Otago Schist

Current kinematic interpretations of the Hyde-Macraes Shear Zone emphasise thrusting (Teagle *et al*. 1990; Winsor 1991) and a later normal sense reactivation of the fault (Angus 1992). These 20th century studies did not take differences in metamorphic and textural grade of the hanging wall and footwall into account. We note that the dip and the brittle-ductile deformation style of the Hyde-Macraes Shear Zone and the RSSZ are similar. Both shear zones are mineralised, and coincide with a textural and metamorphic break separating TZ III chlorite-zone rocks in the hanging wall from TZ IV garnet-biotite-albite-zone rocks in the footwall (Turnbull 2000; Mortimer 2000; Forsyth 2001). As with the RSSZ, a rotation of the Hyde-Macraes Shear Zone to its pre-Waipounamu Erosion Surface orientation shows no significant tilting of its present dip direction. According to the displacement-length relationships for faults longer than 10 km (Cowie & Scholz 1992), a minimum strike length for the RSSZ of 80-150 km is suggested. Even if the method of Cowie & Scholz (1992) gives only a crude estimate of fault length, the calculation shows that the trace of the RSSZ has to be much longer than mapped in the Dunstan Range. A minimum length of c. 80 km suggests that the RSSZ could connect with the Hyde-Macraes Shear Zone. Therefore, we speculate that both shear zones belong to one single top-N net-normal sense shear zone in the Otago Schist. The extensional shear zone correlation does not invalidate interpretations of early contractional deformation on the Hyde-Macraes Shear Zone (Teagle et al. 1990; Angus 1992; Winsor 1991). In this regard we note that the CGSZ is approximately along strike from, and may merge into, the Old Man Fault (Turnbull 2000). A pre-Miocene graben structure mapped SSW of Cromwell (Turnbull et al. 1993) may also be related to the CGSZ.

Timing of shear zone movement

The Waipoumanu Erosion Surface is not offset by the RSSZ and CGSZ (Fig. 2). Although the Waipounamu Erosion Surface is of pre- 85-105 Ma age in coastal and offshore Otago (LeMasurier & Landis 1996; Crampton et al. 1999), the oldest sedimentary rocks resting on the Waipounamu Erosion Surface in inland Otago (near the Dunstan Range) are Miocene and there is some debate about the diachroneity of the erosion surface in inland Otago. Tippett & Kamp (1993) reported apatite and zircon fission track ages for two samples in the Cromwell Gorge and Bendigo areas (Fig. 3). The northern sample (zircon 76±8 Ma, apatite 35±16 Ma, 2 standard deviation errors) is in the hanging-wall block of the RSSZ and the southern sample (zircon 90±10 Ma, apatite 33±8 Ma) is in the footwall block of the RSSZ and CGSZ. The permissibly similar thermochronological histories of these samples support a case for no significant differential movement across the shear zones since the Late Cretaceous. An older age limit on shear zone movement is supplied by the fact that the RSSZ and related shear bands crosscut F3 folds (Winsor 1991). The F3 folds are generally considered to be post-peak metamorphic (Craw 1985), and consequently younger than c. 135 Ma (Little et al. 1999). Thus activity of the RSSZ and CGSZ is broadly placed into the interval between 135 and 105 Ma. This is supported by new $^{40}Ar/^{39}Ar$ data, which suggest extensional exhumation and cooling of the metamorphic core of the Otago Schist from 109-100 Ma (Gray & Foster in press). Further geochronological studies from the shear zones are needed to refine these estimates.

Syn-orogenic versus post-orogenic extension

We have crudely bracketed the timing of activity at the RSSZ and CGSZ between 135 and 105 Ma. An Early Cretaceous formation of the two normal-sense shear zones would fit into two possible tectonic scenarios:

(1) Late-stage accretion in the convergent Torlesse accretionary wedge. Little et al. (1999) speculated that the onset of enhanced cooling and exhumation in the Otago Schist at 135 Ma is related to a phase of crustal thickening as a result of accretion of the Otago Schist to the New Zealand margin along the Livingstone Fault (Fig. 1B). Crustal thickening by underplating may have destabilised the accretionary wedge leading to orogen-parallel normal faulting in the upper rear part of the wedge (cf. Platt 1986). Extensional basins are expected to form above these faults (Wallis et al. 1993). Examples for such basins that formed at convergent margins are the Recent forearc basins of the Hikurangi margin in the North Island of New Zealand (Walcott 1987; Cashman & Kelsey 1990). However, it is unlikely that pre-Albian deposits of this type would be preserved in the internal parts of the Otago Schist. In the Clent Hills Group north of the Otago Schist, weakly indurated Late Jurassic deltaic

deposits rest on highly indurated Late Triassic Torlesse greywacke (Fig. 1A) (Oliver et al. 1982). These sediments are little studied in terms of their provenance and structure but are probably trench-slope rather than extensional basins.

Norris & Bishop (1990), Maxelon et al. (1998), and Deckert et al. (2002) showed that the Otago Schist was subjected to extreme vertical contraction of up to 70% in its internal parts. Great vertical contraction tends, like erosion, to drive a wedge in a subcritical configuration promoting shortening and not extension across the wedge. Thus, the large vertical contraction also makes a syn-accretionary formation of the extensional shear zones unlikely.

(2) New Zealand-wide Albian rifting. In this scenario, the two studied normal-sense shear zones together with the Hyde-Macraes Shear Zone, the Barewood fault system (MacKenzie & Craw 1993), and faults bounding the Albian graben (Fig. 1B) would belong to a distributed regional array of Early Cretaceous normal faults. The aforementioned $^{40}Ar/^{39}Ar$ data of Gray & Foster (in press) also suggest that the RSSZ and CGSZ formed in the Albian. The Albian normal faults aided final exhumation of the Otago Schist during early rifting stages. Support for exhumation at c. 105 Ma is provided by the composition of breccia clasts in the Albian graben sediments of the Kyeburn and Henley Formations. The basal parts of the graben fills are dominated by non-foliated greywacke, whereas clasts in the upper parts are high-grade schist (Mutch & Wilson 1952; Bishop & Laird 1976). This sedimentological evidence suggests that not much of the deeper part of the Otago Schist was eroded and exhumed before rifting. Thus, we postulate that well-known normal faults bounding the Albian graben (Fig. 1B) may represent the structurally higher (and possibly younger) equivalents of extensional shear zones in the inner part of the Otago Schist (e.g. RSSZ, CGSZ, Hyde-Macraes Shear Zone), which were progressively exhumed by erosion and normal faulting.

Conclusion

The main contribution of this study is the recognition of bivergent Early Cretaceous net-normal faulting at the Rise-and-Shine Shear Zone and Cromwell Gorge Shear Zone in the central Otago Schist. This result is based on a kinematic analysis of the shear zones, their relation to paleohorizontal in the Cretaceous, and on breaks in textural and metamorphic grade across the shear zones. Our work contrasts with earlier studies in which low-angle intra-schist shear zones have been described as thrusts. Syn-convergent formation of both shear zones due to destabilisation of the accretionary wedge must be considered but we favour a relationship of the shear zones to New Zealand-wide extension starting in the Albian. The major problem of distinguishing between syn- and post-accretionary formation of the shear zones lies in the poor timing constraints of the Cretaceous shear zones. Future dating will shed light on this controversial issue.

References

Adams, C. J. & Graham, I. J. 1997. Age of metamorphism of Otago Schist in eastern Otago and determination of protoliths from initial strontium isotope characteristics. *New Zealand Journal of Geology and Geophysiscs* 40, 275-286.

Adams, C. J. & Raine, J. I. 1988. Age of Cretaceous silicic volcanism at Kyeburn, Central Otago, and Palmerston, eastern Otago, South Island, New Zealand. *New Zealand Journal of Geology Geophysics* 31, 471-475.

Adams, C. J. & Robinson, P. 1993. Potassium-Argon age studies of metamorphism/ uplift/ cooling in Haast Schist coastal sections of Dunedin, Otago, New Zealand. *New Zealand Journal of Geology and Geophysiscs* 36, 317-325.

Angus, P.V. 1992. The structural evolution of the Hyde-Macraes shear zone at Round Hill, Otago, New Zealand. Proceedings of the 26th Annual Conference, New Zealand Branch, Australasian Institute of Mining & Metallurgy, 11pp.

Ballance, P. 1993. The paleo-Pacific, post-subduction, passive margin thermal relaxation sequence (Late Cretaceous-Paleogene) of the drifting New Zealand continent. In: *Sedimentary Basins of the World*, 2. Elsevier Science, Amsterdam, 93-110.

Berthé, D., Choukroune, P.& Jegouzo, P. 1979. Orthogneiss, mylonite and non-coaxial deformation of granites: the example of the South Armorican shear zone. *Journal of Structural Geology* 1, 31-42.

Bishop, D. G. 1972a. Progressive metamorphism from prehnite-pumpellyite to greenschist facies in the Dansey Pass area, Otago, New Zealand. *Geological Society of America Bulletin* 83, 3177-3198.

Bishop, D. G. 1994. Extent and regional deformation of the Otago peneplain. Institute of Geological & Nuclear Sciences, Lower Hutt, New Zealand.

Bishop, D. G., Bradshaw, J. D., Landis, C. A. & Turnbull, L. M. 1976. Lithostratigraphy and structure of the Caples Terrane of the Humboldt Mountains, New Zealand. *New Zealand Journal of Geology and Geophysiscs* 19, 827-848.

Bolhar, R. & Ring, U. 2001. Deformation history of the Yolla Bolly terrane at Leech Lake Mountain, Eastern belt, Franciscan subduction complex, California Coast Ranges. *Geological Society of America Bulletin* 113, 181-195.

Bradshaw, J.D.; Andrews, P.B.; Adams, C.J.D. 1981. Carboniferous to Cretaceous on the Pacific margin of Gondwana: the Rangitata phase of New Zealand. In: Cresswell, M.M.; Vella, P. ed. Gondwana Five: selected papers and abstracts of papers presented at the Fifth International Gondwana Symposium. Rotterdam, A.A. Balkema, 217-221.

Brandon, M. T. & Fletcher, R. C. 1998. Accretion and exhumation at a steady-state wedge; a new analytical model with comparisons to geologic examples. *Geological Society of America, Abstracts with Programs* 29(6), 120.

Brandon, M. T., Roden-Tice, M. K. & Garver, J. I. 1998. Late Cenozoic exhumation of the Cascadia accretionary wedge in the Olympic Mountains, NW Washington State. *Geological Society of America Bulletin* 110, 985-1009.

Cashman, S.M., Kelsey, H.M. 1990. Forearc uplift and extension, southern Hawke´s bay, New Zealand: Mid-Pleistocene to present. *Tectonics* 9, 23-44.

Corner, N. G. 1988. Bendigo Project. Homestake Exploration activity on the Rise and Shine Shear Zone. Prospecting Licences 31-576 and 31-1490. BHP Gold Mines (NZ) Ltd report CR 5825.

Unpublished open-file mining company report, Institute of Geological & Nuclear Sciences MR 1175.

Cotton, C. A. 1917. Block Mountains in New Zealand. *American Journal of Science* 44, 250-293.

Cowan, D. S. & Brandon, M. T. 1994. A symmetry-based method for kinematic analysis of large-slip brittle fault zones. *American Journal of Science* 294, 257-306.

Cashman, S.M.; Kelsey, H.M. 1990. Forearc uplift and extension, southern Hawke´s bay, New Zealand: Mid-Pleistocene to present. *Tectonics* 9, 23-44.

Crampton, J., Schioler, P., King, P. & Field, B. 1999. Marine Expression of the complex Cretaceous Waipounamu erosion surface in the east coast region, New Zealand. *Geological Society of New Zealand Miscellaneous Publications* 107A, 34.

Craw, D. 1985. Structure of the schist in the Mt. Aspiring region, northwestern Otago, New Zealand. *New Zealand Journal of Geology and Geophysics* 28, 55-75.

Craw, D. 1998. Structural boundaries and biotite and garnet `isograds´ in the Otago and Alpine Schists, New Zealand. *Journal of Metamorphic Geology* 16, 395-402.

Craw, D., Windle, S. J. & Angus, P. V. 1999. Gold mineralisation without quartz veins in a ductile-brittle shear zone, Macraes Mine, Otago Schist, New Zealand. *Mineralium Deposita* 34, 382-394.

Dahlen, F.A., Suppe, J. 1988. Mechanics, growth, and erosion of mountain belts. In: Clark, S.P., Burchfiel, B.C.; Suppe, J. eds. Processes in continental lithospheric deformation. *Geological Society of America Special Paper* 218, 161-208.

Deckert, H.; Ring, U.; Brandon, M.T.; Mortimer, N.; Wohlers, A.& Maxelon, M. 2002. Large vertical shortening in the Otago Schist, New Zealand – Implications for the exhumation of high-pressure metamorphic rocks. TSK IX; Ninth symposium on Tectonics, structural and crystalline geology, *Erlanger Geologische Abhandlungen* Special volume 3, 17-18.

De Ronde, C., Faure, K., Bray, C. J. & Whitford, D. J. 2000. Round Hill Shear-Zone hosted Gold Deposit, Macraes Flat, Otago, New Zealand: Evidence of a magmatic ore fluid. *Economic Geology* 95, 1025-1048.

Forsyth, P.J. comp. 2001. Geology of the Waitaki area. Institute of Geological & Nuclear Sciences 1:250 000 geological map 19. 1 sheet + 64p. Lower Hutt, New Zealand. Institute of Geological & Nuclear Sciences Ltd.

Gray, D.R.; Foster, D.A. in press: New 40Ar/39Ar data from the Otago Schist: record of Gondwana deformation and breakup. In: 11th International Gondwana Symposium Abstracts. Christchurch, New Zealand, University of Canterbury.

Hansen, E. 1971. Strain Facies. Springer Verlag, New York, 207p.

Harms, T.; Jayko, A.S. & Blake, M.C. Jr. 1992. Kinematic evidence for extensional unroofing of the Franciscan Complex along the Coast Range fault zone, northern Diablo Range, California. *Tectonics* 11, 228-241.

Hutton, C. O. & Turner, F. J. 1936. Metamorphic zones in north-west Otago. *Transactions of the Royal Society of New Zealand* 65, 405-406.

Jackson, J., Norris, R. & Youngson, J. 1996. The structural evolution of active fault and fold systems in central Otago, New Zealand: Evidence revealed by drainage patterns. *Journal of .Structural Geology* 18, 217-234.

Korsch, R. J. & Wellman, H. W. 1988. The geological evolution of New Zealand and the New Zealand region. In: The Ocean Basins and Margins (edited by Nairn, A. E. M., Stehli, F. G. & Uyeda, S.) 7B. Plenum Publishing Corporation, 411-482.

Laird, M. 1993. Cretaceous continental rifts: New Zealand region. In: South Pacific Sedimentary Basins. (edited by Ballance, P.). Sedimentary Basins of the World 2. Elsevier Science, Amsterdam, 37-49.

LeMasurier, W. E. & Landis, C. A. 1996. Mantle-plume activity recorded by low-relief erosion surfaces in West Antarctica and New Zealand. *Geological Society of America Bulletin* 108, 1450-1466.

Little, T. A., Mortimer, N. & McWilliams, M. 1999. An episodic Cretaceous cooling model for the Otago-Marlborough Schist, New Zealand, based on 40 Ar/39Ar white mica ages. *New Zealand Journal of Geology and Geophysiscs* 42, 305-325.

Mac Kenzie, D. J. & Craw, D. 1993. Structural control of gold-scheelite mineralisation in a major normal fault system, Barewood, eastern Otago, New Zealand. *New Zealand Journal of Geology and Geophysiscs* 36, 437-445.

MacKinnon, T. C. 1983. Origin of the Torlesse terrane and coeval rocks, South Island, New Zealand. *Geological .Society of America .Bulletin* 94, 967-985.

Maxelon, M.; Wohlers, A.; Halama, R.; Ring, U.; Mortimer, N. & Brandon, M.T. 1998. Ductile strain in the Torlesse wedge, South Island, New Zealand. *Eos* 79 (45) , 889.

Mortimer, N. 1993a. Geology of the Otago Schist and adjacent rocks. Institute of Geological & Nuclear Sciences, Lower Hutt, New Zealand.

Mortimer, N. 2000. Metamorphic discontinuities in orogenic belts: example of the garnet-biotite-albite zone in the Otago Schist, New Zealand. *International Journal of Earth Sciences* 89, 295-306.

Mortimer, N. 2001. Foliation thickness and mica grain size: two new ways to subdivide the Otago Schist, New Zealand. In: Proceedings of the 34th Annual Conference, Dunedin. New Zealand Branch. Australasian Institute of Mining & Metallurgy, 43-49.

Mortimer, N. & Campell, H. J. 1996. Devonian to Jurassic rocks in New Zealand: classification, content and Gondwana context. In: Gondwana Nine. (edited by Guha, P. K. S., Sengupta, S., Ayyasami, K. & Gosh, R. N.). IBH Publishing, New Delhi, Oxford, 783-790.

Mortimer, N., Tulloch, A. J., Spark, R. N., Walker, N. W., Ladley, E., Allibone, A. & Kimbrough, D. C. 1999. Overview of the Median Batholith New Zealand: a new interpretation of the geology of the Median Tectonic Zone and adjacent rocks. *J.African.Earth Sci*. 29, 257-268.

Mutch, A. R. & Wilson, D. D. 1952. Reversal of movement on the Titri Fault. *New Zealand Journal of Science and Technology* B33, 398-403.

Norris, R. J. & Bishop, D. G. 1990. Deformed metaconglomerates and textural zones in the Otago Schists, South Island, New Zealand. *Tectonophysics* 174, 331-349.

Oliver, P. J., Campell, J. D. & Spede, I. G. 1982. The stratigraphy of the Torlesse rocks of the Mt Somers area (S81) mid-Canterbury. *Journal of the Royal Society of New Zealand* 12(243-271).

Passchier, C.W. & Trouw, R.A.J. 1996. Microtectonics. Berlin, Springer. 289 p.

Pettinga, J. R. 1982. Upper Cenozoic structural history, coastal southern Hawke`s Bay, New Zealand. *New Zealand Journal of Geology and Geophysics* 25, 149-191.

Piazolo, S. & Passchier, C.W. 2002. Controls on lineation development in low to medium grade shear zones; a study from the Cap de Creus Peninsula, NE Spain. *Journal of Structural Geology* 24, 25-44.

Platt, J.P., Vissers, R.L.M. 1980. Extensional structures in anisotropic rocks. *Journal of Structural Geology* 2, 397-410.

Platt, J.P. 1986. Dynamics of orogenic wedges and the uplift of high-pressure metamorphic rocks. *Geological Society of America Bulletin* 97, 1037-1053.

Platt, J.P. 1993. Exhumation of high-pressure rocks: a review of concepts and processes. *Terra Nova* 5, 119-133.

Ring, U., Brandon, M.T. 1994. Kinematic data for the Coast Range fault zone zone and implications for the exhumation of the Franciscan Subduction Complex. *Geology* 22, 735-738.

Ring, U. 1995. Horizontal contraction or horizontal extension?: Heterogeneous Late Eocene and Early Oligocene general shearing during blueschist- and greenschist-facies metamorphism at the Pennine-Austroalpine boundary zone in the Western Alps. *Geologische Rundschau* 84, 843-859.

Ring, U. & Brandon, M. T. 1999. Ductile deformation and mass loss in the Franciscan subduction complex: implications for exhumation processes in accretionary wedges. In: Exhumation Processes: Normal faulting, ductile flow and erosion. (edited by Ring, U., Brandon, M. T., Lister, G. S. & Willett, S. D.) 154. *Special Publications of the Geological Society, London*, 55-86.

Teagle, D. A. H., Norris, R. J. & Craw, D. 1990. The structural controls on gold quartz mineralization in a duplex thrust system, Hyde Macraes Shear Zone, Otago Schist, New Zealand. *Economic Geology* 85(1711-1719).

Tippett, J. M. & Kamp, P. J. J. 1993. Fission track analysis of the late Cenozoic vertical kinematics of continental Pacific crust, South Island, New Zealand. *Journal of Geophysical Research* 98, 16119-16148.

Tulloch, A. J. & Kimbrough, D. L. 1989. The Paparoa metamorphic core complex, Westland- Nelson, New Zealand: Cretaceous extension associated with fragmentation of the Pacific margin of Gondwana. *Tectonics* 8, 1217-1234.

Turnbull, I. M. 1987. Geological Map of New Zealand, Sheet 133, Cromwell. Department of Scientific and Industrial Research, Wellington, New Zealand.

Turnbull, I. M., Craw, D. & Norris, R. J. 1993. Pre-Miocene and post-Miocene deformation in the Bannockburn basin, central Otago, New Zealand. *New Zealand Journal of Geology and Geophysiscs* 36, 107-115.

Turnbull, I. M., Mortimer, N. & Craw, D. 2001. Textural zones in the Haast Schist - a reappraisal. *New Zealand Journal of Geology & Geophysics* 44, 171-183.

Turnbull, I. M. c. 2000. Geology of the Wakatipu area. Institute of Geological & Nuclear Sciences, Lower Hutt, New Zealand.

Walcott, R. I. 1987. Geodetic strain and the deformational history of the North Island of New Zealand during late Cenozoic. *Philosophical Transactions of the Royal Society, London,* Series A 321, 163-181.

Wallis, S.R.; Platt, J.P.& Knott, S.D. 1993. Recognition of syn-convergence extension in accretionary wedges with examples from the Calabrian arc and the Eastern Alps. *American Journal of Science* 293, 463-495.

Winsor, C. N. 1991b. Low-angle shear zones in Central Otago, New Zealand - their regional extent and economic significance. *New Zealand Journal of Geology and Geophysiscs* 34, 501-516.

Yardley, B. W. D. 1982. The early metamorphic history of the Haast Schists and related rocks of New Zealand. *Contributions Mineralogy Petrology* 81, 317-327.